MAGYAR ÁLLAMI
EÖTVÖS LORÁND
GEOFIZIKAI INTÉZET

GEOFIZIKAI
KÖZLEMÉNYEK

ВЕНГЕРСКИЙ
ГЕОФИЗИЧЕСКИЙ
ИНСТИТУТ
ИМ Л. ЭТВЕША

ГЕОФИЗИЧЕСКИЙ
БЮЛЛЕТЕНЬ

GEOPHYSICAL
TRANSACTIONS

EÖTVÖS LORÁND GEOPHYSICAL INSTITUTE OF HUNGARY

CONTENTS

VOL. 41. NO. 1–2. APRIL 1997. (ISSN 0016–7177)

BUDAPEST

TARTALOMJEGYZÉK

Lapunk az Ipar Műszaki Fejlesztéséért Alapítvány támogatásával készült.

GEOPHYSICAL TRANSACTIONS 1997
Vol. 41. No. 1-2. pp. 1-21

New results on the theory of the most frequent value procedures

Ferenc STEINER*

New results have been published in the last few years on the theory of the most frequent value (MFV) procedures. In this paper some of these results are presented in a concise manner to show more clearly the differences between the statistical procedures based upon the L_2, L_1 and P-norms, respectively.

Keywords: most frequent value, robustness, P-norms, statistical analysis, type-distance

1. Different attitudes to the actual probability distribution type of measurement errors result in quite different statistical procedures

To facilitate the presentation of the new results, let us start from the definitions of the likelihood function and from that of the I-divergence. There are similarities (or even equalities) and, on the contrary, substantial differences, too. These are summarized in *Table I.*

Table I.

f is assumed to be **unknown** (this corresponds to the overwhelming majority of practical tasks), and therefore it is **substituted** by $g(T,S;x)$ of given analytical form. This substitution results in an **information loss** measured by the 'I-divergence': $$I_g = \int_{-\infty}^{\infty} f(x)\ln\left[f(x)/g(T,S;x)\right]dx.$$	f is assumed to be **a priori known**, including the value of S or T (this latter assumption is implicitly present in the well known book of ANDREWS et al. [1972]). $$\mathcal{L} = \sum_{i=1}^{n} -\ln f(T,S;x_i)$$ is the so-called **likelihood function** which is appropriate for to the basic assumption.

* University of Miskolc, H-3515 Miskolc-Egyetemváros

Manuscript received: 10 October, 1995

Table I. continued

Both I_g and $\mathcal{L}$ should be **minimized.** If S is known, the accepted value of T fulfils:

$$\frac{\partial I_g}{\partial T} = 0 \qquad (1)$$

$$\frac{\partial \mathcal{L}}{\partial T} = 0 \qquad (2)$$

The integral form of Eq. (2) can be trivially given, and similarly Eq. (1) (which is an integral expression) for the data x_i. Astonishingly enough, **both Eqs. (1) and (2) lead to exactly the same formula for *T*-determination.** (In general, iteration is necessary.)
On the contrary, the two approaches belonging to f result in the fact that ***S*-formulae essentially differ from each other:**

To be sure that Eq. (1) really results in **minimum information loss,** the relation

$$\frac{\partial^2 I_g}{\partial T^2} > 0 \qquad (3a)$$

must also hold. The fulfilment of this relation, however, is warranted if

$$\left(H \equiv\right) \int_{-\infty}^{\infty} \frac{\partial^2 g(T,S;x)}{\partial^2 T} \cdot \frac{f(x)}{g(T,S;x)} \mathrm{d}x = 0 \qquad (3)$$

holds [see HAJAGOS 1991]. Eq. (3) defines (with an analytically given g-function) the formula for the calculation of S (i.e., of the parameter of scale).

According to the usual maximum likelihood techniques (see the already cited ANDREWS et al. [1972],)

$$\frac{\partial \mathcal{L}}{\partial S} = 0 \qquad (4)$$

is also demanded and with an analytically given f Eq. (4) results in a formula for determining the parameter of scale. Unfortunately, Eq. (4) leads to such S-formulae which are not resistant (i.e., they are outlier-sensitive).

A new result can already be formulated:
The formulae derived from Eq. (3) and Eq. (4) never coincide with each other except in the Gaussian case.

Notations

x_i : directly measured value ($1 \le i \le n$)

f, $f(x)$, $f(T,S;x)$: *the actual probability density function*

T: parameter of location (this is often the symmetry point). In nearly all of the tasks the unknown of primary interest is the value of T.

S: parameter of scale. We are perhaps not intrinsically interested in its value but the resulting T-value can be heavily influenced by the actual value of S.

Table I. Two different approaches to the type of the actual probability distributions lead to both theoretically and practically different statistics

I. táblázat. Az előforduló valószínűségeloszlások típusára vonatkozó különböző szemléletű alapfeltevések elméleti és gyakorlati szempontból egyaránt eltérő statisztikai eljárásokhoz vezetnek

This new thesis: 'the formulae derived from Eq. (3) and Eq. (4) never coincide with each other except in the Gaussian case', [see CSERNYÁK 1994] is important also concerning the T-determinations inasmuch as using both

methods (namely based on the maximum likelihood principle, on the one hand, and on the other hand, on the *I*-divergence), in just the same manner two formulae are to be fulfilled *simultaneously* (Eqs. (1) and (3) or Eqs. (2) and (4)). Consequently, the formula for the determination of the parameter of scale strongly influences the behaviour of the *T*-determination, e.g. in respect of robustness.

Let us show an example. Choosing the Cauchy type distribution as substitute one (i.e. *g*-function) in the first method, and the same Cauchy-distribution as an a priori known *f* density function in the second one (i.e., in the maximum likelihood method), the actual *T*-formulae derived on the basis of Eqs. (1) and (2) are just the same (as was mentioned earlier in the fourth row of Table I). On the contrary, Eqs. (3) and (4) result in quite other formulae for the parameter of scale, if the Cauchy distribution was chosen as substitute distribution *g*, — but this is in full accordance with the thesis at the end of Table I. If X_i means the residual, i.e., measured value x_i minus computed value (in the simplest case $X_i=x_i-T$ obviously holds), from Eq.(3) it follows that:

$$S^2 = \frac{3\sum_{i=1}^{n} X_i^2 \Big/ \left(S^2 + X_i^2\right)^2}{\sum_{i=1}^{n} 1 \Big/ \left(S^2 + X_i^2\right)^2} \tag{5}$$

and the resulting value is called 'dihesion' (and is denoted by ε). Eq. (4) results in quite another formula (without squares and without the factor '3')

$$S^2 = \frac{\sum_{i=1}^{n} X_i^2 \Big/ \left(S^2 + X_i^2\right)}{\sum_{i=1}^{n} 1 \Big/ \left(S^2 + X_i^2\right)} \tag{6}$$

if the Cauchy-distribution was chosen as substitute distribution *g*.

The question arises as to whether the choice of the determination method of *S*, i.e. of the parameter of scale, is really of significant importance in respect of the determination of *T*? Determination of the value of *T* (or of the values $p_1,p_2,\ldots,p_j,\ldots,p_J$ as components of the unknown parameter vector $\overline{p}$ in multidimensional cases) always has priority in our practical tasks. The question of errors or bias of the *S*-determinations is treated in general as a secondary one, or simply the conventional formulae are used for error-de-

terminations. BARTA and HAJÓSY [1985] showed an astonishing (or even comical or possibly even rather tragic) example concerning determinations of the universal gravity constant: the error intervals given by three authors to their measurements have no common point (*Fig. 1*). Possibly Gaussian error distribution was supposed but the real error seemingly was that nothing was known about this supposition... (The whole range of the three error-intervals divided by the absolute value of the gravity constant is 0.07%, i.e., by several orders of magnitude greater than in the case of some other universal constant, e.g. the velocity of light in vacuum, etc.) Figure 1 shows that error-determinations of classical manner can lead to completely false results.

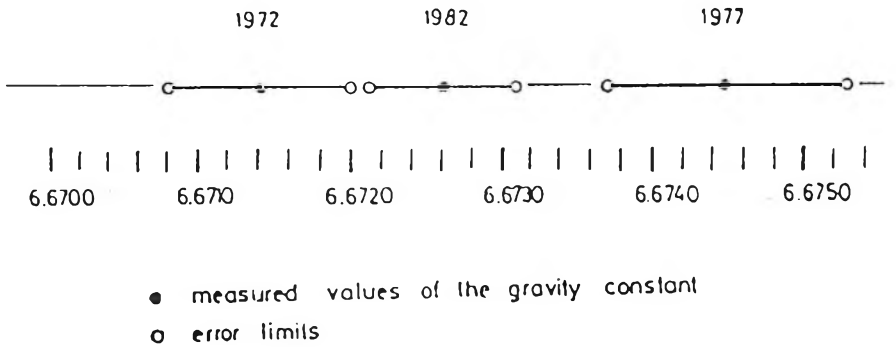

Fig. 1. Error intervals for differing values of the universal gravity constant determined by the measurements of three authors [from BARTA and HAJÓSY 1985]. The error intervals have no common point

1. ábra. Hibaintervallumok az általános tömegvonzási állandónak három szerző által meghatározott értékeihez [BARTA és HAJÓSY 1985 nyomán]. Egyetlen közös pontja sincs a hibaintervallumoknak

2. Essential differences between modern statistics (based e.g. upon the norms P_J, P, P_C, P_{lt}) and the conventional statistical procedures (based on the L_2-norm)

One can perhaps say that some *experimenters* with limited theoretical background work only on the basis of the outdated statistics of the last century. Not at all. Even the Heisenberg relation is formulated for *scatters*, i.e., for minimum values of the old L_2-norm. Incidentally, nowadays primarily norm representations of statistical algorithms are more and more given. The following table (*Table II*) therefore gives the simple expressions of six norms

(expressed by the X_i residuals defined earlier) based on HAJAGOS and STEINER [1993a].

Norm	Formula	Eigen-distribution (for this type of error distribution the norm in question works optimally)
L_1	$\frac{1}{n}\sum_{i=1}^{n}\lvert X_i\rvert$	Laplace
L_2	$\sqrt{\frac{1}{n}\sum_{i=1}^{n}X_i^2}$	Gauss
P_J	$\varepsilon\cdot\left\{\prod_{i=1}^{n}\left[1+\left(\frac{X_i}{3\varepsilon}\right)^2\right]\right\}^{\frac{1}{2n}}$	Jeffreys
P	$\varepsilon\cdot\left\{\prod_{i=1}^{n}\left[1+\left(\frac{X_i}{2\varepsilon}\right)^2\right]\right\}^{\frac{1}{2n}}$	geostatistical
P_C	$\varepsilon\cdot\left\{\prod_{i=1}^{n}\left[1+\left(\frac{X_i}{\varepsilon}\right)^2\right]\right\}^{\frac{1}{2n}}$	Cauchy
P_{lt}	$\varepsilon\cdot\left\{\prod_{i=1}^{n}\left[1+\left(\frac{2X_i}{\varepsilon}\right)^2\right]\right\}^{\frac{1}{2n}}$	(very long-tailed error distributions)
For ε (called dihesion) $\sum_{i=1}^{n}\frac{3X_i^2-\varepsilon^2}{\left(\varepsilon^2+X_i^2\right)^2}=0$ must be fulfilled.		

Table II. Formulae of six statistical norms (the corresponding eigen-distributions are also given)

II. táblázat. Hat statisztikai norma formulája és a normákhoz tartozó sajáteloszlások

Returning to the Heisenberg relation, it is formulated in the literature of the Fourier transforms [see e.g. PAPOULIS 1962] in the following way: if γ is the Fourier-transform of φ, and two density functions are defined as

$$f(x)=\varphi^2(x)\Big/\int_{-\infty}^{\infty}\varphi^2(x)\mathrm{d}x \quad \text{and} \quad g(y)=\gamma^2(x)\Big/\int_{-\infty}^{\infty}\gamma^2(x)\mathrm{d}x \tag{7}$$

(g can be called the 'Heisenberg counterpart' of f), then the product of the scatters (standard deviations) cannot be less than 1/2:

$$\sigma(f)\cdot\sigma(g)\geq\frac{1}{2} \tag{8}$$

It is well known [see e.g. HUBER 1981] that σ is at the same time the asymptotic scatter (A) of the algorithm based on the minimization of the L_2-norm and therefore relation (8) can also be written as

$$A(f)\cdot A(g)\geq\frac{1}{2} \qquad \text{for the } L_2\text{-norm.} \tag{8a}$$

Let us show an example, namely the supermodel $f_a(x)$ (see e.g. in STEINER [1991] the first column of the table at the end of the book):

$$f_a(x)=\frac{\Gamma\left(\frac{a}{2}\right)}{\sqrt{\pi}\cdot\Gamma\left(\frac{a-1}{2}\right)}\cdot\frac{1}{\left(1+x^2\right)^{a/2}} \qquad (a>1). \tag{9}$$

(Incidentally, it is easily seen with this analytically simple density function what an enormous difference exists between the formulae given in Eqs. (5) and (6): if the sum expressions are changed to integral ones and $f_a(x)$ figures in these integrals, Eq. (6) yields $S\to\infty$ if $a\to1$; on the contrary, Eq. (5) yields $S\to2.592$, if $a\to1$, see HAJAGOS and STEINER [1993b].)

The Heisenberg counterpart of $f_a(x)$ is [see STEINER 1991, p. 281]:

$$g_a(y)=\frac{2}{\sqrt{\pi}}\frac{\Gamma\left(\frac{a}{2}\right)}{\Gamma^2\left(\frac{a}{4}\right)\cdot\Gamma\left(\frac{a-1}{2}\right)}\left(\frac{|g|}{2}\right)^{\frac{a-2}{2}}\cdot\left[K_{\frac{a-2}{4}}(|g|)\right]^2 \qquad (a>1). \tag{10}$$

The latter formula is a little bit more difficult (the modified Bessel function K figures in it) but the distributions $g_a(y)$ are symmetric and unimodal (like the $f_a(x)$ distributions). The density curve of $g_a(y)$ e.g. to $a=8$ (*Fig. 2*) proves that for modelling actual cases the types of the supermodel $g_a(y)$ could also be appropriately used.

As was mentioned earlier the scatters in the Heisenberg relation (characterizing primarily the mother distributions themselves) have also the

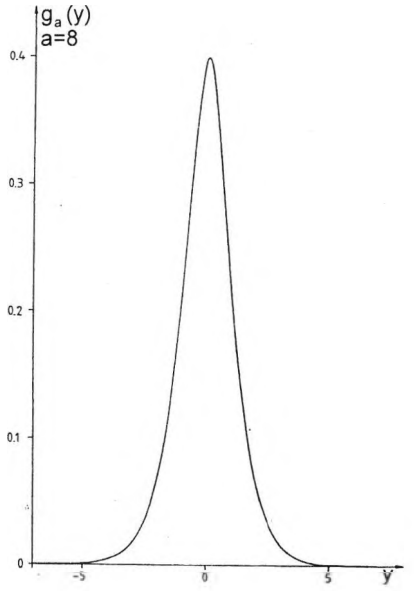

Fig. 2. Probability density function $g_a(y)$ for $a=8$ (see Eq.10); this is the 'Heisenberg counterpart' of the density function $f_a(x)$ for $a=8$

2. ábra. A $g_a(y)$-sűrűségfüggvény $a=8$ esetén (ld. a (10) egyenletet); ez az $a=8$-hoz tartozó $f_a(x)$ valószínűség-sűrűségfüggvény 'Heisenberg-pandantja'

meaning of asymptotic scatters for the case if the L_2-norm is used for determining the parameter of location, e.g. the symmetry point. Consequently, the Heisenberg relation can be written, for the L_2-norm as $A(f_a)\cdot A(g_a)\geq 1/2$ (where equality holds if and only if both f_a and g_a are Gaussian).

And what about the behaviour of the products of the asymptotic scatters of Heisenberg pairs of density functions if the statistical algorithm is defined by minimization of the P_J, P, P_C and P_{lt} norms? Astonishingly enough, they have quite opposite behaviour to that shown by the L_2-norm. The curves of the products $A(f_a)\cdot A(g_a)$ are demonstrated in *Fig. 3:* 1/2 *is no longer the minimum value for the simultaneously reachable accuracy in the two domains of the Fourier-transformation*. This should also be stressed as a new result [see STEINER and HAJAGOS 1995].

Figure 3 shows the products of asymptotic scatters versus $t = 1/(a-1)$ as type-parameter. For comparison in all four cases the same increasing curve concerning the L_2-norm is also shown; if $t = 1/(a-1)$ is equal or greater than 0.5 this error-product for L_2 is infinite.

The descending curves of the new statistical norms start for P_J and P at a value which is not significantly greater than 1/2. The curve for P_{lt} starts at about 1, i.e., twice greater value of this mystical 1/2. No wonder, then, that P_{lt} is defined for error distribution with extremely long tails. It should be

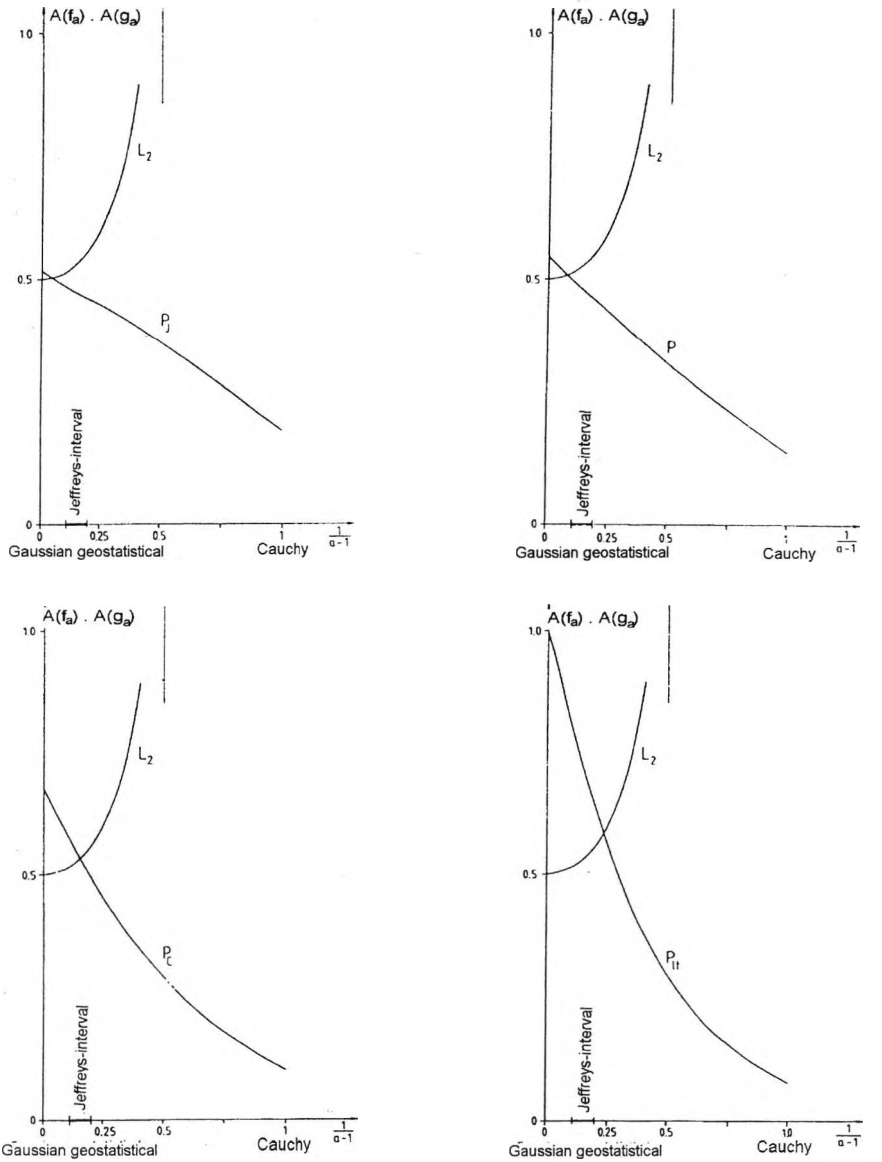

Fig. 3. Descending curves (versus the type parameter $(a\text{-}1)^{-1}$) of the product of asymptotic scatters for 'Heisenberg counterparts' $[A(f_a)\cdot A(g_a)]$ for the statistical norms P_J, P, P_C and P_{II}. In all four cases the corresponding $A(f_a)\cdot A(g_a)$ product-curve for L_2 is also demonstrated, for easier comparison [from STEINER and HAJAGOS 1995]

3. ábra. A $t=1/(a\text{-}1)$ típusparaméter növekedésével a 'Heisenberg-pandantok' aszimptotikus szórásainak $A(f_a).A(g_a)$ szorzatára monoton csökkenő görbék adódnak a P_J, P, P_C és P_{II} normák eseteiben. Mind a négy esetben feltüntettük az L_2 normára vonatkozó, meredeken emelkedő $A(f_a).A(g_a)$ szorzatgörbét is

mentioned, however, that even in this case the product of error-characteristics for $a=5$ is only by 12% greater than 1/2; in cases of P_J, P and P_C is for $t=1/(a-1)=0.25$ i.e., for the so-called geostatistical distribution *the product is significantly smaller than 1/2.*

It is perhaps useful to tabulate this opposite behaviour (see *Table III*).

L_2 -norm:	$A(f_a)\cdot A(g_a)\geq\frac{1}{2}$,	
The *opposite relations* for the *P*-norms at the same limit above are as follows:		
P_J -norm:	$A(f_a)\cdot A(g_a)<\frac{1}{2}$,	if $a<20$ ($f_a(x)$ for $a=20$ is very near the Gaussian type).
P -norm:	$A(f_a)\cdot A(g_a)<\frac{1}{2}$,	if $a<10$ (this means that the opposite relation is valid already for the whole Jeffreys-interval of types).
P_C -norm:	$A(f_a)\cdot A(g_a)<\frac{1}{2}$,	if $a<6$ (i.e., the opposite relation is already valid in the neighbourhood of the so-called geostatistical distribution).
P_{It} -norm:	$A(f_a)\cdot A(g_a)<\frac{1}{2}$,	if $a<4$ (this limit is yet in the domain of distributions of finite variance).

Table III. The product of asymptotic scatters belonging to f_a and to its Heisenberg-counterpart g_a behaves in cases of modern norms inversely to the classical case of the L_2-norm

III. táblázat. Az f_a-hoz és a g_a-val jelölt Heisenberg-megfelelőjéhez tartozó aszimptótikus szórások szorzata a modern normák esetében az L_2 klasszikus esetéhez viszonyítva ellentetten viselkedik

This advantageous behaviour is partly due to the fact that in the new norms the parameter of scale is a constant times the dihesion ε: P_J works with $S=3\varepsilon$, P with $S=2\varepsilon$, P_C with the dihesion itself, and P_{It} with half of it. Let us recall that ε is defined by Eq. (5), i.e., due to Eq. (3) which is based on a train of thought concerning the *I*-divergence.

3. Significance of the right choice of *S* (parameter of scale) in respect of the behaviour of *T*-determinations (the location parameter is denoted by *T*)

Well, we have returned to the significance of the right choice of the parameter of scale S in respect of the behaviour of the determination of T. In *Fig. 4* two curves of statistical efficiencies are presented for the distribution type-interval $0 \le t \le 2$. For $t = 1/(a-1) = 1$ i.e., for the Cauchy type itself, it is evidently indifferent whether Eq. (5) or Eq. (6) is used for the S-determination: in both cases maximum efficiency is achieved. With regard to other types, however, significant differences occur between the efficiencies depending upon whether Eq. (5) ('MFV'-curve, from most frequent value), or Eq. (6) (CML-curve, Cauchy maximum likelihood) is used to calculate the parameter of scale.

Figure 4 is ideal for showing what *robustness* really means. This notion does *not* mean outlier-insensitivity: this latter — also very important — behaviour is called *resistance*. The very meaning of robustness is the

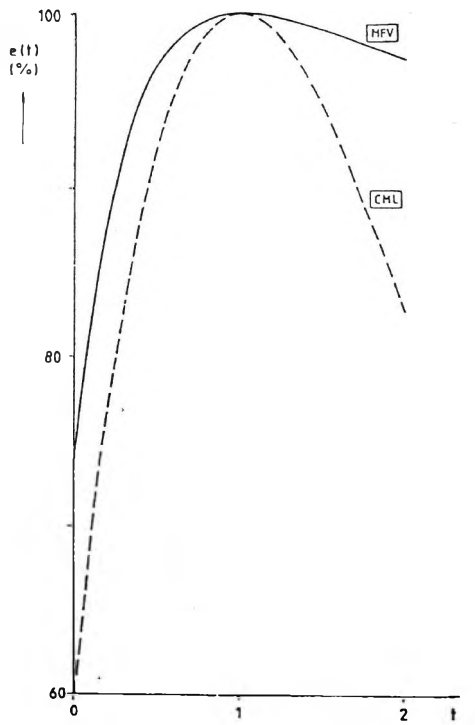

Fig. 4. Significantly different efficiency curves for determining the location parameter [from HAJAGOS and STEINER 1993b], although 'only' the determination method of the parameter of scale is different for the 'MFV' and 'CML' methods

4. ábra. A helyparaméter meghatározására vonatkozó hatásfokgörbék [átvéve HAJAGOS et al. 1993b-ből]; a görbék szignifikáns mértékben különböznek egymástól, noha a helyparamétermeghatározások 'MFV'- és 'CML'-módszerei 'csak' a skálaparaméter számítási módszerében különböznek

following: starting from the maximum efficiency place, with increasing type-distance the efficiency slowly decreases. (The correct definition of the type-distance will be given later in Eq. (11); by good fortune it is approximately constant times of the correctly calculated distances in the Gaussian-Cauchy type-interval, — see also Fig. 5 in this article: the proportionality is almost perfect in the broad neighbourhood of the geostatistical type.) It can be easily concluded on the basis of Fig. 4 that the MFV method is much more robust than the CML method though the ψ-function (see HUBER 1981; nowadays also known as 'influence function') is *just the same* in both methods. Consequently, it is far from satisfactory to give the ψ-function only: we have also to decide which formula must be used to determine S on the basis of the data. Surely, it is possible to give an S-value at random — and not on the basis of data — calling this parameter of scale, for example, an 'empirically proven' value or any arbitrary designation; practices of such kind, however, are out of our present scope of interest. (The ψ-function has a well known fundamental role in the theory of Huber as the function for estimating T on the basis of the measured x_i data. The ψ-functions can be constructed from straight lines, too, if no deeper theoretical background is given; a classical example of this is the ψ-function of the Huber-estimate, see HUBER [1964].)

4. Quantitative characterization of the robustnesses of different norms

The two efficiency-curves in Fig. 4 [cited from HAJAGOS and STEINER 1993b] are excellent for the comparison of robustnesses and the conclusion in that special case obviously is that the MFV method is more robust than the CML estimation. This conclusion is, however, only of qualitative nature. We therefore found it necessary to characterize this property by a numerical value. The formula for this value (as a rate of the robustivity denoted by r) is as follows:

$$r = \int_0^\infty e(t) \cdot q(t) \mathrm{d}t \tag{8}$$

where $e(t)$ is the statistical efficiency of the statistical method in question for the probability distribution type characterized by the type parameter t, and $q(t)$

means the probability density of occurrence of type t in the discipline studied [see STEINER and HAJAGOS1993].

But which $q(t)$ density function can be regarded as adequate for the geosciences? The old statistical literature (not only in the geosciences) often claims that in the overwhelming majority of cases the error-distributions are Gaussian, then called this type 'normal'. (This would mean that $q(t)$ is a Dirac-δ at the point $t=0$.) This dogma was accepted not only because the use of the simplest statistical methods should be justified but also the statistical tests for 'normality' (applying the proposed significance levels) can be misleading. Details about this fact are given in SZŰCS [1993]. For example, the χ^2-test can 'prove' the normality even for data coming from a random variable of a quite different distribution type, if the sample is not sufficiently large.

Only sporadically can reliable information be found about the real type of data although even at the end of the last century NEWCOMB [1886] did not use the L_2-norm for his astronomical data as it was important to exhaust all information contained in the measured values. Briefly speaking, he did not accept the dogma of 'normality'. On the contrary, he concluded that the Gaussian error distribution occurs very rarely.

NEWCOMB is one of the very few scientists who can be regarded as competent in the problem of the really occurring error-types. But also generally: if experts work *only* in the field of geosciences, or *only* in the discipline of mathematical statistics, their opinion about error-types must not be taken into consideration. In this question only such scientists are competent who work deeply enough in *both* disciplines.

As the best example Sir Harold JEFFREYS, the great geophysicist should be cited, who exhausted the information optimally from the seismological data with adequate iteration algorithms, although it was extremely tedious to do this in the thirties of this century: the execution of a single iteration step needed some hours. The book JEFFREYS [1961] written on the theme of probability proves that he was a deep thinking scientist in both disciplines. As for the error-distributions, he concluded that in practice the flanks are not in such a degree short as by the Gaussian, in the best cases $f_a(x)$-like tails can occur for the type-parameter interval $0.1 \leq t \leq 0.2$, or otherwise written for $6 < a < 10$. This interval is marked in the abscissae of Fig. 3 as 'Jeffreys-interval'.

Rather than listing and discussing all the citations, we opted to accept the following expression as $q(t)$-formula for the geosciences:

$$q(t) = 16t \cdot e^{-4t} \ . \tag{9}$$

The q density has its maximum at $t=1/4$, i.e., at $a=5$; this corresponds exactly to a statement of DUTTER [1986/87] about the most commonly occurring type of error in geostatistics. Therefore the type belonging to $t=0.25$ is called 'geostatistical'. As is well known we sometimes have to work with Cauchy-distributed data, too. According to Eq. (9) the probability density $q(1)$ of the Cauchy occurrence is really by far not vanishing: it amounts to 20% of the maximum density ($q_{max}=q(0.25)=5.q(1)$). It should be mentioned, too, that the probability densities of the Jeffreys-interval range from $0.77 \cdot q_{max}$ to $0.98 \cdot q_{max}$ and in the very neighbourhood of the Gaussian, namely for $f_a(x)$ $a=40$ the probability density amounts $0.25 \cdot q_{max}$ ($q=0$ holds only for just the Gaussian as modern authors state that this type never occurs as a mother-distribution in practice see MOSTELLER and TUKEY [1977]). Note also that the t type-distance from the Gaussian of the distribution for $a=40$ is only 10% compared with the t type-distance between the geostatistical and the Gaussian types.

Accepting the $q(t)$-expression given in Eq. (9) for the geosciences, for the rate of robustness the values given in per cent in *Table IV* can be calculated according to Eq. (8) [see STEINER and HAJAGOS 1993].

norm	rate of robustness for geosciences
L_2	36%
L_1	80%
P_J	90%
P	96%
P_C	94%
P_U	75%

Table IV. Quantitative characterization of the robustnesses of different norms
IV. táblázat. Különböző normák robusztusságának kvantitatív jellemzése

The norms for the MFV-algorithms show the greatest values (except P_U which prefers the very long tailed distributions and not the types characterizing the geosciences). It should be mentioned that r is not zero even for L_2 although the statement of the modern statistical literature formulates categorically as follows: 'L_2 algorithms are *not robust*'. This is not really

astonishing: Table IV (and Eqs. (8) and (9)) gives *new results* that characterize the robustness quantitatively. Consequently, our formulations must be more accurate regarding these new results also in other respects. An example: one decade ago the notations 'robustness' and 'resistance' could be used (with a little opportunism) synonymously, but this is no longer allowed — if confusions are to be excluded. We should avoid (or even forget) the wide-spread practice that *resistance* is proved by one or more example and the consequence is formulated as 'the statistical method is *robust*'. (There are examples showing that decreasing robustness occurs simultaneously with increasing resistance, see HAJAGOS and STEINER [1993b].)

The notion 'type-distance' was mentioned earlier for the quantity $t=1/(a-1)$ as Eq. (9), i.e., the $q(t)$ function was discussed. This intuitively introduced quantity has also been investigated by us recently, giving an exact definition for type-distances based upon the well known Kolmogorov distance (K) defined for two arbitrary distributions:

$$K=\max_x \left|F(T_F,S_F;x)-H(T_H,S_H;x)\right|. \tag{10}$$

F and H mean probability distribution functions, the T and S values are parameters of location and that of scale of the distributions in question. (Writing 'sup' instead of 'max' the definition is more correct from the point of view of mathematics.)

The Kolmogorov-distance (the K-value) is obviously strongly influenced by the actual values of T_F, S_F, T_H and S_H. If we are interested primarily on the part of the distance which is caused by the difference of the types, we have to eliminate the effects of these four parameters. Consequently, type-distance between F and H (denoted by $D(F,H)$) can be defined (and calculated) in the following way [see HAJAGOS and STEINER 1994]

$$D(F,H)=\min_{T_F,S_F,T_H,S_H}\left\{\max_x \left|F(T_F,S_F;x)-H(T_H,S_H;x)\right|\right\} \tag{11}$$

(mathematically it is more correct to write 'inf' instead of 'min').

It is generally proven that such 'min-max'definitions fulfil the requirements given for distances (this means, $D(F,F)=0$, $D(F,H)=D(H,F)$ and the triangle-relation is also fulfilled: $D(H_1,H_2)+D(H_2,H_3)\geq D(H_1,H_3)$, see CSERNYÁK [1995]).

The minimization which is to be done actually in our case, is much simpler as is seen in the generally valid Eq. (11). First of all, we compute here only distances of F_a-distributions from the Gaussian; the distribution

function of the latter should be denoted for $T=0$ and $S=1$ by $G(0,1; x)$ (evidently this is the 'standard version' of the so-called 'normal' distribution tabulated in nearly every book written on the subject of probability and mathematical statistics). If $T=0$ is also substituted in F_a, the minimization according to T is already made (functions F_a and G both being symmetrical to T and unimodal). As for the S-values: they have during the minimization no separate role, only the ratio of both S-values influences the D-value. Consequently, the type-difference of any F_a from the Gaussian can be calculated simply as

$$D(F_a,G)=\min_{S}\left\{\max_{x}\left|F_a(0,S;x)-G(0,1;x)\right|\right\}. \tag{12}$$

This exact type-difference is still about the Cauchy-type (astonishingly enough) approximately proportional to the intuitively introduced $t=1/(a\text{-}1)$, (see *Fig. 5*). It would therefore be superfluous to make 'more correct' the abscissae of all figures in the MFV-literature which are given in the overwhelming majority of cases for the Gaussian-Cauchy interval. Even the modification of the definition of the robustness for the geosciences (r) in

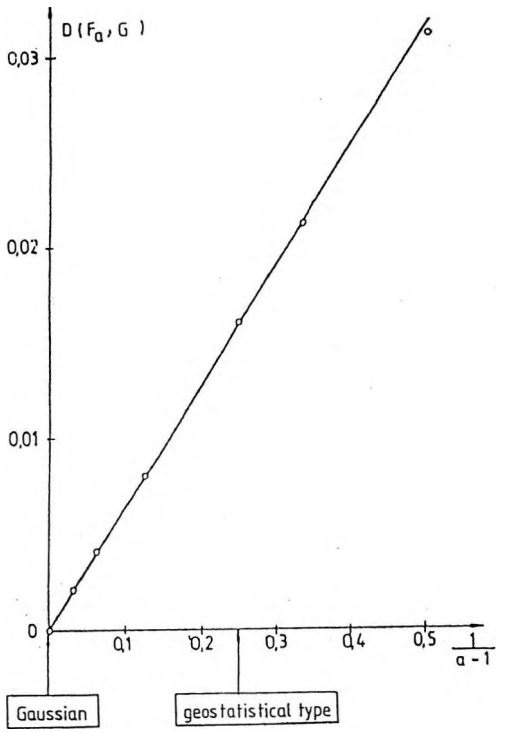

Fig. 5. Type-distance $D(F_a,G)$ (i.e., the distance of type F_a from the Gaussian) versus $t=1/(a\text{-}1)$, showing approximate proportionality between the two quantities in the interval demonstrated [from HAJAGOS and STEINER 1994]

5. ábra. Az F_a típusnak a Gauss-félétől mért $D(F_a,G)$ távolsága az ábrázolt intervallumban közelítő arányosságot mutat a $t=1/(a\text{-}1)$ típusparaméterrel [HAJAGOS et al. 1994 nyomán]

Eq. (8) is not necessary; no significant diminishing is expected if D were to figure in Eq. (8) instead of t.

But what about the much greater D-values, i.e., greater than 0.058? Which value is the Cauchy-Gaussian distance? According to Eq. (8) such types occur very rarely in geophysics and geology practice. We can, however (and, perhaps, we are even obliged) to deal with such questions in a much more general sense, including other geosciences, too, e.g. meteorology, perhaps also astronomy, etc. And finally: exclusion of other disciplines would be unjustifiable if the behaviour of statistical methods in general is to be investigated.

It can be proven [see CSERNYÁK 1995] that $D(F_a, G)$ tends to 0.25 if $a \to 1$ and this value is the maximum possible type-distance among symmetric distributions. This means that the overall behaviour of the statistical methods based on different norms can be easily visualized for the whole supermodel $f_a(x)$ and for $0 \leq D(F_a, G) \leq 0.25$; this is a complete characterization in the sense that characteristic values are shown for all possible type-distances.

In *Fig. 6* the efficiency-curves are shown for the norms listed in Table II versus the type-distance D from the Gaussian from STEINER et al. [1995]. The curve for L_2 quickly drops from 100% to zero. The efficiency curve for the L_1-norm tends to zero if D tends to 0.25; not one of the efficiency-curves of the P_k-norms has such a behaviour. The L_1-curve starts at the value 63.66% ($e = 200/\pi$% being valid for the Gaussian distribution) and reaches a maximum over 80% near to the Cauchy-type; for the latter $e = 800/\pi^2 = 81$% holds.

For the whole supermodel $f_a(x)$ (except the close neighbourhood of the Gaussian type) the L_1-curve shows very great advantages over the conventional statistics characterized by the L_2-curve. Fig. 6 shows, however, that the norms $P_{\sqrt{\ }}$, P_{-}, P_C and P_{lt} have significant advantages even compared with the efficiency curve of the L_1-method. With a slight overstatement this property of these four P_k-norms can be called 'overall robustness'. Note, for example, that the P_C-curve shows for this *as long as theoretically possible type-interval* an e-value never less than 74%.

The 'overall robustness' (OR) for the $f_a(x)$ supermodel, however, can also be characterized quantitatively supposing that all distances $D(F_a, G)$ occur with the same probability density, i.e., $q \equiv 4$ holds for the complete type domain, neglecting special aspects of various disciplines. In this case the definition of the 'overall robustness' is:

$$OR = 4 \cdot \int_0^{0.25} e(D)\mathrm{d}D \tag{13}$$

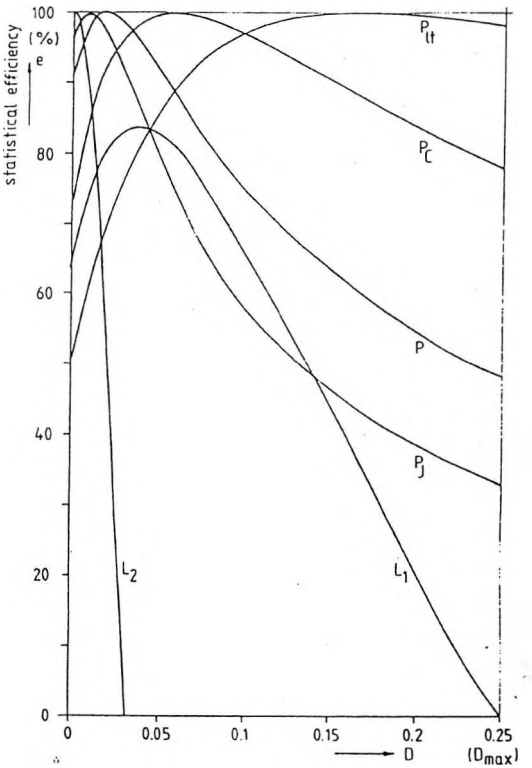

Fig. 6. Efficiency curves for norms listed in Table II versus type-distance $D=D(F_a, G)$ [from STEINER et al. 1995]. The demonstrated D interval is as long as theoretically possible for symmetrical error distribution types

6. ábra. A II. táblázatban felsorolt normák hatásfok-görbéi a Gauss-típustól mért $D=D(F_a, G)$ típustávolság függvényében [STEINER et al. 1995 nyomán]. Az ábrázolt D-intervallum szimmetrikus esetekre vonatkozóan az elmélet szerint a lehető leghosszabb

[see STEINER et al. 1995]; $e \equiv 100\%$ would obviously result in $OR = 100\%$. — For the six norms in Table II, the *OR*-values are given in *Table V.*

L_p	L_2: 7.8% L_1: 50.1%
norms of the MFV-procedures	P_J: 59.3% P : 71.5% P_C: 90.7% P_{tt}: 92.6%

Table. V. 'Overall robustnesses' for different norms

V. táblázat. Különböző normák általános robusztussága

The conclusions can be formulated as follows:

1. The overall robustness of L_2 can really be regarded as nearly vanishing;
2. The overall robustnesses of the norms resulting in MFV procedures are greater (or even significantly greater) than the overall robustness of the L_1-norm.

Also in respect of the overall robustness of the standard version P has a significantly greater OR-value compared with that of L_1:

$$OR(P)\text{-}OR(L_1) = 21.4\ \%.$$

It is perhaps more interesting that

$$OR(L_1)\text{-}OR(L_2) = 42.3\ \%$$

and

$$OR(P_{lt})\text{-}OR(L_1) = 42.5\ \% \qquad (14)$$

hold and this nearly full coincidence of the differences means not less than (concerning overall robustness) the choice of P_{lt} instead of L_1 has the same advantage that we could have reached using L_1 instead of the conventional L_2-norm.

5. 'Philosophies' in statistics

The rates of robustness (the values of r and OR) are very helpful in choosing the appropriate statistical norm for a given task, but this is far from being satisfactory. It must also be taken into consideration which 'philosophies' are behind the formulae. Finally, let me show a table (*Table VI*) for orientation (from CSERNYÁK et al. [1995]).

All three philosophies can be applied appropriately in different disciplines. For example, in the case of the geosciences (where outliers often occur and modelling can rarely be exact), the statistical method must be sufficiently resistant — and this is warranted in the philosophy of the MFV-procedures. Accepting e.g. the P-norm and its philosophy we have to decide additionally whether or not neglecting more than 50% of the data is acceptable from the point of view of a well defined task to be solved in a framework of a given discipline.

MULTIPARAMETER REGRESSION, GEOPHYSICAL INVERSION	
Philosophy	Theoretically best elaborated and experimentally proved alternative is the minimization of the given norm of the residuals
Classical philosophy: The greatest values of the squared residuals should not be too large, **even if the values characterizing the concentration of the residuals differ significantly from zero.**	L_2-norm
Median-type philosophy: Positive and negative residuals must be in equilibrium with regard to their absolute values, **no group of the data should be neglected.**	L_1-norm
MFV-philosophy: Residuals must concentrate possibly close around zero, even if some data (or occasionally even a significant part of the data) are practically neglected.	P_J-norm, P-norm, P_C-norm, P_{lr}-norm

Table VI. Different philosophies in statistics and the corresponding norms [CSERNYÁK et al. 1995]

VI. táblázat. Különböző statisztikai filozófiák és az azoknak megfelelő normák [CSERNYÁK et al. 1995]

Acknowledgements

Some of the new results presented were obtained by research work supported by the Hungarian Science Foundation. This whole project was realized in cooperation with researchers of the Institute of Geodesy and Geophysics in Sopron. On behalf of the whole team working in Miskolc on this topic, I should like to express our thanks not only for fruitful consultations and discussions with the researchers of this institute (in the first place with the leader of this project J. SOMOGYI and with J. VERŐ), but also for the

computer-technical support: without the latter some of the new results could not have been presented in the present paper.

REFERENCES

ANDREWS D. F., BICKEL P. J., HAMPEL F. R., HUBER P. J., ROGERS W., TUKEY J. W. 1972: Robust Estimation of Location. Princeton University Press, Princeton. 373 p.

BARTA Gy., HAJÓSY A. 1985: New procedure for determination of the gravity constant. Ann. Univ. Sci. Budapestiensis de Rolando Eötvös Nom. Sectio Geoph. et Meteorologica **1–2**, pp. 5–12

CSERNYÁK L. 1994: A thesis on the difference of the determination methods of the scale parameter (CML≠MFV). Acta Geod. Geoph. Hung. **29,** (1–2), pp. 255–257

CSERNYÁK L. 1995: Distance of probability distribution types. (Study of the distance of the normal and the generalized Student-distributions.) Acta Geod., Geoph. Hung. **30**, pp. 281–284

CSERNYÁK L., HAJAGOS B., STEINER F. 1995: The philosophy of the most frequent value procedures. Acta Geod., Geoph. Hung. **30**, pp. 265–280

DUTTER R. 1986/1987: Mathematische Methoden in der Montangeologie. Vorlesungsnotizen. Leoben 22 p.

HAJAGOS B. 1991: The most frequent value as estimation with minimum information loss. *In* STEINER (ed.) 1991: as Chapter X Eq.(10-11).

HAJAGOS B., STEINER F. 1993a: Determination of fault's position in mines using different norms in inversion. Annales Univ. Sci. Budapestiensis de Rolando Eötvös Nom. Sectio Geophysica et Meteorologica **9,** pp. 101–146

HAJAGOS B., STEINER F. 1993b: Investigations concerning resistance — importance of the choice of the formula determining the scale parameter. Geophysical Transactions **38,** (4), pp. 211–230

HAJAGOS B., STEINER F. 1994: Definition der Entfernung von Wahrscheinlichkeitsverteilungstypen u.s.w. Publ. Univ. of Miskolc, Series D, Natural Sciences **35,** 4, pp. 97–108

HUBER P. J. 1981: Robust Statistics. Wiley, New York, 308 p.

HUBER P. J. 1964: Robust estimation of a location parameter. Ann. Math. Statist. **35,** pp. 73–101

JEFFREYS H. 1961: Theory of Probability. Clarendon Press, Oxford

MOSTELLER F., TUKEY J.W. 1977: Data Analysis and Regression. Addison-Verlag, Reading, Mass

NEWCOMB S. 1886: A generalized theory of the combination of observations so as to obtain the best result. American Journal of Mathematics **8,** pp. 343–366

PAPOULIS A. 1962: The Fourier Integral and its Applications. McGraw-Hill, New York

STEINER F. (ed.) 1991: The Most Frequent Value. Akadémiai Kiadó, Budapest, 315 p.

STEINER F., HAJAGOS B. 1993: Practical definition of robustness. Geophysical Transactions **38,** 4, pp. 193–210

STEINER F., HAJAGOS B. 1995: Opposite behaviour of the P-norms compared to that of the L_2-norm with respect to the simultaneously achieved accuracy in the space- and frequency-domain. Acta Geod. Geoph. Hung. **30**, pp. 293–299

STEINER F., HAJAGOS B., PÁSZTOR P. 1995: Curves of statistical efficiency versus type distance of generalized Student-types from the Gaussian. 'Overall robustness' of the P-norms. Acta Geod., Geoph. Hung. **30,** pp. 285–291

SZŰCS P. 1993: Comment to an old dogma: 'The data are normally distributed.' Geophysical Transactions **38,** 4, pp. 231–238

A leggyakoribb érték (MFV) eljárások elméletének új eredményei

Ferenc STEINER

Az MFV-filozófia szerinti elmélet, azaz a leggyakoribb érték-eljárások elvi problémaköre több új eredménnyel gyarapodott az elmúlt néhány évben. A publikációk különböző szakfolyóiratokban jelentek meg, így indokolt, hogy ebben a dolgozatban az eredmények egy részének tömör összefoglalása történjék meg abból a célból, hogy a maximum likelihood-elven, valamint az L_2-, L_1- és P-normákon alapuló statisztikai eljárások lényegi különbségei minél tisztábban álljanak előttünk.

GEOPHYSICAL TRANSACTIONS 1997
Vol. 41. No. 1-2. pp. 23-35

Mutual effects of porosity–permeability and both irreducible water saturation and displacement pressure: the Törtel Formation, Hungary

Abdel Moktader A. EL SAYED*

On the basis of reservoir heterogeneity in both clastic and carbonate rocks, the porosity–permeability relation of a certain reservoir zone sometimes elucidates more than one trend because of the many petrophysical factors directly or indirectly affecting such a relation. These factors tend to be interrelated to different extents.

The well known Kozeny–Carman equation and its modified version indicate that the porosity–permeability relation is mainly affected by the irreducible water saturation which is, in turn, directly related to the clay content and rock texture including grain size and clay distribution. An attempt was made to investigate the mutual effects of both irreducible water saturation and displacement pressure and total porosity, effective porosity, and laboratory measured permeability data of the clastic interval belonging to the Törtel Formation encountered in the Algyő oil and gas field.

Some significant linear relations have been obtained indicating that the mutual effect between the irreducible water saturation, porosity and permeability is more efficient than that of the same combination with the estimated displacement pressure. The calculated permeability based on the modified Kozeny–Carman equation reveals reliable relationships with strong correlations with the effective and total porosity data and even laboratory measured permeability. The calculated regression line equations, characterized by high correlation coefficients, give an order of magnitude greater accuracy in permeability assessment based on effective porosity and/or total porosity measured data of the sandstone of the Törtel Formation.

Keywords: porosity, permeability, saturation, Törtel Formation

* Dept. of Geophysics, Faculty of Science, Ain Shams University, Cairo, Egypt

Manuscript recevied (revised version): 29 January, 1996

1. Introduction

Numerous experimental data obtained in major rock physics laboratories suggest that there exists a relatively simple relation between porosity and permeability and such important other parameters as irreducible water saturation, specific surface area, pore space framework, and clay content [EL SAYED 1981, VERNIK 1994].

The relationship between the absolute permeability and porosity has been extensively addressed from both theoretical [CARMAN 1937, SCHEIDEGGER 1974] and experimental [e.g. TIMUR 1968, EL SAYED 1981, HERRON 1987, ADLER et al. 1990, CHILINGRIAN et al. 1990, EHRENBERG 1990] perspectives. The well known Kozeny–Carman equation [SCHEIDEGGER 1974] has been expressed as

$$k = \left(A\phi^3\right) \Big/ \left\{s^2(1-\phi)^2\right\} \tag{1}$$

where s is the specific surface area, A is an empirical constant, and k is the absolute permeability in millidarcies. This equation is limited in application because (1) it strictly applies only on loose sand, and (2) the surface area is difficult to estimate in consolidated rock formations and is not directly measurable by logging. TIMUR [1968] developed a modified version of the original Kozeny equation as follows,

$$k = \left\{0.136\left(\phi^{4.4}/S_{wi}^2\right)\right\} \cdot 10^5 \tag{2}$$

where k is the absolute permeability in millidarcies, and S_{wi} is the irreducible water saturation. This equation was successfully tested on 155 sandstone samples related to three different sedimentary basins [VERNIK 1994]. The porosity exponent (n) in the above equation ranges from 4 to 5 [ADLER et al. 1990].

It is mentioned that in some sedimentary facies (especially clean arenite sandstone defined by VERNIK and NUR 1992), the irreducible water saturation is almost independent of porosity in a wide range from $\phi = 6$ up to 36 % and average $S_{wi} = 10$ to 5 % [VERNIK 1994]. Therefore the irreducible water saturation–porosity relation ($S_{wi} = f\phi$) should be developed for each sedimentary facies or even reservoir zone instead of the generalized expressions theoretically assumed in order to predict absolute permeability based on porosity measured data using the Kozeny modified version.

In the present work, using experimental measurements of 52 core samples from the Törtel Formation encountered in the Algyő oil and gas field

(Hungary), the relationship between both porosity and permeability and irreducible water saturation and displacement pressure have been studied. The Törtel Formation (comprising number of sandstone reservoirs) of the Great Hungarian Plain is penetrated by more than 900 holes drilled in the Algyő field. The aims of the present study are: (1) to investigate the mutual relations between porosity, permeability, irreducible water saturation, and displacement pressure; (2) to develop some specific relations to allow permeability prediction based on porosity measurements; and (3) to test the relationship between calculated permeability [TIMUR 1968] and the laboratory measured permeability.

The Törtel Formation (Pannonian s.l.) conformably overlies the Algyő Formation and underlies the Zagyva Formation. It is interpreted as deltaic sandstone of three major deltaic rock genetic types: (1) distributary channel, (2) barrier bar, and (3) deltaic fringes [EL SAYED 1981, BÁN, EL SAYED 1986, JUHÁSZ 1991]. On the other hand, the intercorrelation of capillary pressure derived parameters of this formation has been studied by EL SAYED [1993 and 1994] to enhance methods for reservoir development.

2. Methodology

The gas permeability of the samples that were studied was measured using the Ruska gas permeameter. The measuring technique is outlined by EL SAYED [1981]. Mercury porosimetery is used to approximate reservoir conditions and to allow accurate determination of both effective and total porosity of the sandstone of the Törtel Formation. Capillary pressure measurements using a Carlo Erba porometer were performed to calculate the irreducible water saturation and displacement pressure. Capillary pressure is defined as the pressure difference across the curved interface between two immissible fluid phases jointly occupying the interstices of a rock, while it is due to the tension of the interfacial surface. The capillary pressure formula modified by WARDLAW [1976] from WASHBURN [1921] and BERG [1975] is:

$$P_c = 2\gamma \cos\theta / r \tag{3}$$

where P_c is the capillary pressure (kPa), γ is the surface tension of Hg (485 mN/m), θ is the contact angle (140°) and r is the radius of pore aperture for a cylindrical pore; thus, r (μm) = $741.9/P_c$ (kPa).

The 52 samples taken from the Törtel Formation were mainly of calcareous and argillaceous sandstones and siltstones. The displacement pressure was determined graphically from the mercury pressure injection curves as the pressure at 10% mercury saturation [SCHOWALTER 1979]. The irreducible water saturation was calculated graphically on the mercury capillary injection curves as the corresponding water saturation while the curve is almost parallel to the pressure axis.

3. Results and discussions

From the standpoint of reservoir rock physics, the obtained relationships for the sandstone of the Törtel Formation (Algyő field) gave considerable information about the mutual effects between either irreducible water or displacement pressure and both porosity and permeability, which are the most important reservoir parameters. The significance of the permeability prediction from either total and/or effective porosity is also investigated as discussed below.

Irreducible water saturation versus porosity

The total porosity versus irreducible water saturation relation (*Fig. 1A*) elucidates the intermediate correlation coefficient ($r=-0.69$), the calculated linear regression equation is represented as

$$S_{wi} = 64.05 - 2.12\phi_t \tag{4}$$

where S_{wi} is the irreducible water saturation (%), and ϕ_t is the total porosity (%). On the other hand, the relationship between effective porosity and the irreducible water saturation exhibits (*Fig. 1B*) a relatively high correlation coefficient ($r=-0.80$) and is represented by a linear equation:

$$S_{wi} = 53.5 - 1.937\phi_e \tag{5}$$

where ϕ_e is the effective porosity (%) and S_{wi} is the irreducible water saturation (%).

The irreducible water saturation (Fig.1B) shows a stronger dependence on the effective porosity than the total porosity. This may be due to the existence of stagnant pore spaces (precluding saturation) which are mainly filled earlier by gases and therefore do not share in reservoir capacity.

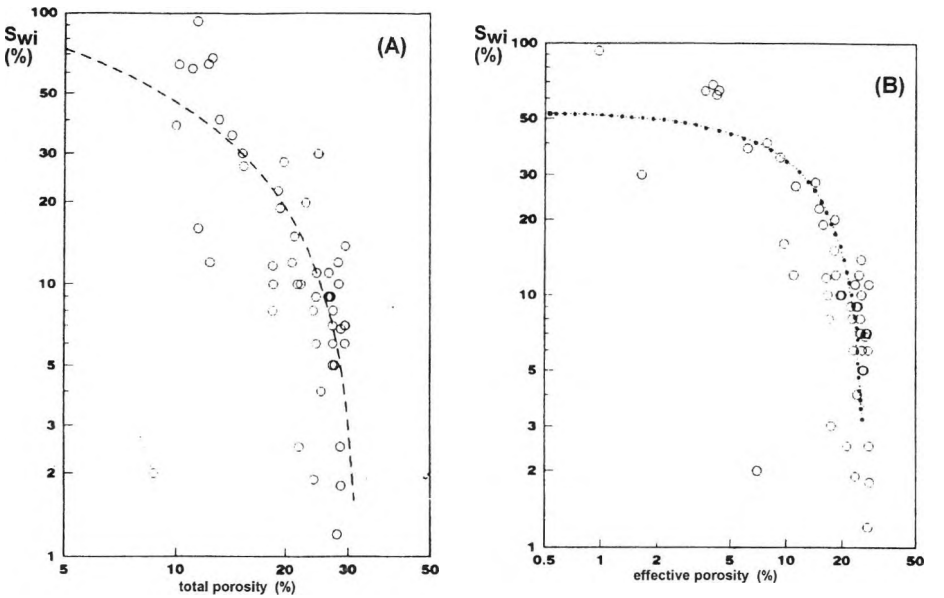

Fig. 1. Irreducible water saturation versus total (A) and effective porosity (B)
1. ábra. A vissza nem állítható viztelítettség a teljes (A) és az effektív (B) porozitás függvényében

Displacement pressure versus porosity

Displacement pressure data were plotted against total and effective porosity (*Figs. 2A, 2B*) . These plots show weak correlation while the majority of samples were characterized by displacement pressure values range from 5 kPa up to 400 kPa. The scattering of the data points may indicate weak dependence of displacement pressure on either total or effective porosity. However, at least two sample groups (A&B) could be determined while each of them has a certain characteristic pore space history. They suffered from post depositional cycles of different nature of diagenesis by which different pore geometries were created. Therefore, we can conclude in general, that the effect of porosity on the displacement pressure is sometimes unequal and can give misleading relations.

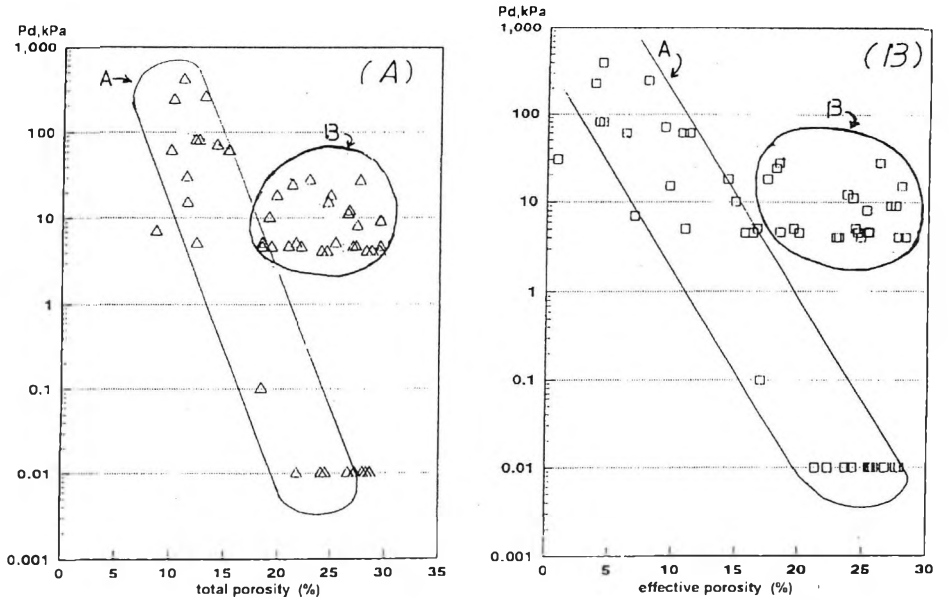

Fig. 2. Displacement pressure versus total (A) and effective porosity (B)

2. ábra. Az elmozdulási nyomás a totális (A) és az effektív (B) porozitás függvényében

Irreducible water saturation versus permeability

The measured gas permeability versus irreducible water saturation has been constructed (*Fig. 3A*). This figure reveals an intermediate correlation between the two investigated parameters while the exponential equation representing this relation is

$$k_m = 192.65e^{-0.092} S_{wi} \tag{6}$$

where k_m is the measured permeability (μm^2), and S_{wi} is the irreducible water saturation (%). The calculated correlation coefficient for the relationships between the irreducible water saturation and both porosity and permeability shows that it is strongly dependent on porosity rather than the reservoir permeability.

Displacement pressure versus permeability

The gas permeability versus displacement pressure relation (Fig. 3B) reveals two groups of data points confirming the same groups obtained with

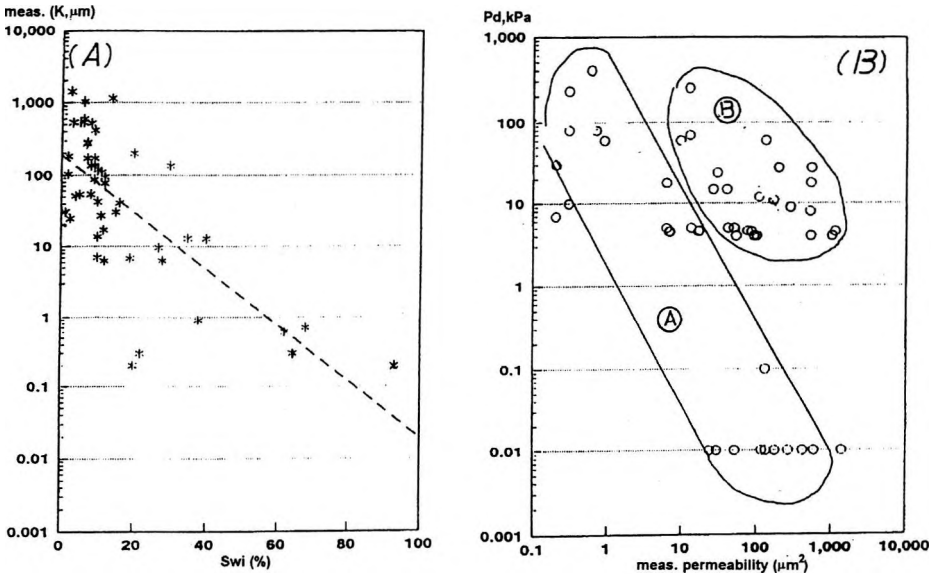

Fig. 3. Measured permeability versus irreducible water saturation (A) and displacement pressure (B)

3. ábra. A mért permeabilitás a vissza nem állítható víztelítettség(A) és az elmozdulási nyomás (B) függvényében

porosity data, while the same interpretation previously mentioned for porosity should be adequate. It is clear that the displacement pressure could be dependent on more than one formation parameter; it does not directly depend on either porosity or permeability.

Porosity versus measured permeability

The relationship between porosity and permeability is unequal for different reservoir rocks depending on other petrophysical factors such as clay content, rock texture and pore space framework. The prediction of permeability based on porosity data is commonly done in practice using least squares regression analysis. It is appreciated that the relationship between the dependent and independent variables may be expressed in other forms using other means [CHAPMAN 1983, CHORK et al. 1994]. The statistical approach performs well if the two variables concerned are strongly corre-

lated. In the event that they are poorly correlated, other forms of equations involving additional independent variables such as pore size, specific surface area, displacement pressure, and residual water saturation may have to be used to give reliable results.

Figure 4A &B, show the porosity-measured permeability relations for the sandstones of the Törtel Formation. On the basis of our knowledge, the correlation coefficient controlling the relation (Fig. 4A) between the measured permeability and total porosity (r=0.82) is slightly higher than that obtained for the same relation with the effective porosity (r=0.8). The linear regression equations representing these relations (Figs. 4A&B) are,

$$k_m = 0.12 \times 10^{-5}(\phi_t)^{5.69} \qquad r = 0.82, \tag{7}$$

and

$$k_m = 0.019(\phi_e)^{2.73} \qquad r = 0.8 \tag{8}$$

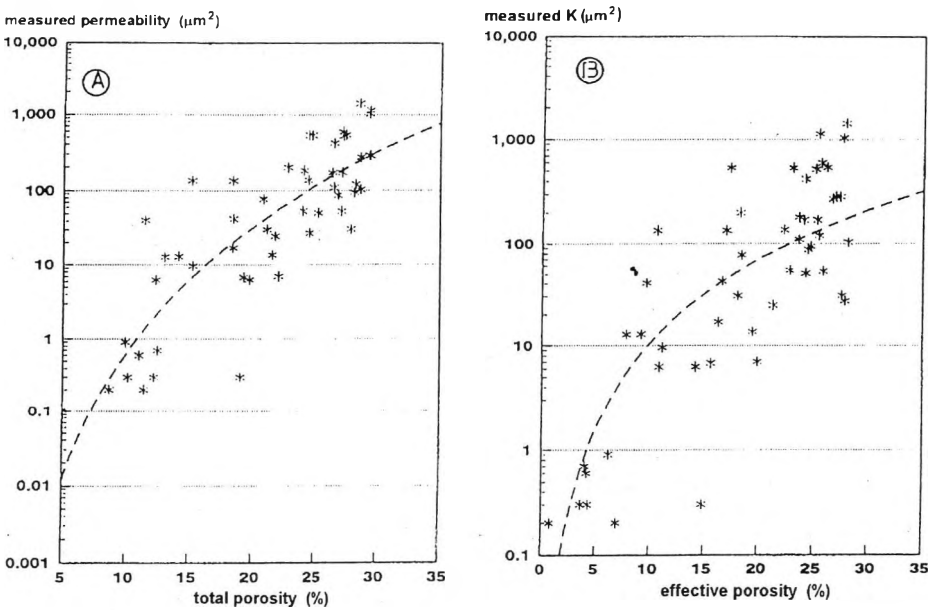

Fig. 4. Measured permeability versus total (A) and effective porosity (B)

4. ábra. A mért permeabilitás a totális (A) és az effektív (B) porozitás függvényében

where k_m is the laboratory measured permeability (μm^2), ϕ_t is the total porosity (%), and ϕ_e is the effective porosity (%).

Measured permeability vs. calculated permeability

The permeability of the samples was calculated using the modified Kozeny equation [TIMUR 1968] while the porosity exponent was equal to 4.5 [ADLER et al. 1990]. *Figure 5A* shows a relatively strong correlation between the measured and calculated permeability. The correlation coefficient characterizing this relation ($r=0.81$) is sufficiently reliable, while the relation is represented by

$$k_{cal} = 5.33(k_m)^{0.647} \tag{9}$$

where k_{cal} is the calculated permeability in μm^2. Therefore, the above equation is successfully applicable to the sandstone of the Törtel Formation thereby enabling one to predict either permeability or irreducible water saturation using the effective porosity.

Permeability prediction

An attempt was made to relate the calculated permeability to both total and effective porosity (*Figs. 5B&C*). Figure 5B reveals the calculated permeability–total porosity relationship, showing a strong correlation. A few data points are scattered above and below the best fit line especially at high sample porosity. This may be due to the effect of the irreducible water saturation. The values of the irreducible water saturation have been plotted and contoured, while their trends seem to be parallel to the fitting line (general curve trend). The values of the irreducible water saturation decrease while the permeability increases.

The relationship (Fig. 5B) is characterized by a high correlation coefficient ($r=0.9$) allowing one to estimate reliable values of calculated permeability using the total porosity data. The relationship is represented by a regression line equation as

$$k_{cal} = 0.01e^{0.48\phi_t} \tag{10}$$

On the other hand, Figure 5C, exhibits a reliable and applicable relationship between calculated permeability and effective porosity. This relation is characterized by a strong correlation coefficient ($r=0.94$) thereby

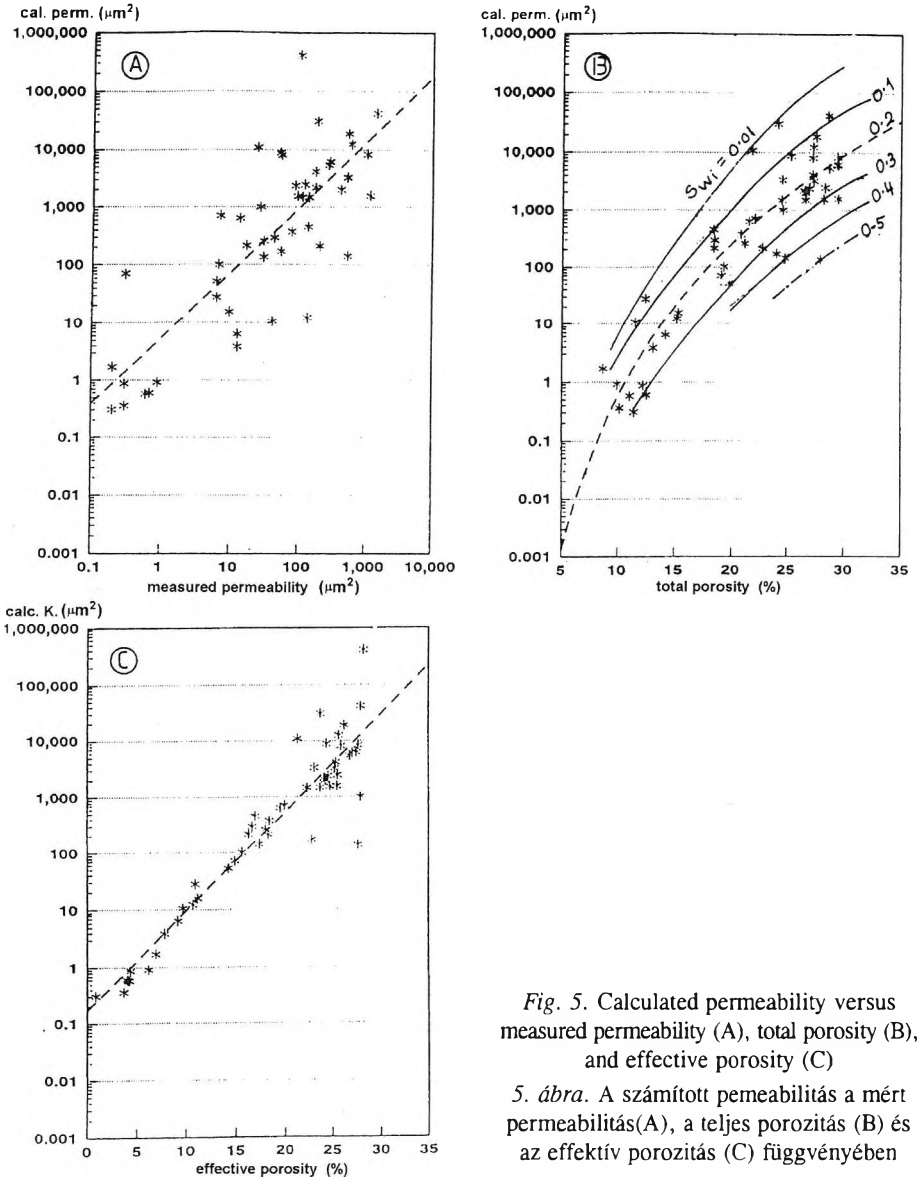

Fig. 5. Calculated permeability versus measured permeability (A), total porosity (B), and effective porosity (C)

5. ábra. A számított pemeabilitás a mért permeabilitás(A), a teljes porozitás (B) és az effektív porozitás (C) függvényében

allowing one to predict a calculated permeability value from the effective porosity data. The relationship is represented by a regression line equation as

$$k_{cal} = 0.169e^{0.403\phi_e} \tag{11}$$

where ϕ_e is the effective porosity (%), and k_{cal} is the calculated permeability (μm^2).

4. Conclusions

— The irreducible water saturation significantly affects porosity; however, the effective porosity seems to be more sensitively affected than the total porosity.

— The effect of both porosity and permeability on the displacement pressure could not be cancelled while the constructed relations indicate weak correlation between displacement pressure and effective porosity.

— The laboratory measured permeability seems to be greatly affected by the irreducible water saturation.

— The estimated permeability using Timur's equation gives reliable relationships using the laboratory measured permeability, total porosity, and effective porosity. The effective porosity could be considered as the most important parameter for permeability prediction for the studied sandstone samples of the Törtel Formation.

Acknowledgments

This work was supported by the Hungarian Petroleum Corporation (MOL Rt) during 1994 on the basis of a consultation contract. I wish to thank this organization for its financial support. Special thanks are due to dr. J. PÁPAY, dr. E. BALÁZS and J. MORGENSTERN of the Hungarian Oil & Gas Laboratory for their continuous help and fruitful discussions.

REFERENCES

ADLER P. M., JACQUIN C. G., QUIBLIER J. A. 1990: Flow in simulated porous media. Inter. J. Multiphase Flow **16**, pp. 691–712

BÁN Á., EL SAYED A. M. A. 1986: Genetic delineation of deltaic rock types in terms of log curve shape in the Algyő-2 hydrocarbon reservoir, Hungary. Acta. Geol. Hung. **30**, 1–2, pp. 231–240

BERG R. 1975: Capillary pressure in stratigraphic traps. AAPG Bull. **59**, pp. 939–956

CARMAN P. C. 1937: Fluid flow through granular beds. Amer. Inst. Chem. Eng. Trans. **15**, pp. 150–166

CHAPMAN R. E. 1983: Petroleum geology. Elsevier, Amsterdam, 415 p.

CHILINGARIAN G. V., CHANG J., BAGRINTSEVA K. I. 1990: Empirical expression of permeability in terms of porosity, specific surface area, and residual water saturation of carbonate rocks. J. Pet. Sci. and Eng. **4**, pp. 317–322

CHORK C. Y., JAIN F. X., TAGGART I. J. 1994: Porosity and permeability estimation based on segmented well log. J. Pet. Sci. and Eng. **1**, pp. 227–239

EHRENBERG S. N. 1990: Relationship between diagenesis and reservoir quality in sandstones of Garn Formation, Haltenbanken, Mid Norwegian Continental shelf. AAPG. Bull., **10**, pp. 1538–1558

EL SAYED A. M. A. 1981: Geological and petrophysical studies for the Algyő-2 reservoir evaluation, Algyő oil and gas field. Ph. D. Thesis, Hungarian Acad.of Sci., Budapest, 166 p.

EL SAYED A. M. A. 1993: Relationship of porosity and permeability to mercury injection derived parameters for sandstones of the Törtel Formation, Hungary. Geophysical Transactions **38**, pp. 35–46

EL SAYED A. M. A. 1994: Intercorrelation of capillary pressure derived parameters for sandstones of the Törtel Formation, Hungary. Geophysical Transactions **39**, 1, pp. 77–87

HERRON M. M. 1987: Estimating of intrinsic permeability of clastic sediments from geochemical data. Trans., SPWLA, p. h-h

JUHÁSZ Gy. 1991: Lithological and sedimentological framework of the Pannonian (s.l.) sedimentary sequence in the Hungarian Plain (Alföld), Eastern Hungary. Acta. Geol. Hung. **34**, 1-2, pp. 53–72

SCHEIDEGGER A. E. 1974: The physics of flow through porous media. Univ. of Toronto press, Toronto (3^{d} ed.), 353 p.

SCHOWALTER T. T. 1979: Mechanics of secondary hydrocarbon migration and entrapment. AAPG. Bull. **63**, pp. 723–760

TIMUR A. 1968: An investigation of permeability, porosity, and residual water saturation relationships. Trans. Soc.Petrol. and Well Log Analysts

VERNIK L. 1994: Predicting lithology and transport properties from acoustic velocities based on petrophysical classification of siliciclastics. Geophysics **59**, 3, pp. 420–427

VERNIK L., NUR A. 1992: Petrophysical classification of siliciclastics for lithology and porosity prediction from seismic velocities. AAPG. Bull. **76**, pp. 1295–1309

WARDLAW N. C. 1976: Pore geometry of carbonate rocks as revealed by pore casts and capillary pressure. AAPG. Bull. **60**, pp. 245–257

WASHBURN E. W. 1921: Note on a method of determining the distribution of pore sizes in porous materials. Proc. National Acad. Sci., USA, **7**, pp. 115–116

A permeabilitás, a porozitás, a vissza nem állítható víztelítettség és elmozdulási nyomás kölcsönatása a Törtel formációban (Magyarország)

Abdel Moktader A. EL SAYED

A törmelékes és karbonátos kőzetekben lévő tározók is heterogének. Egy adott zónában a porozitás és permeabilitás közti összefüggés vizsgálata rávilágít arra, hogy ezt a kapcsolatot sok kőzetfizikai tényező befolyásolhatja, közvetve vagy közvetlenül, és ezek a tényezők egymástól is függenek.

A jól ismert Kozeny–Carman egyenlet és ennek egy módosított változata azt jelzi, hogy a porozitás és permeabilitás közötti kapcsolatot főként a helyre nem állítható víztelítettség befolyásolja. Ez ugyanis közvetlen kapcsolatban van az agyagtartalommal és a kőzet szövetével, amely viszont magában foglalja a szemcseméretet és az agyag eloszlását is. Megkíséreltük meghatározni a vissza nem állítható víztelítettség és az elmozdulási nyomás hatását a porozitásra, az effektív porozitásra és a laboratóriumban mért permeabilitásra a Törtel formáció (algyői olaj- és gázmező) törmelékes kőzeteinek egy adott intervallumában. Néhány olyan lineáris kapcsolatot sikerült feltárni, amelyek azt jelzik, hogy a vissza nem állítható víztelítettség, a porozitás és a permeabilitás között sokkal szorosabb a kapcsolat mint ugyanezen paraméterek és a becsült elmozdulási nyomás között. A módosított Kozeny–Carman egyenlet alapján számított permeabilitás jól korrelál mind az effektív, mind a teljes porozitással és a laboratóriumban mért permeabilitással is. A regresszió korrelációs együtthatója nagy és az effektív és/vagy teljes porozitáson alapuló permeabilitás becslés pontossága jelentősen javul a Törtel formáció homokkövei esetében.

GEOPHYSICAL TRANSACTIONS 1997
Vol. 41. No. 1-2. pp. 37-63

Reservoir diagnosis for the Szolnok Formation in the middle part of the Great Hungarian Plain

A. M. A. EL SAYED* and Balázs KISS**

The Szolnok Formation encountered in all drilled wells in the middle part of the Great Hungarian Plain is composed mainly of turbidite clastic deposits while the siltstones present are intercalated by sandstone beds and streaks of marls. For this study, 494 core samples were collected and subjected to laboratory investigations using various petrophysical techniques. The capillary pressure technique was utilized to outline pore throat size distribution, pore space volume corresponding to pore radius of different dimensions (*pvc*), and effective porosity. On the other hand, both the horizontal and the vertical permeability were measured for reservoir parameter correlation purposes and the helium porosity was also measured.

The petrophysical data obtained were handled as one population for all studied samples regardless of lithology. Moreover, each lithologic facies of the Szolnok Formation was treated separately in order to calculate reliable mathematical relations of high significance for reservoir diagnosis. A new technique was used for pore throat size measurements; this technique allows enhancement and evolution pathways of pore space characterizing the Szolnok deposits to be detected and/or predicted through different stages of reservoir sedimentation and lithification.

In the case of sandstone facies, cross-plots performed for pore throat size measurements indicated that we have two different genetic types whereas this phenomenon does not clearly appear by using either porosity or permeability data. On the other hand, both horizontal and vertical permeability give clear diagnostic features for reservoir heterogeneity in case of marls and siltstones. Both porosity and permeability versus some special sizes of pore spaces usually elucidate reservoir heterogeneity in all types of lithologic facies of the Szolnok Formation. Lithologic facies in the Szolnok Formation were distinguished and a number of reservoir parameter combinations were proved to be effective. In addition, reliable relations were obtained for reservoir effective pore radius, porosity and or permeability prediction.

Keywords: reservoirs, Szolnok Formation, porosity, permeability

* Ain Shams Univ. Fac. of Sciences, Dept. of Geophysics, 11566 Cairo, Egypt
** MOL plc., Hungarian Oil &Gas Lab., H-1311 POB 43, Budapest, Hungary

Manuscript recevied: 15 September, 1995

1. Introduction

The results of pore throat size distribution in combination with porosity and permeability can be used by geologists, petrophysicists, and petroleum engineers to evaluate reservoir genesis, heterogeneity, and pore space history through the time of deposition and lithification. On the other hand, based on the correlation of these data reservoir quality as well as reservoir classification can be determined. Correlation of pore throat size with either reservoir porosity or permeability is important because pore throat distribution governs all reservoir parameters. Investigation of pore space evolution is very difficult task while an understanding of its evolution paths is of great significance for outlining reservoir behaviour. Even a partial understanding of pore throat evolution and their recent distribution helps in reservoir performance and enhancement projects. The Szolnok Formation of the Great Hungarian Plain was the target of the present study; it is penetrated by a great number of drilled wells. The Great Hungarian Plain, attributable to the Late Miocene in age (Pannonian s.l.), lies in eastern part of Hungary (*Fig. 1*). It comprises

Fig. 1. Location map of the study area
1. ábra. A vizsgált terület helyzete

an area of approximately 40,000 sq. km. The term Pannonian is mainly related to sedimentary facies, which range in age from the Miocene to the Pliocene, and are distributed throughout the Pannonian basin. The structural pattern of the basement was most likely formed by the Neo-Alpine orogeny which took place during the Miocene and extended in some parts to Pliocene times.

The Pannonian basin is of large extension especially in the eastern part of Hungary; it is characterized by various sedimentary environments through time and space, while near the edges, fluvial, alluvial and deltaic facies were the most predominant. The Pannonian basin is composed mainly of a series of different sizes sub basins, therefore some formations are not of uniform thickness or may even be discontinuous. These sub basins are more or less connected to each other. The sedimentary sequence of the Pannonian basin in the Great Hungarian Plain has been studied from the geological viewpoint and stratigraphically classified by a number of authors [e.g. SZELES 1962, 1966; KÖRÖSSY 1968, 1971; MUCSI and RÉVÉSZ 1975; MAGYAR and RÉVÉSZ 1976; JÁMBOR 1980 and 1989; EL SAYED 1981; GAJDOS et al. 1983; BÉRCZI and PHILLIPS 1985; BÁN and EL SAYED 1987; RÉVÉSZ et al. 1989; and JUHÁSZ 1991 and 1994]. Periodic rapid sedimentation and huge amount of sediments occurred during Late Miocene times (Pannonian s.l., 2.4–12 Ma).

The sedimentary sequences (*Fig. 2*) developed in the Pannonian basin during late Miocene times, having characteristic depositional environments which seem to be unchanged through that long time. The lithologic associations formed in the Pannonian sub basins are almost similar to each other although they become younger in the south-eastern part of Hungary. The sedimentary sequences attributed to the Late Miocene (Pannonian s.l.) in the Great Hungarian Plain can be summarized from top to bottom as;

Bükkalja Formation: composed of lignite and brown coal beds especially in the northern part of the Great Hungarian Plain.

Zagyva Formation: mainly a thick clastic association of fluvial origin and partly of limited extent in the basin. It contains thin beds of siltstones, marls and sandstone intercalations. Thin lignite beds are frequently present. The uppermost part of the Zagyva Formation contains variegated clays and terrestrial fauna. The most likely depositional environment is alluvial plain sediments.

Törtel Formation: this is mainly composed of embedded sandstones intercalated with siltstones, marls, lignite and carbonized plant fragments. Sandstone bodies were interpreted as distributary channel, barrier and mouth

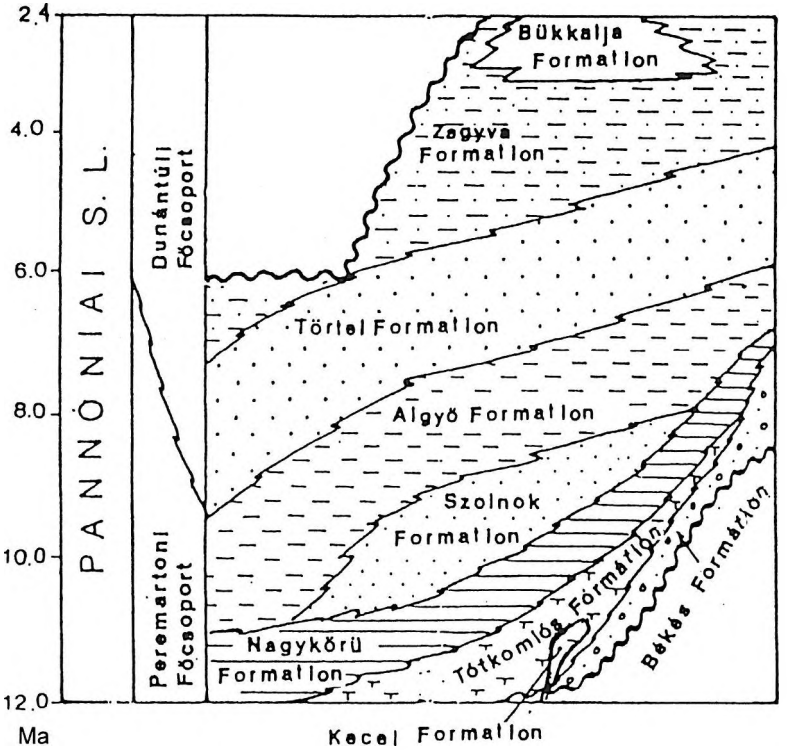

Fig. 2. Stratigraphic classification of the Pannonian s.l. [after GAJDOS et al. 1983]
2. ábra. A pannon s.l. rétegtani felosztása [GAJDOS et al. 1983 nyomán]

bars, and deltaic fringe deposits [EL SAYED 1981]. The environment of deposition of the Törtel Formation varies from shallow lake and fluvial marsh to terrestrial and fluvially dominated delta. The Törtel Formation is conformably underlain by the Algyő Formation. It is classified into five superimposed reservoir bodies, in the Algyő field, from bottom to the top as: Algyő-1, Algyő-2, Szeged-1, Szeged-2, and Szeged-3. Both the Algyő-2 reservoir sequence as well as the Törtel Formation were petrophysically studied by EL SAYED [1981, 1993 and 1994]. The previously mentioned reservoir sequences of the Törtel Formation are considered as the most important oil producing zones in the Algyő field, while their reservoir characteristics have been outlined by a number of authors, e.g. EL SAYED [1991] and EL SAYED and VOLL [1992].

Algyő Formation: mainly of argillaceous marls, siltstones and sandstone of deltaic slope and neritic environments [JUHÁSZ 1994]. It conformably overlies the Szolnok Formation especially in the deep parts of the basin.

Szolnok Formation: composed mainly of sandstone beds intercalated with marls and siltstone laminations while grain size increases downward. Direct contacts between sandstones and siltstone beds are frequently present. Coal seams, plant debris and fragments are recorded. Turbidite deposits characterizing the Szolnok Formation in the Great Hungarian plain were created in a prodelta subenvironment while the north western direction of delta system was prevailing. This formation is conformably underlain by calcareous marls of the Nagykörű Formation [GAJDOS et al. 1983]. The encountered thickness of the Szolnok Formation in the Szarvas area increases with increasing depth; its minimum thickness was about 449 m [JUHÁSZ 1991]. The Szolnok Formation is underlain from place to place by two diachronous marl units (Nagykörű and Tótkomlós formations). These units are underlined by the basement.

Nagykörű Formation: this is composed mainly of argillaceous facies and gradually changes downward to calcareous marls of the Tótkomlós Formation; the coastal conglomerates are of very limited extension around the pre-existing islands and represent what is known as the Békés Formation.

The main aim of the present study is an attempt to introduce a new technique of reservoir data manipulation for diagnosing the Szolnok reservoir on the basis of pore throat, permeability and porosity measurements.

2. Methods and techniques

In natural hydrocarbon reservoirs at least two fluids are present, viz. water and oil and/or gas. If the reservoir rock was wet (with water), most grains will be surrounded by a thin film of water, whereas the oil does not usually come into contact with grains but it will be in contact with the water which surrounds the rock grains. When the rock grains are fine, they are closely packed with very small pore throats. Oil will not move in the pores until it develops a sufficient pressure to overcome capillary forces. The best method to determine effectively the minimum size of rock pore throats is the mercury injection technique [MAPSTONE 1973; EL SAYED 1981 and 1994; KISS 1994].

In the present study, 494 core samples obtained from the Szolnok Formation, which were encountered in some small fields in the middle part of the Great Hungarian Plain (*Fig. 3*) have been prepared (sample size of 1.0 cm diameter and 5.0 cm length). The prepared clean (hydrocarbon free)

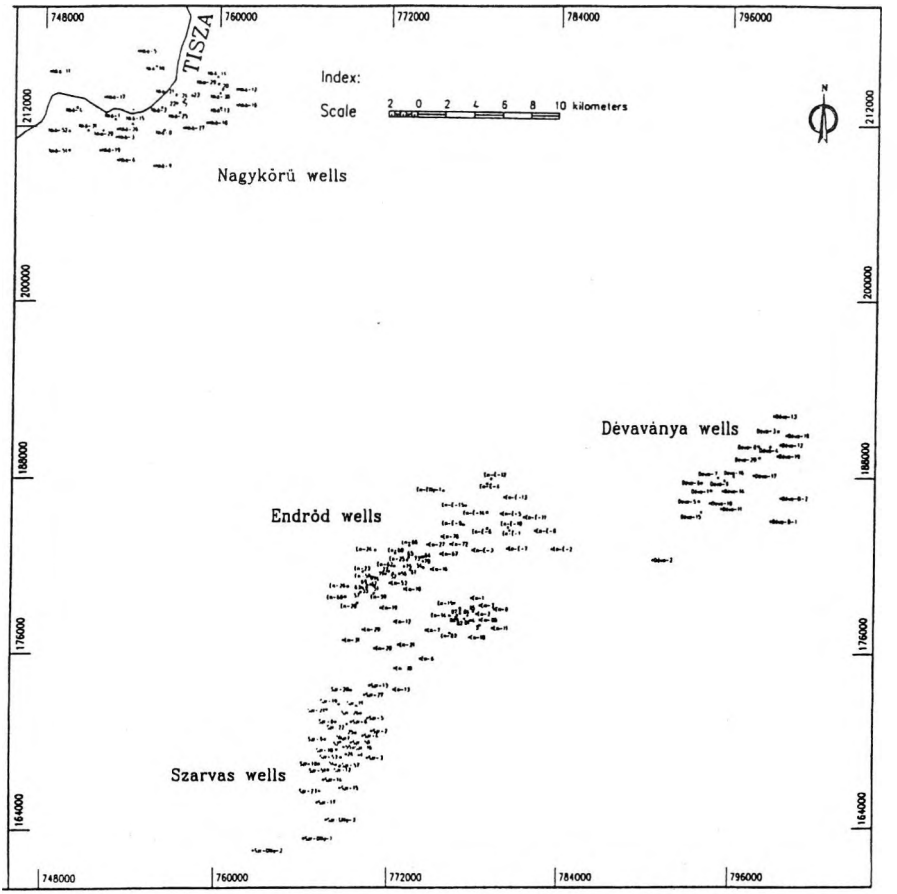

Fig. 3. Location map of the studies wells
3. ábra. A vizsgált kutak elhelyezkedése

sample is placed in a metal chamber of a Carlo Erba porosimeter (model 2000) and then evacuated. Mercury is forced into the evacuated core sample at low pressure starting with 1.0 kg/sq.cm, which is maintained until no more mercury enters the sample. The volume of mercury entering the sample at this pressure level is recorded by the pressure measuring circuit of the

porosimeter. The process is repeated through a range of pressure (1.0–2000.0 kg/sq.cm) while the recorded volume of mercury injected with each pressure increment step is used to calculate directly the percentages of total pore spaces which can be saturated. The fraction of the one volume accounted for by all pore sizes between 75,000 Å and 37 Å is calculated according to the following equation:

$$Vp = (Hp_{max} - Hp_r)/Hp_{max} \tag{1}$$

where Hp_{max} = corrected value of mercury level displacement in mm at maximum pressure, Hp_r = corrected value of mercury level displacement in mm at the pressure step recorded.

The sample mercury porosity, in the present work, is determined according to the equation

$$\Phi = (aHp_{max} \cdot Q)/A.L \tag{2}$$

where Φ = porosity; fraction a = the instrument dilatometer cross-sectional area (sq.mm); Q = sample weight (g), referred to as one gram of sample; A = core sample cross-sectional area, (sq.mm); L = core sample length.

On the other hand, the sample helium porosity is determined by use of both mercury pump porosimeter for bulk volume (Vb) and the helium porosimeter with matrix cup core holder for grain volume (Vg). Hence, porosity is calculated as;

$$\Phi = 1.0 - (Vg/Vb) \tag{3}$$

The sample permeability was measured in the laboratory using a Hassler type core holder in which the sample was subjected to dry nitrogen gas at a pressure of 1378.9 kPa. The gas permeability is calculated as ;

$$K = \{(C.Q.hw.L)/200.Vb\} \tag{4}$$

where: K= permeability (μm^2); C = value of mercury height (mm); Q = orifice value; hw = orifice manometer reading (mm); L = sample length (cm); Vb = sample bulk volume (cubic cm).

2.1. Suggested reservoir model

The suggested new technique for pore throat measurements is based mainly on the reservoir model shown in *Fig. 4*, the total volume of the proposed cube simulating the reservoir rock is 1.0 cubic cm and comprises:

1. grain volume (total volume of solids) = 0.75 cm^3
2. pore volume (total volume of voids) = 0.25 cm^3.

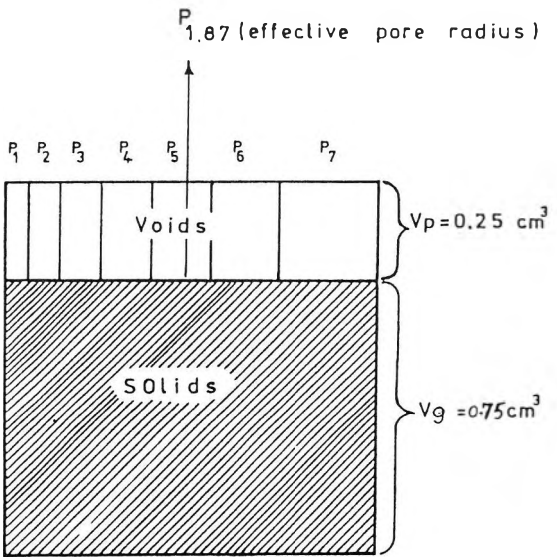

$P_1 = pvc_1$ (0.0075 μm)
$P_2 = pvc_2$ (0.01 μm)
$P_3 = pvc_3$ (0.075 μm)
$P_4 = pvc_4$ (0.25 μm)
$P_5 = pvc_5$ (0.75 μm)
$P_6 = pvc_6$ (2.5 μm)
$P_7 = pvc_7$ (7.5 μm)

$Vg = 0.75\ cm^3$ Grain Volume

$Vb = 1\ cm^3$ Bulk Volume

$Vp = 0.25\ cm^3$ Pore Volume

$$Pv = TTh(np_1r^2p_1 + np_2r^2p_2 + np_3r^2p_3 + np_4r^2p_4 + np_5r^2p_5 + np_6r^2p_6 + np_7r^2p_7)$$

$$\sum P_1 + P_2 = \text{Pore Volume} \quad < \quad pvc_2$$

$$\sum P_1 + P_2 + P_3 + P_4 = \text{Pore Volume} \quad < \quad pvc_4$$

Fig. 4. Suggested reservoir model
4. ábra. A javasolt tároló modell

Therefore, the rock porosity in this case should be equal to 0.25. In fact, this is the summation by product of all sizes of pore spaces present while both the number and radius of these clusters of pores are usually different. The measured pore throat size distribution data of the Szolnok Formation are classified into seven groups (from P_1 to P_7) each of which covers a subgroup of pore clusters having a small range of pore radius. The volume of voids making up a cluster of a certain pore radius can be calculated as

$$P = \prod r^2 \cdot h \tag{5}$$

where r = average pore radius of the cluster of pore cylinders (cm), having height (h).

The volume of a pore space subgroup can be determined as;

$$pvc = \prod r^2 \cdot n \cdot h \tag{6}$$

where pvc = volume of pore radius corresponding to a certain size of pore space subgroup (cubic cm) and n = number of pores of the same radius in the reservoir rock model. The relative pvc (%) = (pvc/Vp) . 100

Thus, the total pore volume is given by

$$Vp = \prod h\left(r_1^2 n_1 + r_2^2 n_2 + r_3^2 n_3 + r_4^2 n_4 + r_5^2 n_5 + r_6^2 n_6 + r_7^2 n_7\right) \tag{7}$$

or

$$Vp = pvc_1 + pvc_2 + pvc_3 + pvc_4 + pvc_5 + pvc_6 + pvc_7 \tag{8}$$

where Vp = sample total pore volume, h = height of pore cylinder, all pores in this model are suggested to be of circular cylindrical shape, and n is the distribution parameter as function of pore number of each subgroup pore type. The pore radius in sandstone reservoirs usually ranges from 0.0075 μm up to at least 4.2 μm or more. The effective pore radius for hydrocarbon production is identified as 0.5 μm [PITTMAN 1992] while the suggested size in the present study is 1.87 μm and is known as $P_{1.87}$ [EL SAYED 1991].

3. Results and discussion

All core samples under investigation were petrographically studied by the staff of MOL plc, OGIL Lab. and classified into two main groups: (a) sandstones (324 samples) and (b) siltstone and marl (170 samples). The petrophysical

data including porosity, permeability, and pore throat size distribution for the above-mentioned two groups are treated as one sample population. On the other hand, each group was treated separately in order to investigate the efficiency of the suggested reservoir model (Fig. 4) to discriminate between sandstone and siltstone–marl lithologic facies. The following part is devoted to discussing the cross plots regarding the reservoir diagnostic features and validity of the suggested model.

3. 1. Helium versus mercury porosity

The cross plots (*Fig. 5a, b,* and *c*) elucidate the relationships between helium porosity and mercury porosity for sandstone (Fig. 5a), siltstone–marl facies (Fig. 5b) and all samples (Fig. 5c). In fact, the sandstone porosity (Fig. 5a) seems to start its lower limit from $\Phi H = 7.0\%$ and $\Phi M = 6.0\%$. The lowest porosity values of the sandstone facies are mainly represented by samples belonging to the Déva and Endrőd wells. The samples of Kisújszállás are characterized by higher porosity values while both porosity types (ΦH and ΦM) are more than 25%. The calculated regression line equation characterizing this relation is;

$$\Phi H = 0.999\,\Phi M + 2.326 \tag{9}$$

where ΦH = helium porosity (%), and ΦM = mercury porosity (%).

This equation is supported by a high correlation coefficient ($r = 0.9$) which enables it to be used to predict one porosity from the other. The maximum recorded porosity of the siltstone–marl facies is generally lower than 8% (Fig. 5b); most of these samples are attributed to the Nagykörű and Endrőd wells. The regression line equation recognizing this relation is

$$\Phi H = 0.74\,\Phi M + 2.26 \tag{10}$$

The relationship governing all the samples (Fig. 5c) is calculated as;

$$\Phi H = 1.054\,\Phi M + 1.54 \tag{11}$$

This equation contains a high correlation coefficient ($r = 0.9$) enabling porosity to be predicted and the costs and time of laboratory measurements to be reduced. It is worthy of mention that both of the defined siltstone and sandstone areas (Fig. 5c) could be beneficial during lithofacies studies of the Szolnok Formation.

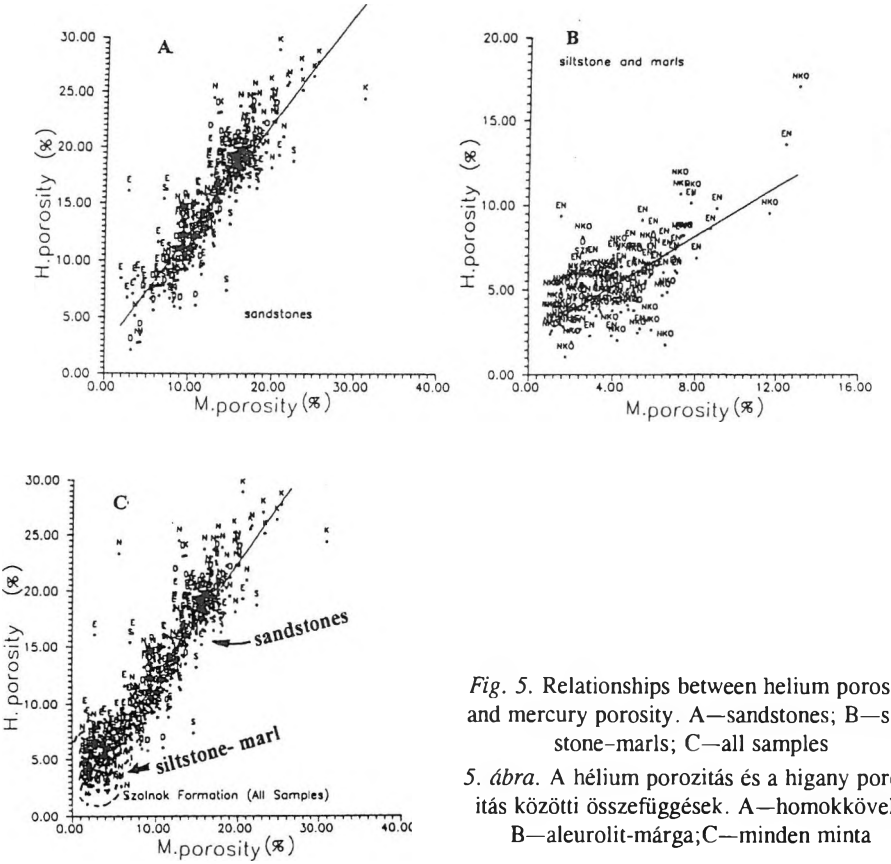

Fig. 5. Relationships between helium porosity and mercury porosity. A—sandstones; B—siltstone–marls; C—all samples

5. ábra. A hélium porozitás és a higany porozitás közötti összefüggések. A—homokkövek; B—aleurolit-márga;C—minden minta

3. 2. Porosity versus permeability

The relationships between helium porosity and horizontal permeability for sandstones, siltstone–marl facies and all samples are shown in *Figs. 6a, b*, and *c* respectively. Figure 6a exhibits a linear relation with reliable coefficient of correlation ($r = 0.75$), while a sandstone subtrend of abnormally high permeability is observed (*s* or *sz* symbol on graphs). The calculated regression line equation for sandstones facies is

$$\log Kh = 0.189\,\Phi H - 2.37 \qquad (12)$$

where Kh = horizontal permeability (μm^2).

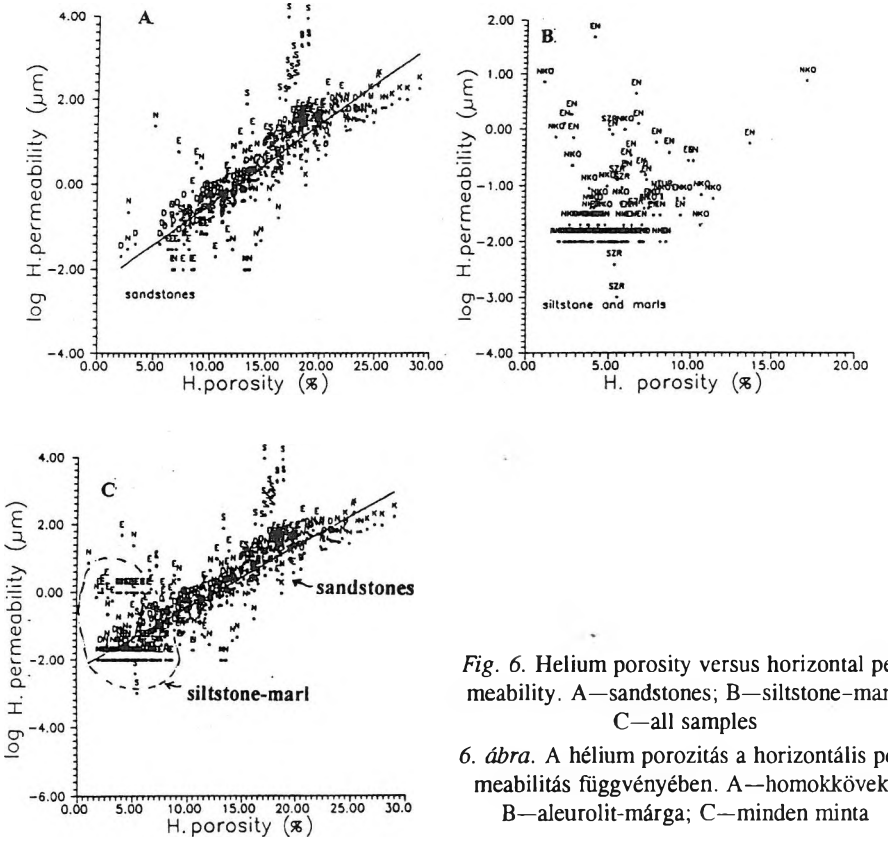

Fig. 6. Helium porosity versus horizontal permeability. A—sandstones; B—siltstone–marl; C—all samples

6. ábra. A hélium porozitás a horizontális permeabilitás függvényében. A—homokkövek; B—aleurolit-márga; C—minden minta

The relationship (Fig. 6b) representing siltstone–marl facies has mainly cloud shaped sample points indicating that permeability does not depend on sample porosity. On the other hand, Fig. 6c shows the probable partitioned areas of both sandstone and siltstone–marl facies. The regression line equation governing this relation, which is supported by a reliable coefficient of correlation ($r = 0.72$) is

$$\log Kh = 0.183\,\Phi H - 2.29 \tag{13}$$

The helium porosity versus vertical permeability relations (*Figs. 7a, b*, and *c*) exhibit the same features — as was mentioned earlier — while the siltstone–marl area is slightly changed. The sample behaviour of abnormally high permeability which belongs to samples obtained from the Szarvas wells

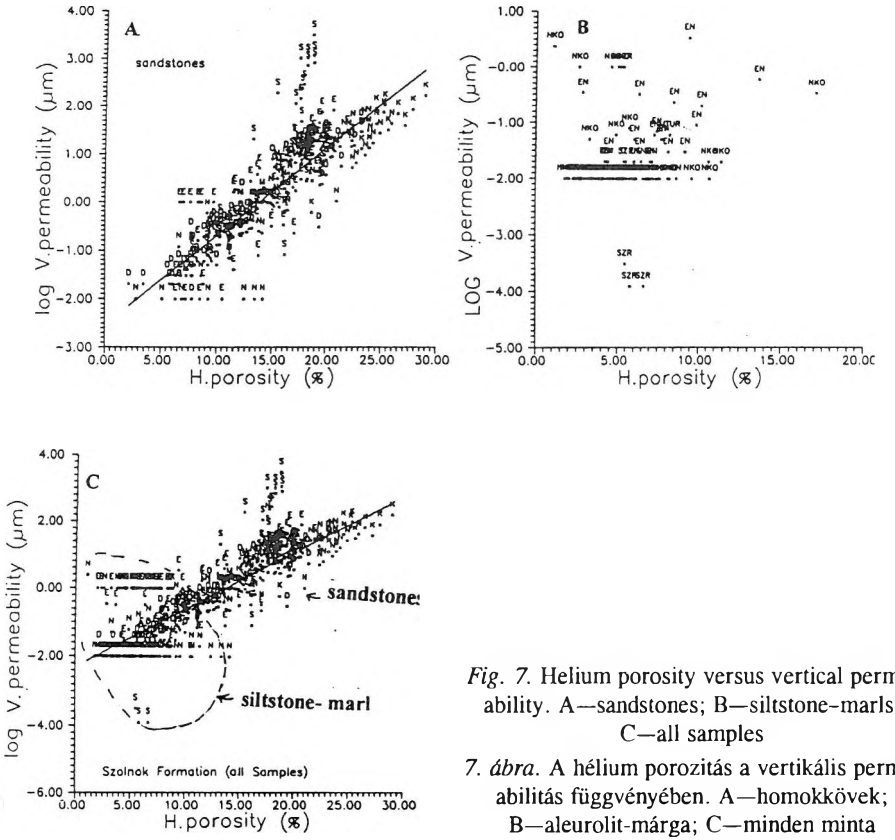

Fig. 7. Helium porosity versus vertical permeability. A—sandstones; B—siltstone-marls; C—all samples

7. ábra. A hélium porozitás a vertikális permeabilitás függvényében. A—homokkövek; B—aleurolit-márga; C—minden minta

still exists. The regression equations calculated for both sandstone facies and all samples are:

$$\log Kv = 0.183\,\Phi H - 2.54 \qquad \text{(for sandstones)} \qquad (r = 0.84) \tag{14}$$

and

$$\log Kv = 0.169\,\Phi H - 2.23 \qquad \text{(for all samples)} \qquad (r = 0.81) \tag{15}$$

where Kv = vertical permeability (μm^2).

3. 3. Horizontal versus vertical permeability

Figures 8a, b, and *c* show good relations between horizontal and vertical permeability of sandstones attributed to the Szolnok Formation. The calculated formulae representing both sandstone lithologic facies and all studied samples have slightly high coefficients of correlation ($r = 0.8$ and 0.78) respectively, they are:

$$\log Kh = 0.862 \log Kv + 0.29 \qquad \text{(for sandstones)} \qquad (16)$$

and

$$\log Kh = 0.36 + 0.76 \log Kv + 0.073 \log Kv \qquad \text{(for all samples)} \qquad (17)$$

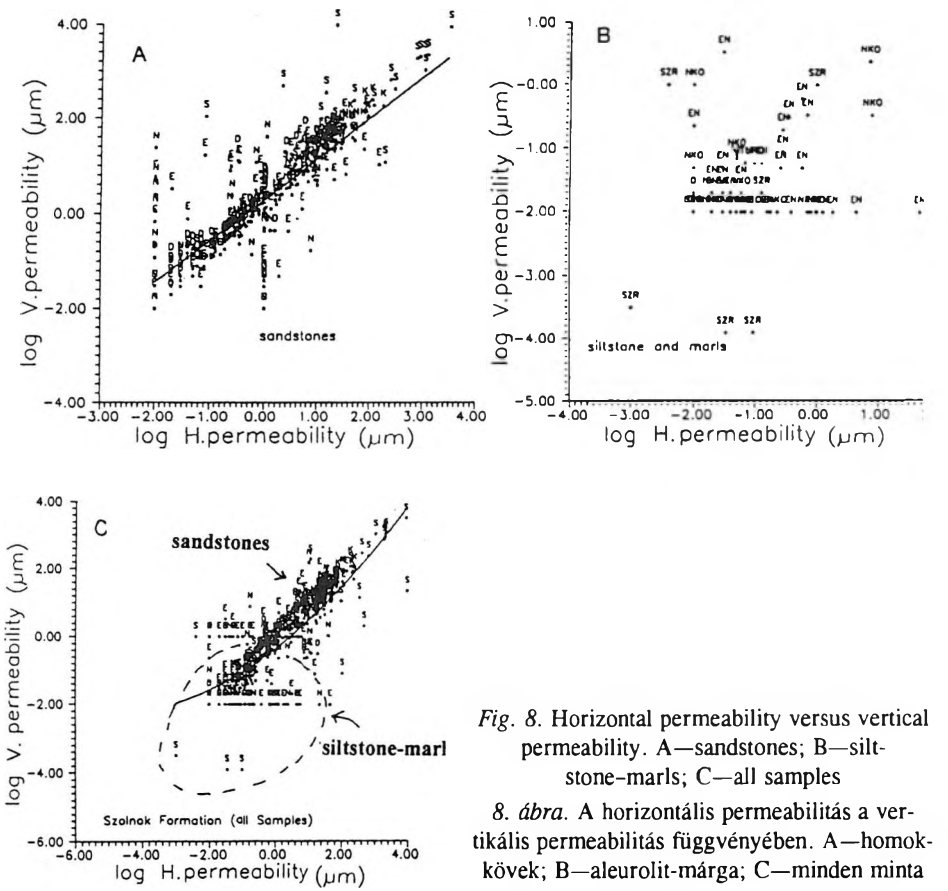

Fig. 8. Horizontal permeability versus vertical permeability. A—sandstones; B—siltstone-marls; C—all samples

8. ábra. A horizontális permeabilitás a vertikális permeabilitás függvényében. A—homokkövek; B—aleurolit-márga; C—minden minta

The correlation between sample plots in Figs. 8b and 8c allows identification of limits of siltstone–marl facies of the Szolnok Formation see Fig. 8c and this therefore facilitates allocation of areas for further reservoir studies.

3. 4. Permeability versus pvc_7

The pore volume corresponding to pore radius of 4.28 μm in size is defined in the present study (Fig. 2) as pvc_7. The permeability–pvc_7 relations (*Figs 9a, b*, and *c*) seem to be slightly effective for siltstone–marl discrimination. Some sort of sub-facies (probably silty sandstones) which may be assumed petrographically to sandstone facies have appeared and partially overlap siltstone–marl areas in some combinations (Figs. 9a , b & c). These combinations lead to some difficulties in differentiating between silty sand-

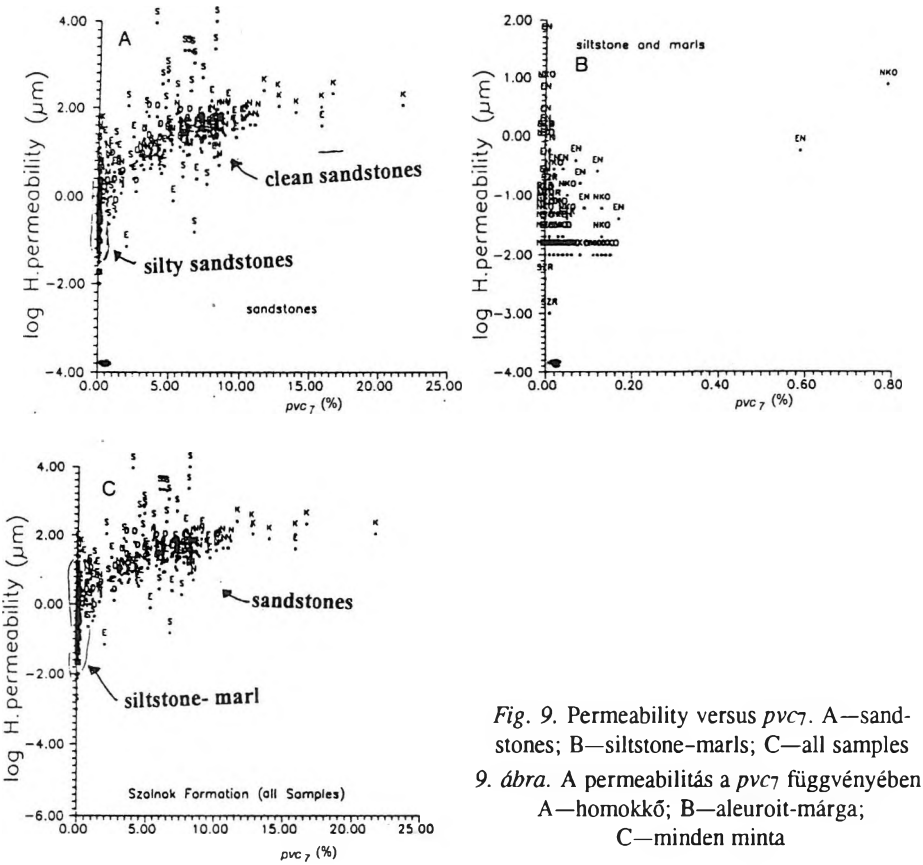

Fig. 9. Permeability versus pvc_7. A—sandstones; B—siltstone-marls; C—all samples

9. ábra. A permeabilitás a pvc_7 függvényében. A—homokkő; B—aleuroit-márga; C—minden minta

stone and siltstone–marl facies in view of which either we have to look for another effective cross plot or assume both silty sandstones and siltstone–marl as one petrophysical facies (petrofacies).

3. 5. Mercury porosity versus pvc_2

pvc_2 is defined as the pore volume corresponding to pore radius of 0.01 μm. The combination of mercury porosity and pvc_2 (*Figs. 10a, b* and *c*) proves to be very effective in discriminating between clean sandstones, silty sandstones, and siltstone–marl facies. The obtained inclined V-shaped sample points distribution is a specific feature characterizing this cross-plot. The examination of Figs. 10a, b and c indicates that silty sandstone facies is more or less overlapped in some parts by siltstone–marls. In addition, it can be proved that clean sandstones have a very low pvc_2 %, while silty sandstone

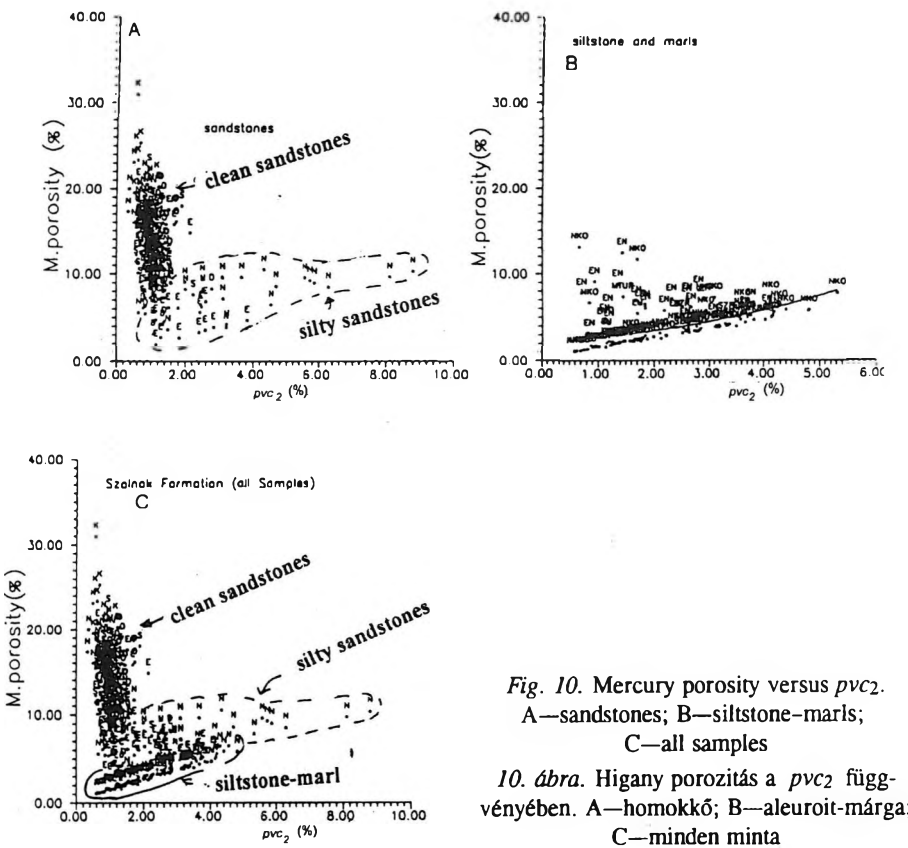

Fig. 10. Mercury porosity versus pvc_2. A—sandstones; B—siltstone–marls; C—all samples

10. ábra. Higany porozitás a pvc_2 függvényében. A—homokkő; B—aleuroit-márga; C—minden minta

and siltstone–marls have a range of pvc_2 % from 1.0 up to 10.0 of total pore volume. A linear regression line equation has been calculated for siltstone–marl facies, this being:

$$\Phi M = \exp\cdot(0.259 pvc_2)\cdot 2.06 \qquad (18)$$

This equation could be used for either siltstone or clean sandstone determination; while the latter has a pvc_2 value of $<2.0\%$.

3. 6. Mercury porosity versus pvc_7

The relationships between mercury porosity and pvc_7 (*Figs. 11a, b* and *c*) for sandstone, siltstone–marl and all samples have a certain efficiency of lithologic facies differentiation. The siltstone–marl facies have a percentage of pvc_7 ranges from 0.0 to 1.8, while clean sandstone facies attains pvc_7 from

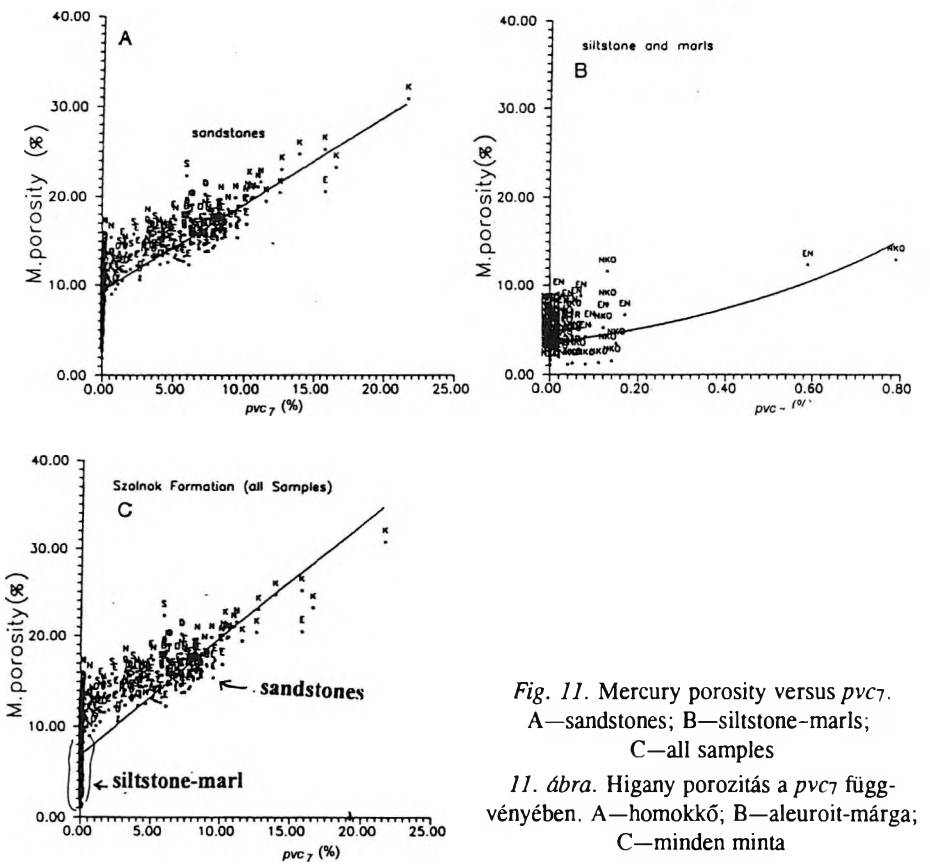

Fig. 11. Mercury porosity versus pvc_7. A—sandstones; B—siltstone-marls; C—all samples

11. ábra. Higany porozitás a pvc_7 függvényében. A—homokkő; B—aleuroit-márga; C—minden minta

2.0 up to 25. In addition, siltstone–marl facies are characterized by low mercury porosity ranging from 1.0 to 9.0 %, the porosity of the silty and clean sandstones ranges from 3.0 to 30.0%. It is mentioned that this combination fails to discriminate silty sandstones. The regression line equations calculated for both sandstones and all samples are supported by reliable coefficients of correlation equal to $r = 0.75$ and 0.65, respectively. The equations representing these relations are:

$$\Phi M = 0.975(pvc_7) + 9.37 \qquad \text{(for sandstones)} \qquad (19)$$

and

$$\Phi M = 1.3(pvc_7) + 6.82 \qquad \text{(for all samples)} \qquad (20)$$

3.7. (Vp < pvc$_6$) versus pvc$_3$

The pore volume (*Vp*) less than pvc_6 is defined in the present study as the summation of all pore volumes corresponding to a pore radius starting from 0.0075 μm (pvc_1) up to 2.5 μm (pvc_6). pvc_3 is defined as the pore volume corresponding to pore space radius of 0.075 μm in size. The relationships (*Figs. 12a, b* and *c*) exhibit a sample point distribution of L-shape. Most siltstone–marl sample points are concentrated in the area with maximum pvc_3 equals 4.0 and ($Vp < pvc_6$) equals 7.0. In fact the silty sandstone facies and the siltstone–marl have a mutual overlapping zone, whereas the clean sandstone facies is sharply isolated and easily identified (Fig. 12c).

3.8. (Vp < pvc$_5$) versus pvc$_5$

The pore volume (*Vp*) less than pvc_5 is defined as the summation of all pore spaces, which corresponds to pore radius starting from 0.0075 μm (pvc_1) up to 0.75 μm (pvc_5).The relationships (*Figs. 13a, b* and *c*) elucidate the efficiency of such combinations in lithologic facies discrimination. The correlation between these figures helps in allocating areas of different lithologic facies. The silty sandstones, exposed by different previously examined cross-plots, are usually accompanied in some parts by siltstone–marl facies. As complete separation between them using the present technique seems to be difficult, we suggest to put them altogether as one petrophysical facies.

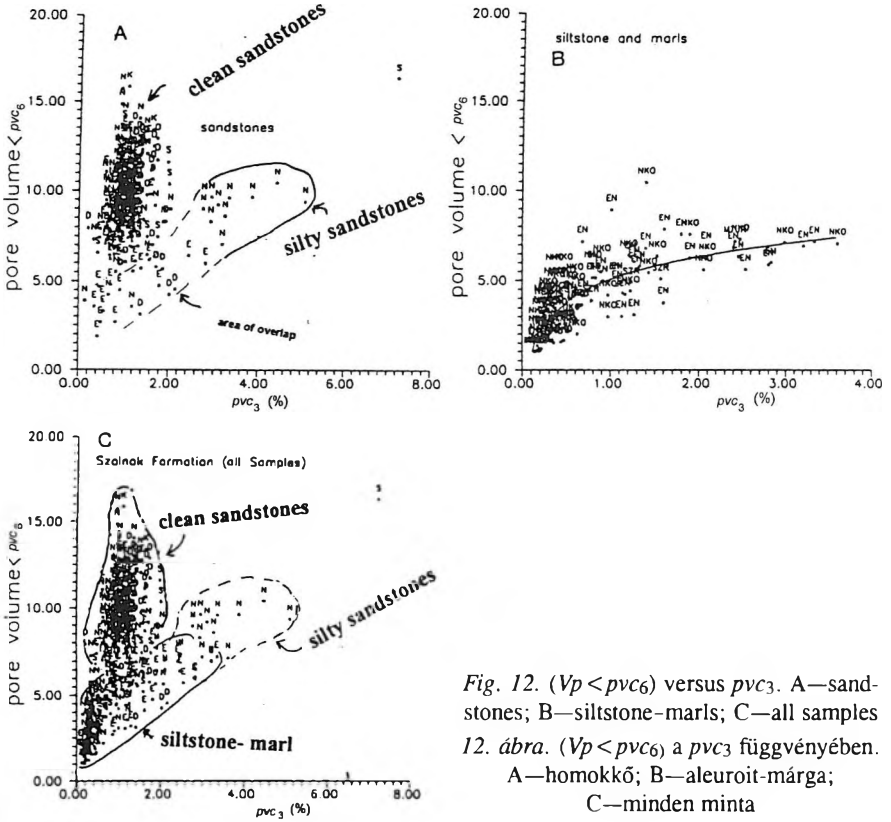

Fig. 12. ($Vp < pvc_6$) versus pvc_3. A—sandstones; B—siltstone-marls; C—all samples

12. ábra. ($Vp < pvc_6$) a pvc_3 függvényében. A—homokkő; B—aleuroit-márga; C—minden minta

3.9. ($Vp < pvc_6$) versus pvc_2

Examination of the relationships (*Figs. 14a, b* and *c*) indicates that we can easily differentiate between sandstones and siltstone–marl facies. Both the siltstone–marl and silty sandstones still have an overlapping area, which represents poor reservoir type in the Szolnok Formation.

3. 10. Effective radius versus mercury porosity

Here, the effective pore radius, is defined as the pore volume corresponding to pore radius of 1.87 μm in size. The relationships (*Figs. 15a, b* and *c*) between effective pore radius and mercury porosity for sandstones, siltstone–marls and all samples are useful for facies discrimination despite exhibiting linear trends in the case of clean sandstone samples. It is clear that

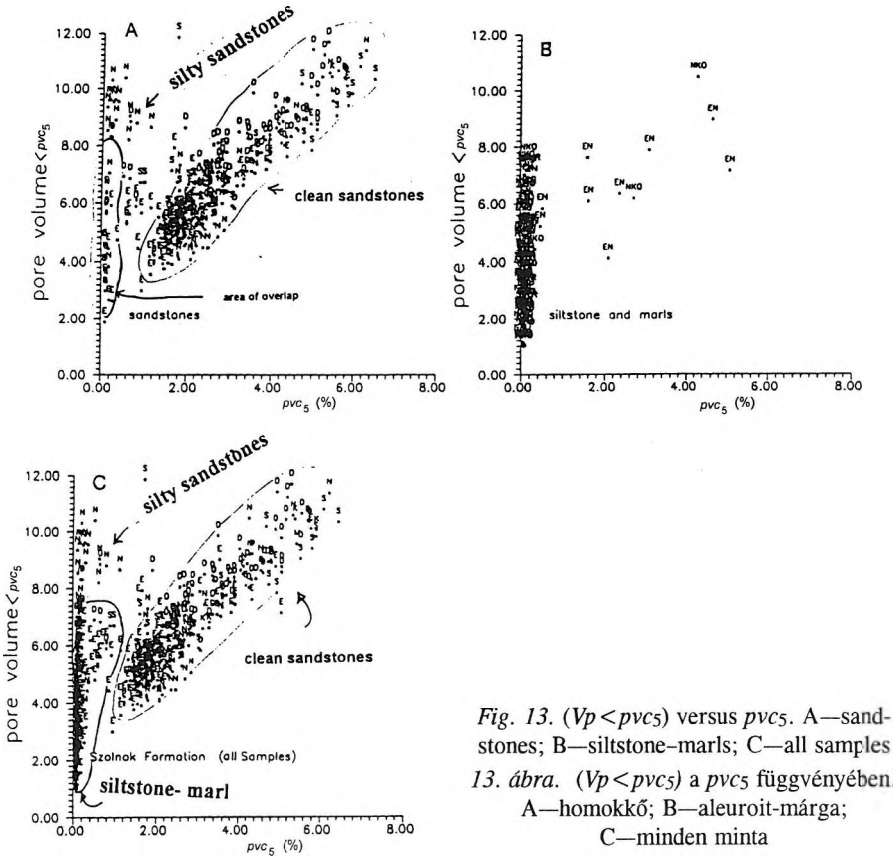

Fig. 13. (*Vp*<*pvc*5) versus *pvc*5. A—sandstones; B—siltstone-marls; C—all samples
13. ábra. (*Vp*<*pvc*5) a *pvc*5 függvényében. A—homokkő; B—aleuroit-márga; C—minden minta

effective pore radius has little or no positive contribution to increase porosity in the case of both silty sandstones and siltstone-marl facies of the Szolnok Formation. The regression line equations calculated are distinguished by reliable coefficients of correlation: $r = 0.86$ and 0.71 for sandstones and all samples respectively. The equations are;

$$\Phi M = 0.902(P_{1.87}) + 8.95 \qquad \text{(for sandstones)} \qquad (21)$$

and

$$\Phi M = 1.187(P_{1.87}) + 6.48 \qquad \text{(for all samples)} \qquad (22)$$

where $P_{1.87}$ = effective pore radius (μm).

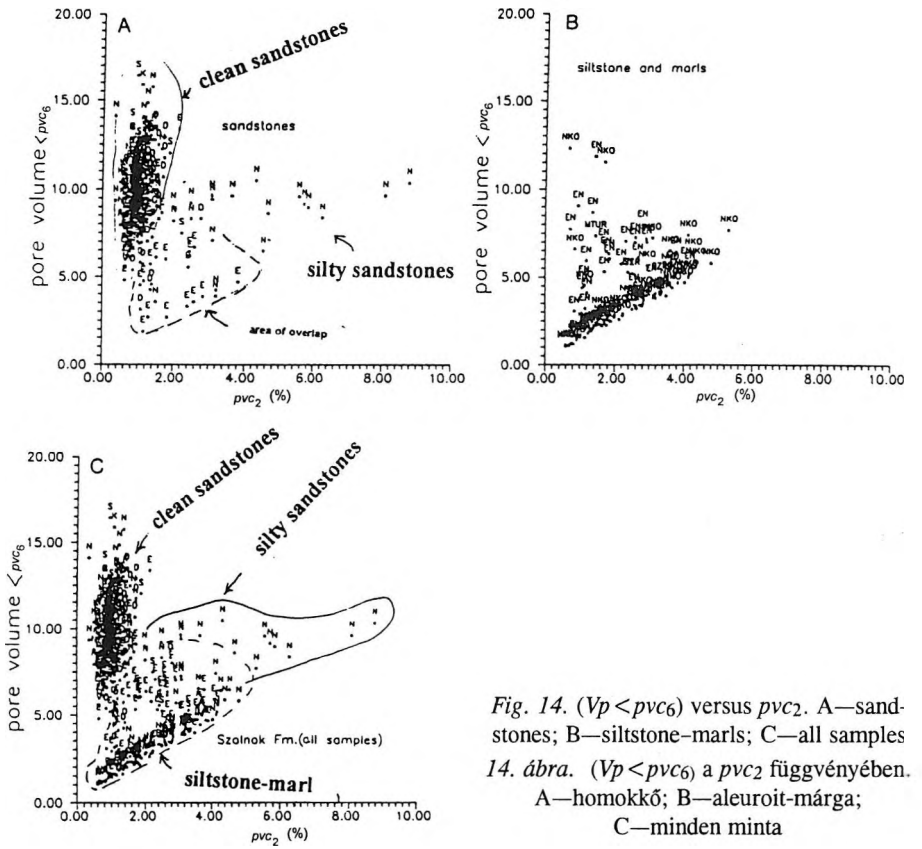

Fig. 14. ($Vp < pvc_6$) versus pvc_2. A—sandstones; B—siltstone-marls; C—all samples

14. ábra. ($Vp < pvc_6$) a pvc_2 függvényében. A—homokkő; B—aleuroit-márga; C—minden minta

By using these relations one can determine the effective pore radius, which is difficult in measurements as well as being expensive, from the routine porosity data of the Szolnok Formation.

3. 11. Effect of calcite content on pore structure

During the sedimentary history, both chemical and physical diagenetic processes have a great effect on the rock pore space framework. Therefore, the today's rock pore space structures are mainly the net product of either syn-sedimentary or post-sedimentary processes. Study of the primary porosity is not enough for pore structure investigation, while the chemical diagenetic processes (solution, cementation, etc.) can negatively or positively affect reservoir parameters such as pore structure, porosity and permeability.

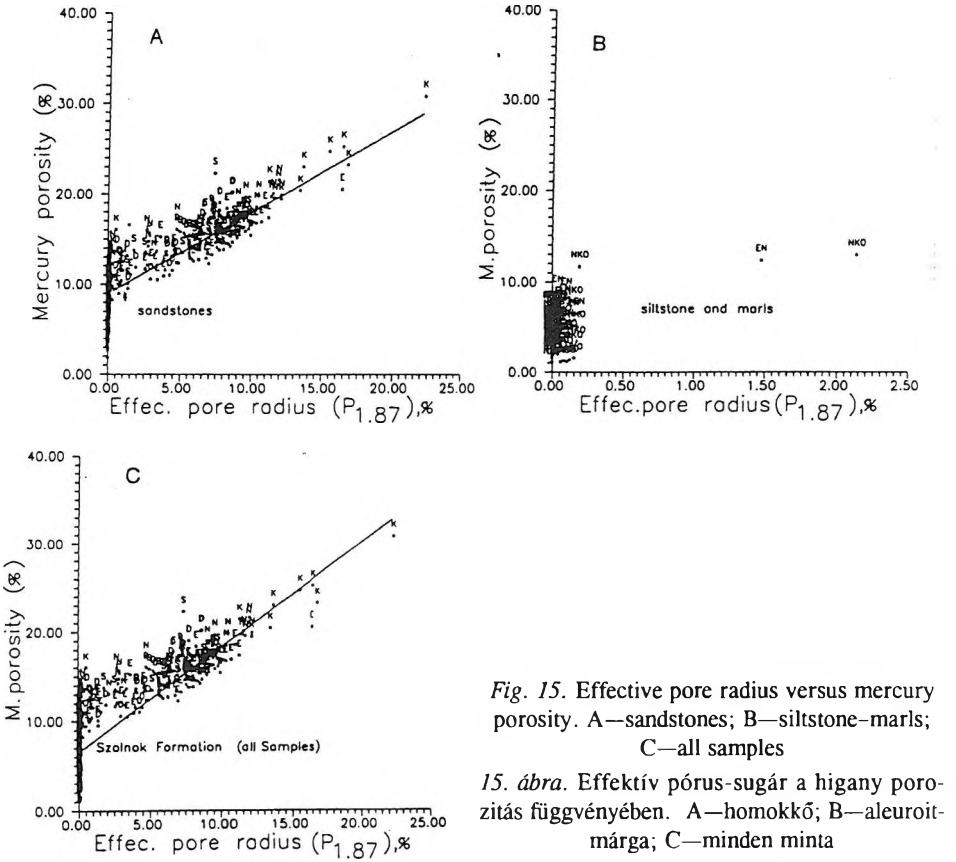

Fig. 15. Effective pore radius versus mercury porosity. A—sandstones; B—siltstone-marls; C—all samples

15. ábra. Effektív pórus-sugár a higany porozitás függvényében. A—homokkő; B—aleuroit-márga; C—minden minta

The low percentages of calcite content as a rock formation fines occurring in the pore spaces usually occupy the larger pore throat size fractions (*Fig. 16*). On the other hand the percentages of calcite content increase at the expense of the large pore throats. Figure 16 elucidates that the large pore size fractions have been destroyed step by step from the largest size fraction downward by the gradual increase of the percentages of the calcite content in the pore space framework of the sandstones belonging to the Szolnok Formation. We can conclude that the increase in the percentages of calcite contents up to 22% can destroy all pore throats having a radius larger than 0.25 μm, in this case the sandstone reservoir could not be suitable for storing fluids.

An attempt was made to investigate the calcite cement and its effect on reservoir fluid production. For this purpose some sandstone samples were acidified with 15% HCl acid while both porosity and pore throat size

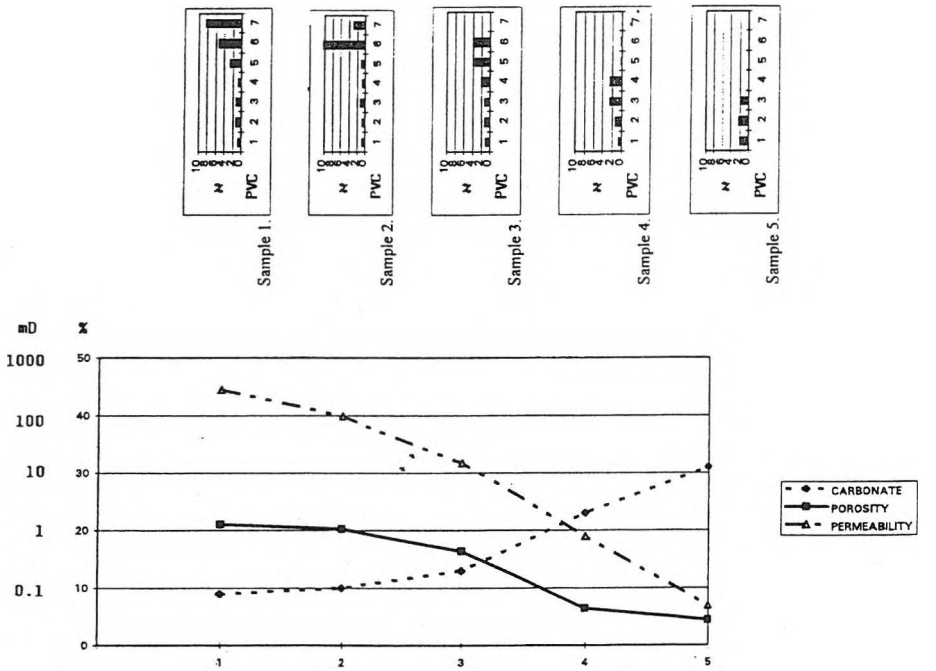

Fig. 16. Permeability, porosity, and *pvc* interrelationships for some selected samples from Szarvas area

16. ábra. Permeabilitás, porozitás és *pvc* összegüggések néhány Szarvas környéki mintára

parameters are measured before and after the acidification (*Figs. 17a* and *b*). Based on the data presented in Figures 17a and b, we can find two different types of sandstone reservoir behaviour in the Szolnok Formation. The first type (Fig. 17a) exhibits that the enhancement of the rock porosity after acidification goes in accordance with that before acidification. This can be explained by the dissolving of the calcite without any major changes in the shape of the original rock pore structure. The permeability of this sandstone type is slightly increased. The second reservoir type (Fig. 17b) shows that the largest pore throat size (pvc_7) is drastically increased at the expense of pvc_5 and pvc_6, while the permeability of this type is greatly enhanced after the acidification processes. Therefore, we can conclude that the formation fines were only calcite in the pore throats which are now completely dissolved

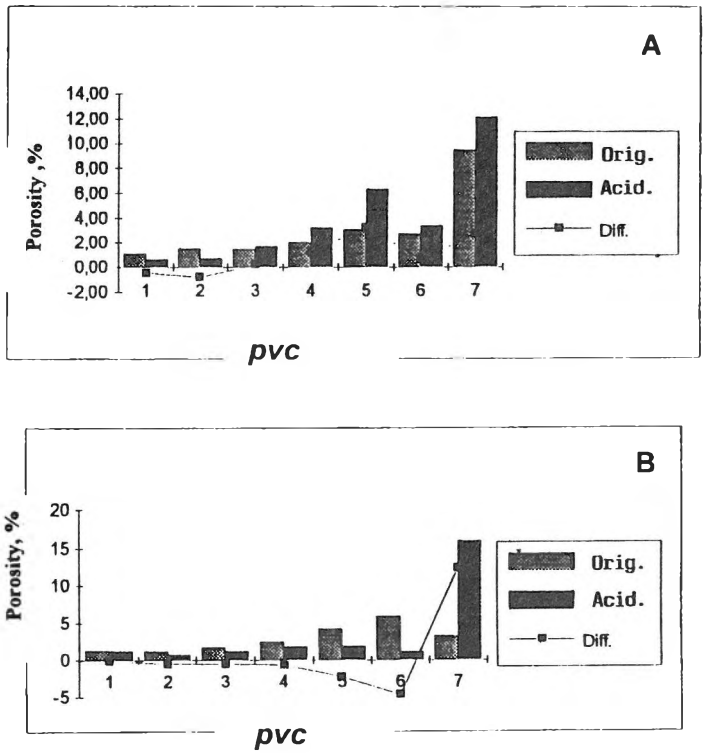

Fig. 17. Effect of calcite cement on both porosity and permeability before and after acidification (Szarvas area). A—sandstone reservoir type-1; B—sandstone reservoir type-2

17. ábra. A kalcit cement hatása a porozitásra és a permeabilitásra savazás előtt és után (Szarvasi terület). A—1-es típusú homokkő tározó; B—2-es típusú homokkő tározó

and thus they enhance pore throat size as well as porosity and permeability. It is mentioned that reservoir enhancement using acidification of sandstones depends mainly on the nature of pore throats, pore spaces and mode of occurrence of formation fines and its mineralogy .

4. Conclusions

The petrophysical data obtained for the Szolnok Formation have been treated as one population for all samples. However, both sandstone and siltstone-marl facies were processed separately. The application of the

suggested reservoir model permits lithologic discrimination with high efficiency using some graphical combinations. This technique is extremely important for Szolnok reservoir diagnosis. It facilitates separation and identification of the present lithofacies.

The pore throat size classification based on the proposed model proves its appilicability for lithologic facies discrimination as well as for prediction of some important reservoir parameters. Cross-plotting of the petrophysical measurements has indicated that the Szolnok Formation comprises two main lithologic groups: (a) clean sandstone, (b) silty sandstone, siltstone and marls. It means that by using these plots one can easily differentiate between very good and intermediate or even bad reservoirs; each lithologic facies has a characteristic trend.

The prediction of one type of porosity and/or permeability from another using the least squares fitting method has great significance for Szolnok reservoir evaluation. Both the porosity and permeability variation range characterizing the detected lithologic facies of the Szolnok Formation are useful for reservoir zonation.

Some pore volume sizes — especially pvc_2 and pvc_7 as defined by the suggested reservoir model — could be predicted from either measured permeability or porosity. Intercorrelation between some pore space volumes is very effective for lithologic facies separation and identification.

It should be mentioned that reservoir enhancement using acidification processes depends mainly on the nature of pore throats, pore spaces, and the mode of occurrence of formation fines and its mineralogy.

Acknowledgements

This work was supported by the MOL plc, OGIL Lab. of Budapest, Hungary during 1995 on the basis of a consultation contract. The authors wish to thank this organization for financial support and permission for publication. Special thanks are due to Prof. József PÁPAY, Dr. István BÉRCZI, and Dr. Endre BALÁZS for their continuous help and fruitful discussions.

REFERENCES

BÁN Á., EL SAYED A. M. A. 1987: Genetic delineation of deltaic rock types in terms of log curve shape in the Algyő-2 hydrocarbon reservoir, Hungary. Acta Geol. Hung. **30**, 1–2, pp. 231–240

BÉRCZI I., PHILIPS R. L. 1985: Processes and depositional environments within Neogene deltaic-lacustrine sediments, Pannonian Basin, southeast Hungary. Geophysical Transactions **31**, 1–3, pp. 55–74

EL SAYED A. M. A. 1981: Geological and petrophysical studies for the Algyő-2 reservoir evaluation, Algyő oil and gas field, Hungary. Ph.D. thesis, Hungarian Acad. of Sci., Budapest, 166 p.

EL-SAYED A. M. A. 1991: Reservoir evaluation for the Törtel Formation. Internal report, SZKFI, Budapest, 48 p.

EL SAYED A. M. A., VOLL L. 1992: Empirical prediction of porosity and permeability in deltaic sandstones of the Törtel Formation, Hungary. Sci. Bull, Ain Shams Univ., **30**, pp. 461–487

EL SAYED A. M. A. 1993: Relationship of porosity and permeability to mercury injection derived parameters for sandstones of the Törtel Formation, Hungary. Geophysical Transactions **38**, pp. 35–46

EL SAYED A. M. A. 1994: Intercorrelation of capillary pressure derived parameters for sandstones of the Törtel Formation, Hungary. Geophysical Transactions **39**, 1, pp. 77–87

GAJDOS I., PAPP S., SOMFAI A., VÖLGYI L. 1983: Lithostratigraphic units of the Pannonian s.l. formations in the Hungarian plain (in Hungarian). MÁFI, Budapest, 70 p.

JÁMBOR Á. 1980: Basic features of the stratigraphy of the Pannonian formations (in Hungarian). Ált. Föld. Szemle, Budapest, **14**, pp. 113–124

JÁMBOR Á. 1989: Review of the geology of the s.l. Pannonian formations of Hungary. Acta Geologica Hungarica **32**, pp. 269–324

JUHÁSZ Gy. 1991: Geological framework of the Neogene formations of the Szarvas region, Middle Hungarian plain, Hungary (in Hungarian). Földt. Közlöny, (Bull.of the Hung. Geol. Soc.) **121**, pp. 111–124

JUHÁSZ Gy. 1994: Comparison of the sedimentary sequences in Late Neogene sub basins in the Pannonian basin, Hungary (in Hungarian). Földt. Közlöny, (Bull.of the Hung. Geol. Soc.) **124**, pp. 341–365

KISS B. 1994: Numerical analysis of pore structure for reservoir sediments (in Hungarian). Kőolaj és Földgáz **127**, pp.10–13

KÖRÖSSY L. 1968: Entwicklungsgeschichtliche und Palaogeographische Grundzüge des Ungarischen Unterpannons. Acta Geol. Acad. Sci. Hung. **12**, pp. 199–217

KÖRÖSSY L. 1971: Subsurface geology and evolution history of the Pannonian in Hungary. *In*: GÓCZÁN F. & BENKŐ J. (eds.): Investigations of the Pannonian formations in Hungary (in Hungarian). Akad. Kiadó, Budapest, pp. 253–344

MAGYAR L., RÉVÉSZ I. 1976: Data on the classification of Pannonian sediments of the Algyő area. Acta Mineralogica-Petrographica **22**, pp. 276–283

MAPSTONE N. V. 1973: Porosity, permeability and pore throat size distribution in Danian and Maastrichtian limestone from the North Sea and Denmark. Bp. Research Center, Report EPR/R8081. pp. 1-13

MUCSI M., RÉVÉSZ I. 1975: Neogene evolution of the southeastern part of the Great Hungarian Plain on the basis of sedimentological investigations. Acta Mineralogica-Petrographica **22**, pp. 29-49

PITTMAN E. D. 1992: Relationship of porosity and permeability to various parameters derived from mercury injection -capillary pressure curves for sandstones. AAPG Bull. **76**, pp. 723-760

RÉVÉSZ I., BÉRCZI I., PHILIPS R. L. 1989: Lower Pannonian sedimentation in the Békés basin (in Hungarian). Magyar Geofizika, **XXX**/2-3, pp. 98-113

SZELES M. 1962: Molluskenfaunen von Beckensedimenten des Unterpannons. Földt. Közlöny, (Bull.of the Hung. Geol. Soc.) **92**, pp. 53-60

A Szolnoki Formáció tárolóinak diagnózisa az Alföld középső részén

A. M. A. El SAYED és KISS Balázs

Az Alföld középső részén minden mélyfúrásban megtalálták a Szolnok Formáció képződményeit többnyire turbidites törmelékes üledék alakjában. Az aleuritban közbetelepülő homokkő rétegek és márga csíkok is vannak. Jelen tanulmány céljára 494 db magmintát gyűjtöttek össze és vetették alá különböző kőzettani laboratóriumi vizsgálatoknak. A kapilláris nyomás módszerét (MICP) alkalmazták a pórusnyílás méreteloszlásának, a különböző dimenziójú pórus átmérőknek megfelelő pórustérfogat (*pvc*) és az effektív porozitás vizsgálatára. Másrészről a tároló paraméterének korrelációja céljából mind a horizontális, mind a vertikális permeabilitást és a hélium porozitást is mérték.

A kőzetfizikai adatokat a litológiától függetlenül minden mintára egyetlen halmazként kezelték. Továbbá, a Szolnoki Formáció minden litológiai fáciesét külön kezelték azért, hogy megbízható, nagy pontosságú matematikai összefüggéseket állíthassanak fel a tároló értékeléséhez. Új eljárást alkalmaztak a pórusnyílások mérésére; ez a módszer lehetővé teszi a szolnoki üledékeket jellemző pórusterek keletkezésének és fejlődésének becslését a tároló üledékképződésének és kőzetté válásának során.

Homokkő fáciesek esetében a pórusnyílás mérések korrelációja jelzi, hogy két genetikai típus létezik, míg ez a jelenség nem ilyen egyértelmű, ha csak porozitási vagy permeabilitási adataink vannak. Másrészt mind a horizontális, mind a vertikális permeabilitás világosan jelzi a tároló heterogenitását márgák és aleurolit esetében. Mind a porozitás, mind a permeabilitás ábrázolása a különböző pórustér méretek függvényében világossá teszi a tároló heterogenitását a Szolnoki Formáció minden kőzetfácies-típusában. A Szolnoki Formációban a litológiai fácieseket elkülönítették és egy sor tároló-paraméterkombináció hatékonyságát a gyakorlatban is bizonyították. Továbbá, megbízható összefüggéseket kaptak a tároló effektív pórusátmérője, porozitása és/vagy permeabilitása becslésére.

GEOPHYSICAL TRANSACTIONS 1997
Vol. 41. No. 1-2. pp. 65-94

Modelling the history of burial, temperature, and hydrocarbon generation of sedimentary basins. Application to the Aars-1A well

Peter Klint JENSEN*

The history of burial and subsurface temperature is calculated for the Danish well Aars-1A using simple analytical expressions. Compaction of the sedimentary sequences is taken into account. Vitrinite reflectance and hydrocarbon generation are simulated using a general chemical simulation model. The model is flexible with regard to modifications of chemical reactions. A method for calculating the heat flow history by inversion of measured vitrinite reflectance values is suggested. 1-D basin modelling is performed for the Danish well Aars-1A. The uncertainty of the calculated heat flow (relative to the present heat flow) is 25%, 100 mill. years ago. Before that time the uncertainty increases further. The hydrocarbon generation of the F-III Member of the Fjerritslev Formation is calculated using the heat flow history derived from geodynamic modelling.

Keywords: burial history, sedimentation, compaction, geothermics, maturity, vitrinite reflectance, hydrocarbon generation, simulation

1. Introduction

The ultimate goal of basin modelling is to calculate the amount of hydrocarbons generated in source rocks through time and to predict accumulations in reservoirs. The basic principles of basin models are given in YÜKLER et al. [1978], UNGERER et al. [1984] and CAO and LERCHE [1986]. A simple

* Department of Geology and Geotechnical Engineering, Technical University of Denmark, byg. 204, DK-2800 Lyngby, Denmark

Manuscript received (revised version): 2 January, 1995

one dimensional computer model was presented in JENSEN et al. [1985]. This model is able to calculate the history of 1) burial including compaction of sedimentary sequences, 2) formation temperatures, 3) vitrinite reflectance; however it is not suitable for calculating hydrocarbon migration. The model is based mainly on analytical expressions some of which are so simple that they can be used in connection with hand calculations. The model was used in a basin model study of the Aars-1A well [JENSEN et al. 1985].

In the present study a general model for simulating chemical reactions is implemented in the above mentioned 1D-basin model. Chemical reactions are traditionally simulated by deriving analytical expressions for the production rates of species. Although in certain cases the expressions may be solved analytically, in most cases they are solved numerically. Despite the analytical method being computationally efficient it is also time consuming and non-flexible. Thus, the introduction of more reactions needs re-evaluation of the analytical expressions and re-programming. SØRENSEN, STEWART [1980] showed that modelling of chemical reactions can also be performed by applying a general computation scheme with a flexible input data procedure. Reactions are specified in the input data file. This paper describes the application of the general chemical simulation method to kerogen transformation chemistry. It is shown that modification of the model by BURNHAM, SWEENEY [1989] is necessary for obtaining reasonable vitrinite reflectance values.

Past heat flow is traditionally calculated by repeated forward modelling. The assumed heat flow function is modified until there is reasonable accordance between calculated and measured vitrinite reflectance values. [LERCHE et al. 1984, LERCHE 1988a and 1988b]. Although useful results have been obtained with forward modelling there are a number of assumptions which have not been addressed, e.g. no rules are given for the choice of heat flow function, a method which determines the number of free variables is needed, the chosen function may be either too stiff or too soft. If the function is too stiff there may be cases where a rapid change of heat flow, e.g. in connection with intrusions or hydrothermal activity, cannot be satisfactorily simulated; if it is too soft the inverted heat flow history may fluctuate due to uncertain vitrinite reflectance measurements.

In this study an inversion procedure is suggested in which a piece by piece linear heat flow function is constructed on the basis of the measured vitrinite reflectance values and their uncertainties. Alternative heat flow

functions which all result in simulated vitrinite reflectance values close to measured values, are derived.

In the following the mathematical background is given for 1-D basin modelling.

2. Burial history

Sedimentary sequences are often divided into a number of formations each with a distinct lithology. Looking at a particular formation it may be reasonable to assume that the layer resulted from a continuous and steady sedimentation process. During burial the sediments are compacted due to rearrangement of the grains and of diagenesis. The grains themselves are considered incompressible. In due course the formation water occupying the pore volume escapes the diminishing pores. Empirical observations have shown that sediments often compact with the porosity decreasing exponentially with depth [ATHY 1930]. Each formation has its own characteristic exponential function. Limitations to this approach will be discussed below. The mathematical formulation of burial history including compaction, given here, is based on the principle of conservation of the solid particle mass. The sediment volume, not occupied by solid particles, is assumed to be filled with water. Once the movement and the compaction of the solid particles are given, the movement of the water may be readily found since the water just occupies the volume left over by the solid particles.

The following description is divided into two parts: the first part discusses the derivation of equations for the surface layer, the second describes underlying layers.

The sedimentation process of a surface layer may be regarded as a flow of solid particles relative to the surface, towards the depth. The rate at which solid mass is added to the surface is assumed constant from time $t=0$, when the sedimentation process started. It is assumed that the lithology and the porosity profile of the layer are constant in time during sedimentation. This means that any lump of sediment experiences equivalent burial paths. Analytical equations of the burial history of a surface layer including compaction may be deduced by considering conservation of the solid particle mass. The particles are packed with depth. This is expressed by increasing density of the solid with depth. The density is calculated as the mass of solid, per total volume of sediment, including water. The flow of compacting solid

particles may then be regarded as analogous to the flow of a compressible fluid. A differential equation may be derived from which the relation between time and depth can be determined [HUTCHINSON 1985 and JENSENet al. 1985];

$$t(z) = \frac{1}{v_0(1-\Phi_0)}\left[z + \frac{\Phi_0}{a}\left(e^{-az} - 1\right)\right] \tag{1}$$

where $t(z)$ is the time it takes a sediment grain to reach depth z, Φ_0 is the surface porosity, a is the compaction coefficient determining the compaction of sediments:

$$a = -\frac{1}{z}\ln\left(\Phi(z)/\Phi_0\right) \tag{2}$$

$\Phi(z)$ is the exponential porosity depth function. The surface velocity υ_0 is determined from:

$$\upsilon_0 = \frac{1}{(1-\Phi_0)t_b}\left[h + \frac{\Phi_0}{a}\left(e^{-ah} - 1\right)\right] \tag{3}$$

where the total surface layer thickness, h, is known from well information, and t_b is equal to an age date of the base of the layer, thus Eq. (1) is the expression governing the relation between time and depth for the sedimentation process including compaction. Given the depth, the time necessary for a sediment particle to reach this depth can be calculated simply form Eq. (1). If, on the other hand, the time is given the depth must be found from Eq. (1) by an iterative procedure (see Appendix A).

We now turn to layers underlying the surface layer. SCLATER, CHRISTIE [1980] showed that the following relation can be used to calculate the depth to the base of a layer z_4:

$$z_4 + \frac{\Phi_0}{a}e^{-az_4} = z_2 - z_1 + \frac{\Phi_0}{a}\left(e^{-az_2} - e^{-az_1} + e^{-az_3}\right) + z_3 \tag{4}$$

where z_1 and z_2 are respectively the depth to the top and the base of the layer at a given time, and z_2 and z_3 are respectively the depth to the top and the base of the layer at another time (see *Fig. 1*).

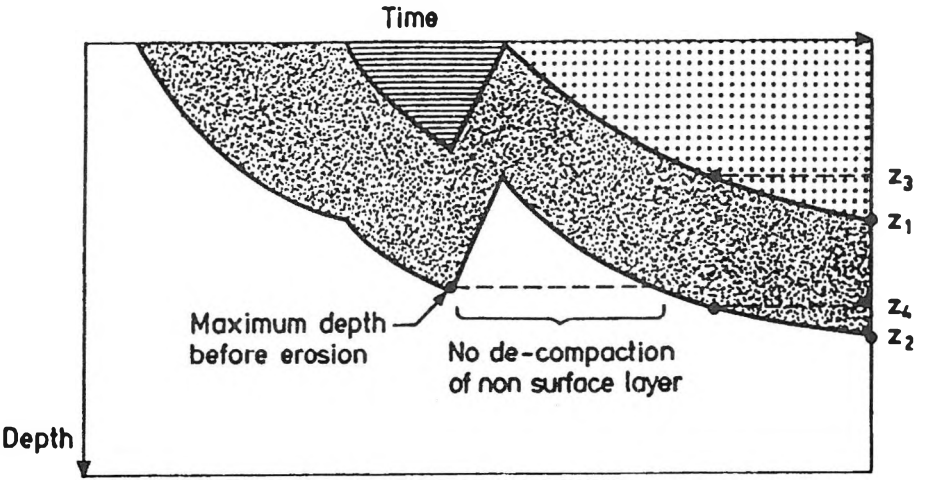

Fig. 1. Schematic drawing showing the burial history of sedimentary layers
1. ábra. Az üledékes rétegek feltöltődésének sematikus vázlata

In this equation depths z_1 and z_2 might be known from well data; z_3 may be calculated from Eq. (1); z_4 is then determined by an iterative procedure from Eq. (4), Appendix A.

The equations given above provide the foundation for calculating a multilayer sedimentation process. In sedimentary basins uplift and temporaneous erosion is a common feature. It is a general experience that sediments do not undergo much decompaction when they are uplifted. Since the elastic rebound, which is of the order of a few per cent is disregarded here, the depth history of the sediments during erosion may be modelled as a linear decrease of depth with no decompaction and with a constant uplift rate. Compaction starts when the burial depth is greater than the previous maximum depth. The maximum depth is determined by an iterative procedure. The calculations start at the present where the previous maximum depth are assumed to be zero. The formations are decompacted except during uplift. After one backstripping a first estimate of the maximum depths before erosion is calculated and the time interval with no decompaction of the formations is determined (Fig. 1). The process is repeated until the maximum depths are determined with confidence and the final estimate of the burial history is thus determined.

3. Formation temperature through time

Steady state formation temperature is calculated analytically for a given surface temperature and a given heat flow. Heat production and transport of heat by water and grain movements are not considered. The conductivity is a function of the depth dependent porosity. The conductivity function considered is

$$K = K_F + (1-\Phi)^2 (K_S + pC - K_F) \tag{5}$$

This equation is due to ROBERTSON [1979]. The conductivity is a function of fluid conductivity K_F, solid conductivity K_s for zero content of quartz, and quartz content p (percentage). The influence of the quartz content, p, is governed by multiplying by C which is a constant for each formation. Results of measurements on a large number of sedimentary rocks are given in ROBERTSON [1979] where the necessary constants in Eq. (5) may be found for different rock types. For an exponential depth decrease of porosity, and applying the conductivity given by ROBERTSON [1979] one obtains an expression for the formation temperature. For a given formation the temperature at its base $T(z_2)$ is [JENSEN et al. 1985]:

$$T(z_2) = T(z_1) + W \frac{1}{aA} \frac{1}{(K_F/A)+1} (g_1 - g_2) \tag{6}$$

where $A = K_S + pC - K_F$, $\Phi_i = \Phi_0 e^{-az_i}$, and

$$g_i = \ln \Phi_i - \tfrac{1}{2} \ln\left(\frac{K_F}{A} + (1-\Phi_i)^2 \right) - \frac{1}{K_F/A} \arctan\left(\frac{1-\Phi_i}{K_F/A} \right) \tag{7}$$

for $i = 1, 2$. Hints concerning the derivation of the above given expression are detailed in Appendix B.

4. Maturity modelling

Quantification of maturity of source rocks is often performed by measuring the vitrinite reflectance. Vitrinite reflectance is time and temperature

dependent and has been modelled by Lopatin's time-temperature index TTI [WAPLES 1980]. WAPLES related the time-temperature index to measured vitrinite reflectance values for a large number of wells world-wide. This relation can then be used to predict the maturity of source rocks by reconstructing the temperature history and calculating the time-temperature index. Other authors such as, for example, FALVEY, DEIGHTON [1982], used a time-temperature integral to calculate the vitrinite reflectance.

Although the above mentioned methods were great steps forward in this type of modelling, a number of major problems regarding these models should be noted. The concept of using maximum temperature and effective time will in some cases lead to erroneous results. In particular it is to be expected that degradation of vitrinite is a function of the whole temperature history. Another problem is that many authors do not take compaction and time dependent conductivity into account. Neither do they include the time varying surface temperature. Furthermore, only a few models include the temperature effect of water movements caused by the compaction of the sediments [YÜKLER et al. 1978 and BETHKE 1985]. For a one-dimensional case HUTCHINSON [1985] showed that the effect of water movement is important only for rapidly subsiding basins. In the case history presented below for the Aars-1A well, water movements have not been taken into account.

Founded upon the above given criticism it is not to be expected that the maturity relations given by WAPLES [1980] and FALVEY, DEIGHTON [1982] can be used with success using a basin model including compaction, time dependent conductivities, surface temperature history, and the whole time-temperature history. In this paper the chemical kinetic vitrinite maturation model by BURNHAM and SWEENEY [1989] is applied for calculating vitrinite reflectance.

5. Simulation of hydrocarbon generation

Degradation of kerogen is calculated using 35 parallel first order reactions [BURNHAM, SWEENEY 1989]. Kerogen is divided into 19 groups with different activation energies; it may be thermally degraded into H_2O, CO_2, CH_n and CH_4. The degradation of kerogen is described mathematically by first order differential equations. The activation energies and frequency factors were, according to BURNHAM, SWEENEY [1989], found from the modelling of pyrolysis experiments on samples in the laboratory and the

modelling of kerogen degradation in nature. In the latter case basin models are used to model the temperature history. BURNHAM and SWEENEY [1989] give the activation energies, the frequency factors and the initial amounts of kerogen in each group. In this study the author multiplied the original frequency factors by $0.5\ 10^{-2}$ to obtain a reasonable match between calculated and measured vitrinite reflectance values.

Since the amount of a certain species is generally the result of several reactions, the calculations may be quite complicated. However, the calculations can be systematized by utilizing matrix calculation [SØRENSEN, STEWART 1980]. The production rates of species are calculated by matrix multiplication of the reaction rates and the stoichiometric matrix.

Consider the stoichiometric matrix

$$\mathbf{v} = \begin{array}{c} \begin{array}{ccccc} S_1 & . & S_j & . & S_n \end{array} \\ \begin{pmatrix} \nu_{1,1} & \nu_{1,2} & . & . & \nu_{1,n} \\ . & . & . & . & . \\ \nu_{i,1} & . & \nu_{i,j} & . & \nu_{i,n} \\ . & . & . & . & . \\ \nu_{m,1} & . & \nu_{m,j} & . & \nu_{m,n} \end{pmatrix} \end{array} \tag{8}$$

Each row represents a chemical reaction, each column is assigned to the species S_j given above the columns, $\nu_{i,j}$ represents the stoichiometric weight of the species. By convention $\nu_{i,j}$ is negative for the elements on the left side of the reaction equation and positive for elements on the right side. The exercise is now to calculate the concentration of each species as a function of time given the initial concentrations. First, this is done by calculating the production rate R_j as a function of time. This may be the result of several reactions, and the total production rate is

$$R_j = \sum_{i=1}^{m} \nu_{i,j} \cdot r_i \tag{9}$$

where r_i is the reaction rate. The production rate is defined

$$R_j = \frac{\partial c_j}{\partial t} \tag{10}$$

where c_j is the concentration of species j, and t is the time. Equation (9) may be expressed in matrix form

$$\mathbf{R}^{\mathrm{T}} = \mathbf{r}^{\mathrm{T}}\mathbf{v}\,. \tag{11}$$

Here the transposed matrices $\mathbf{r}^{\mathrm{T}}$ and $\mathbf{R}^{\mathrm{T}}$ are column vectors. Given the initial concentrations, at a later time the concentrations can be calculated by integrating the reaction rates for each species. Integration of the non-linear differential equations is performed by LSODE, the Lawrence Livermore solver for ordinary differential equations [HINDMARSH 1980]. Simple calculation examples using matrices are given in SØRENSEN [1982].

The reaction rate is usually a function of species concentration

$$r_i = k_i \cdot \left[\prod_j c_j^{\varepsilon_{i,j}} - \frac{1}{K_i} \prod_j c_j^{\nu_{i,j}+\varepsilon_{i,j}} \right] \tag{12}$$

where $c_j = [S_j]$ is the source rock concentration of a species, $\varepsilon_{i,j}$ is an element in the reaction order matrix $\underline{\underline{\varepsilon}}$. $\varepsilon_{i,j}$, may be determined from published reaction rate expressions; k_i is the forward reaction rate constant, and K_i is the equilibrium constant. k_i may be temperature dependent

$$k_i(T) = A_i\left(T_{k,i}\right) \exp\left[\frac{E_i}{R_{Ad}} \left(\frac{1}{T_{k,i}} - \frac{1}{T} \right) \right] \tag{13}$$

where T is the temperature (Kelvin), A_i is the frequency factor at the base temperature $T_{k,i}$ (usually 25 °C), E_i is the activation energy, and R_{Ad} is Avogadro's number.

The equilibrium constant is also temperature dependent

$$K_i(T) = K_{b,i}\left(T_{K,i}\right) \exp\left[\frac{\Delta H_i}{R_{Ad}} \left(\frac{1}{T_{K,i}} - \frac{1}{T} \right) \right] \tag{14}$$

where $K_{b,i}$ is the equilibrium constant at the base temperature $T_{K,i}$ (in degrees K), ΔH_i is the reaction enthalpy. The stoichiometric matrix is here derived from the reaction kinetics given by BURNHAM, SWEENEY [1989]. The matrix is quite large therefore only the submatrix for the reactions involving water production is shown here. The stoichiometric sub-matrix is in this case

$$\mathbf{v}_w = \begin{array}{c} \begin{matrix} P_1 & . & P_8 & R_1 & . & R_8 & H_2O \end{matrix} \\ \begin{pmatrix} -1 & . & 0 & 1 & . & 0 & 1 \\ . & . & . & . & . & . & . \\ 0 & . & -1 & 0 & . & 1 & 1 \end{pmatrix} \end{array} \tag{15}$$

where $P_1 \ldots P_8$ are the kerogen precursors for water, and R_1–R_8 are the kerogen residuals. The rows of the stoichiometric matrix express the transformation of the water kerogen precursor to kerogen residual and water. The reaction order matrix is

$$\underline{\underline{\varepsilon}}_w = \begin{array}{c} \begin{matrix} P_1 & . & P_8 & R_1 & . & R_8 & H_2O \end{matrix} \\ \begin{pmatrix} 1 & . & 0 & 0 & . & 0 & 0 \\ . & . & . & . & . & . & . \\ 0 & . & 1 & 0 & . & 0 & 0 \end{pmatrix} \end{array} \tag{16}$$

Applying the equations (15) and (16) in equation (12) and using $K_i = \infty$ one obtains the reaction rates $r_i = k_i[P_i]$, $i = 1, \ldots, 8$, which is a first order reaction as expected. The matrices for the chemical reactions producing CO_2, CH_n, and CH_4 are similar to matrices (15) and (16).

The reaction rate r_i is computed from Eq. (12) with the equilibrium constant being infinity. The forward rate constant is calculated from Eq. (13).

Multiplication of the reaction rate vector and the stoichiometric matrix, Eq. (11), results in the production rate vector for:

$$\begin{pmatrix} R_{P_1} \\ . \\ R_{P_8} \\ R_{R_1} \\ . \\ R_{R_8} \\ R_{H_2O} \end{pmatrix} = \begin{pmatrix} r_1 \\ . \\ r_8 \end{pmatrix} \begin{array}{c} \begin{matrix} P_1 & . & P_8 & R_1 & . & R_8 & H_2O \end{matrix} \\ \begin{pmatrix} -1 & . & 0 & 1 & . & 0 & 1 \\ . & . & . & . & . & . & . \\ 0 & . & -1 & 0 & . & 1 & 1 \end{pmatrix} \end{array} \tag{17}$$

The last element, R_{H_2O}, in the production rate vector is the total water production rate. The species concentration as a function of time may then be calculated by integrating the production rate vector, given the initial concentrations.

6. Estimation of past heat flow

Heat flow history may be calculated by inversion of vitrinite reflectance depth profile measurements [MIDDLETON 1982, LERCHE 1988a and 1988b]. In these papers variables of an initially assumed heat flow function are adjusted until there is a reasonable match between calculated and measured vitrinite reflectance values. However, no rules are given for the choice of function or its number of degrees of freedom. A procedure for calculating past heat flow as a piece by piece linear function is given in the following. Sedimentation age increases with depth. *Figure 2* illustrates a simple approach to inverting the vitrinite reflectance values. A piece by piece linear heat flow function is used (Fig. 2). The figure shows three co-ordinate systems: the uppermost is used for the heat flow history, the right one is used for the vitrinite reflectance values, the lower left co-ordinate system is for the burial history. The linear segment of the heat flow history which is valid for the most recent time, has an endpoint at the present and the other endpoint at the age of the uppermost

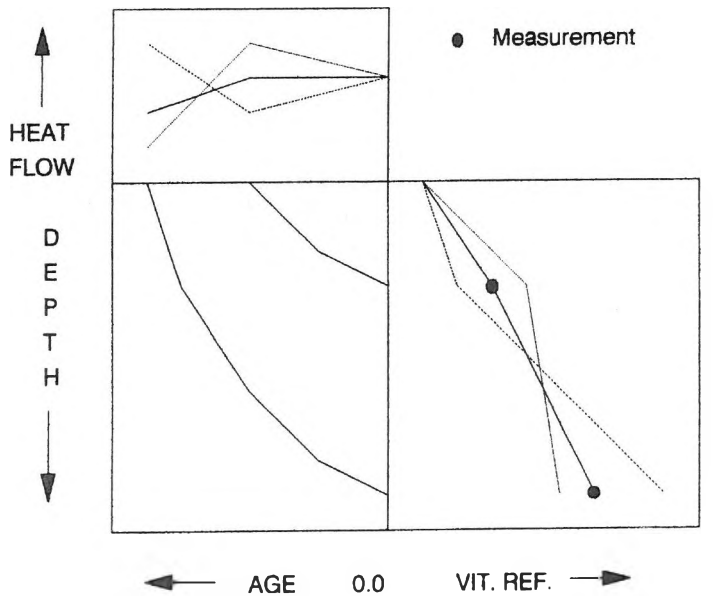

Fig. 2. The lower left co-ordinate system shows the burial history for two vitrinite reflectance samples. The reflectance values are given in the lower right co-ordinate system. Three heat flow functions are given in the uppermost coordinate system

2. ábra. A bal alsó koordináta rendszer a feltöltődés menetét mutatja két vitrinit reflektivitási mintára. A reflektivitás értékek a jobb alsó koordináta rendszerben láthatók. A legfelső koordináta rendszer három alternatív hőáram függvényt mutat

sample. The next (older) segment is valid for the time span between the age of the uppermost sample and the next deeper sample. In this case the number of degrees of freedom for the heat flow function is equal to the number of samples. For the first segment the endpoint at the present has a heat flow value equal to the present day heat flow value; the heat flow value at the other endpoint may be calculated iteratively by simulating the uppermost vitrinite reflectance value. The heat flow function may be continued further back in time provided that deeper samples are available. The next segment may be calculated similarly using the next deeper sample.

Uncertainties of the vitrinite reflectance values lead to uncertainties in the inverted heat flow function. This is illustrated in Fig. 2, where three heat flow functions are shown. The function which leads to a close match between simulated and measured vitrinite reflectance values has already been discussed. The other two functions are determined such that their corresponding calculated vitrinite reflectance values are at the outer limit of the error bars for the measured vitrinite reflectance values (Fig. 2). As the depth distance of the samples becomes small the uncertainty of the calculated heat flow becomes large, and even unrealistically large fluctuations may be obtained. This problem may be solved by enlarging the distances between vitrinite reflectance measurements. Enlarging the distances means that the segments of the heat flow function cover larger time intervals. Since the heat flow history is constructed by line segments beginning at the most recent time and progressing back in time, the uncertainty of a segment is dependent on the uncertainty of the preceding segment, but not on the following one. The uncertainty is thus increasing back in time. To avoid steadily larger fluctuations of the calculated heat flow backwards in time the length of the line segments has to be increased.

7. Basin modelling of the Aars-1A well

The basin model described above is used to simulate hydrocarbon generation for the Danish well Aars-1A.

The Aars-1A well is situated in the Danish Sub-basin, *Fig. 3*. A subdivision in stage/formation/member and a brief summary of the regional setting are given in THOMSEN et al. [1987]. The post Chalk Group erosion is here assumed to be 600 m [JAPSEN 1993]. The potential source rock is the F-III Member of the Fjerritslev Formation, *Fig. 4* [ØSTFELDT 1986]. The age

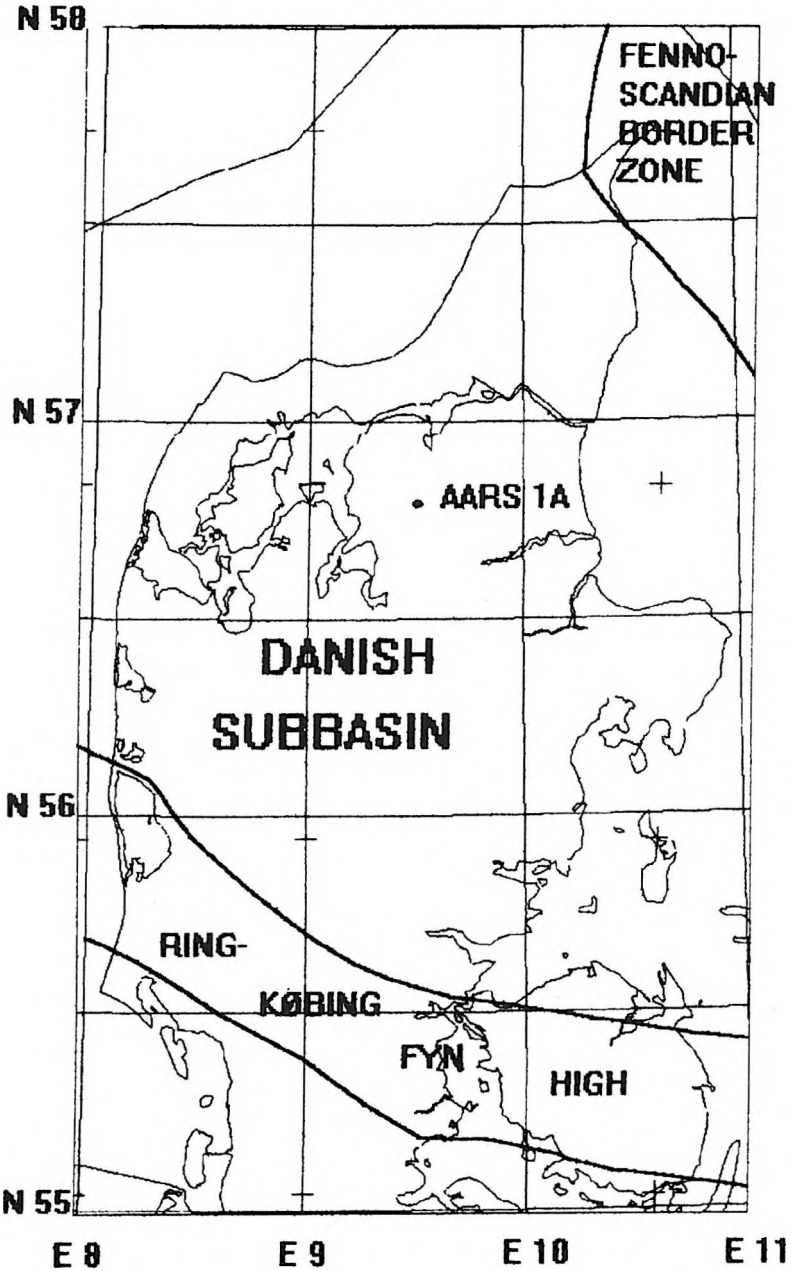

Fig. 3. Map of the Danish Sub-basin and location of the Aars-1A well [after MICHELSEN 1982]

3. ábra. A dán al-medence térképe és az Aars-1A mélyfúrás helyzete [MICHELSEN 1982 nyomán]

dates are based on HAQ et al. [1987]. The total time span of 210 mill. years is divided into 13 events comprising time intervals of sedimentation or erosion. The compaction constants are determined from assumed surface porosities and from a semi-log plot of porosities versus depth for the

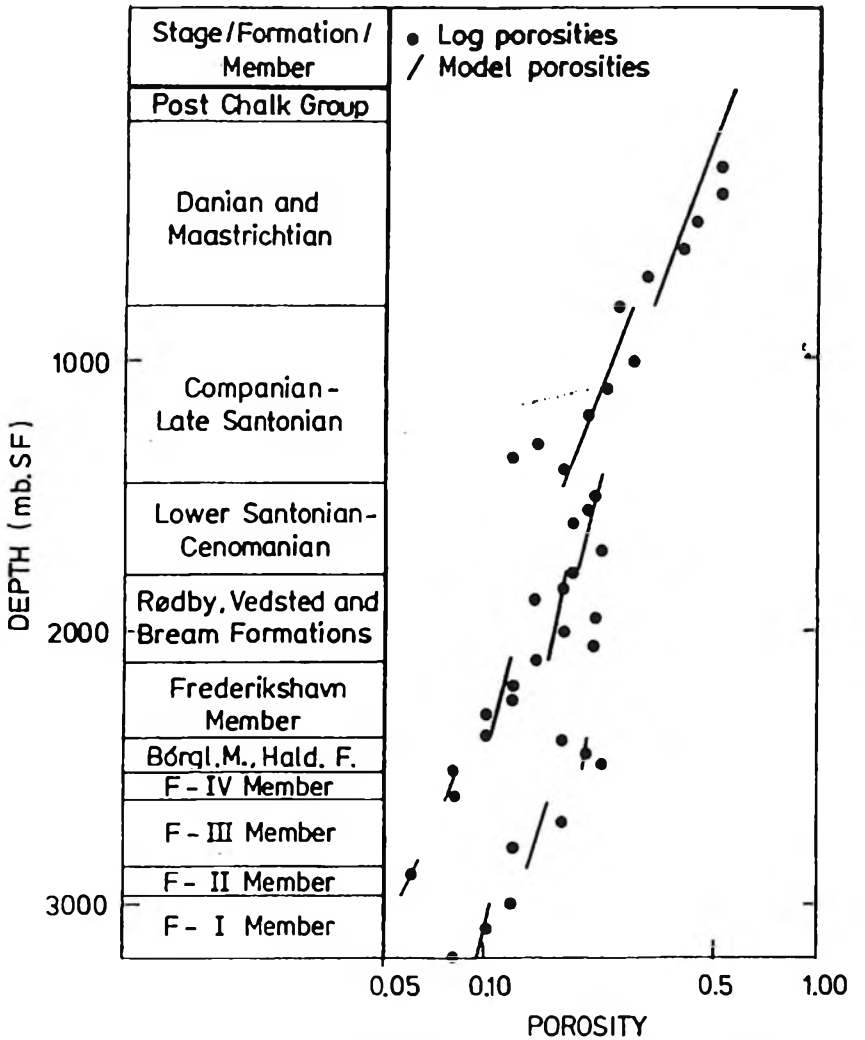

Fig. 4. Log derived and model porosities as a function of depth. The straight lines are exponential function approximations used in the modelling

4. ábra. Karotázs mérésekből levezetett és modell-porozitás értékek a mélység függvényében. Az egyenes vonalak a modellezés során használt exponenciális függvény közelítő értékeit adják meg

individual formations (Fig. 4). The calculated burial history is shown in *Fig. 5.*

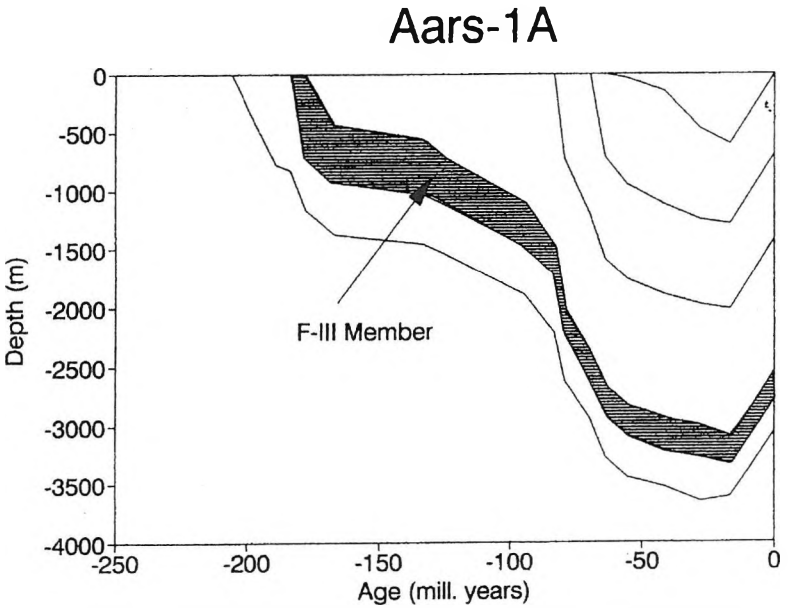

Fig. 5. Simulated burial depth as a function of time including compaction of the sediments

5. ábra. Szimulált feltöltődési mélységek az idő függvényében, figyelembe véve az üledékek kompakcióját is

The sediment surface temperatures (*Fig. 6*) are given by BUCHARDT [1978] for the period back to 60 mill. years. Data for older times were obtained after personal communication with B. BUCHARDT**. The thermal constants determining the conductivities of the rocks using Robertson's model, Eq. (5), are shown in Table 3 in JENSEN et al. [1985]. These constants are found stepwise. First a set of constant is found from figures given by ROBERTSON [1979] for each lithology knowing the porosity and the quartz content. Based on this conductivity model the input heat flux is adjusted to obtain a calculated temperature profile as close as possible to the measured temperature profile. The temperature profile was measured 1 1/2 years after

** Institute of Historical Geology and Palaeontology, University of Copenhagen, Østervoldgade 10, DK-1350 Copenhagen K, Denmark

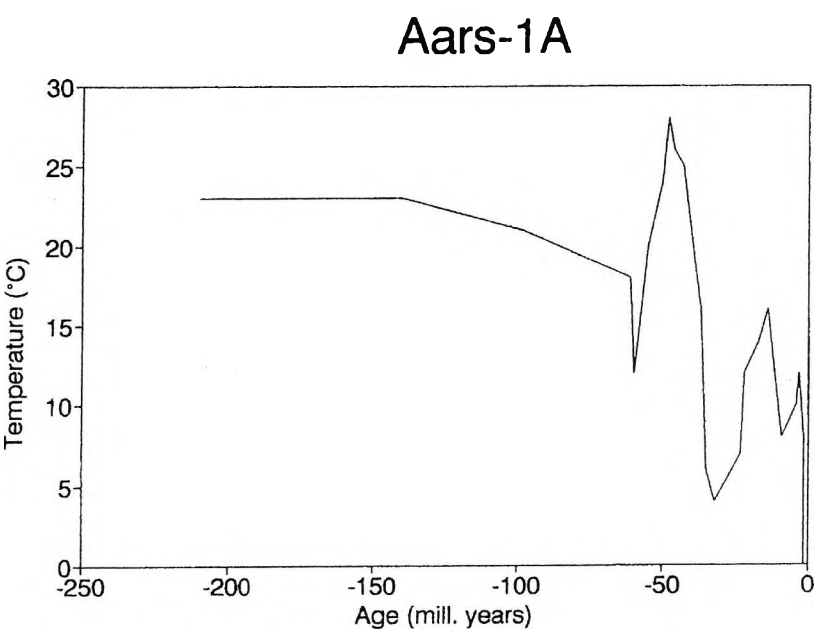

Fig. 6. Surface temperature as a function of time. The surface temperature is due to BUCHARDT [1978]

6. ábra. Felszíni hőmérséklet az idő függvényében BUCHARDT adatai alapján [1978]

cessation of the circulation [BALLING1986] and it is expected that the measured temperatures are within ± 1–2 °C of the true formation temperature. In this way the present heat flow is estimated to be 55 mWm^{-2}, which value is slightly lower than the mean value of 60 mWm^{-2} estimated for the area based on conductivity measurements and temperature logging, BALLING [1986]. A better match (*Fig. 7*) is then obtained by adjusting the constant C in Robertson's conductivity equation, Eq. (5).

The heat flow history calculated by VEJBÆK [1989] is utilised to calculate the formation temperature history (Fig. 7). The heat flow history is based on geodynamic modelling. LARSEN [1986] estimated the formation temperature of the Gassum Formation (just below the Fjerritslev Formation) to be above 130 °C in the early Tertiary. Oxygen $^{18}O/^{16}O$ measurements of formation water were used. The estimate is in accordance with the simulation shown in *Fig. 8.*

The 1-D-basin model is run applying the kinetics by BURNHAM, SWEENEY [1989]. Calculation of the vitrinite reflectance is based on the calculated composition of the residual kerogen as described by BURNHAM, SWEENEY

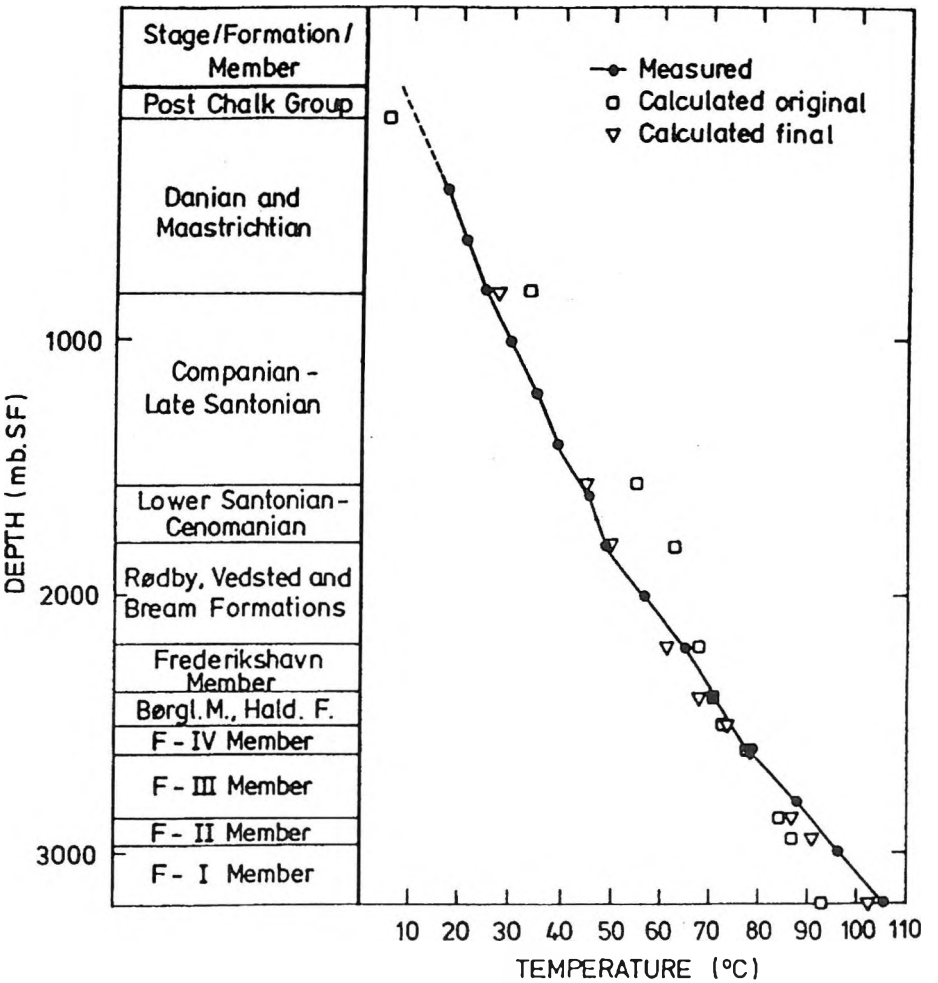

Fig. 7. Measured [BALLING 1986] and calculated temperatures for the Aars-1A well
7. ábra. Mért [BALLING 1986] és számított hőmérséklet értékek az Aars-1A mélyfúrásra

[1989]. A too low calculated vitrinite reflectance value 1.5 % R_0 at the bottom of the well was obtained (*Fig. 9*). A parameter study showed that realistic heat flow histories could not be obtained with the kinetic parameters given by BURNHAM, SWEENEY [1989]. It is necessary to adjust the kinetic model to avoid unrealistic heat flow histories. A reasonable match (Fig. 9) is obtained using the geodynamic heat flow model [VEJBÆK 1989] and the surface

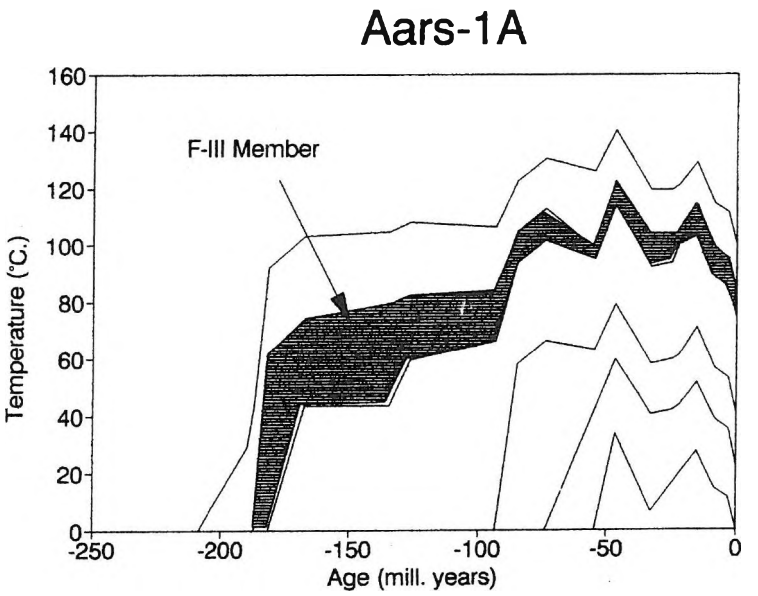

Fig. 8. Simulated formation temperatures as a function of time
8. ábra. Szimulált formáció hőmérsékletek az idő függvényében

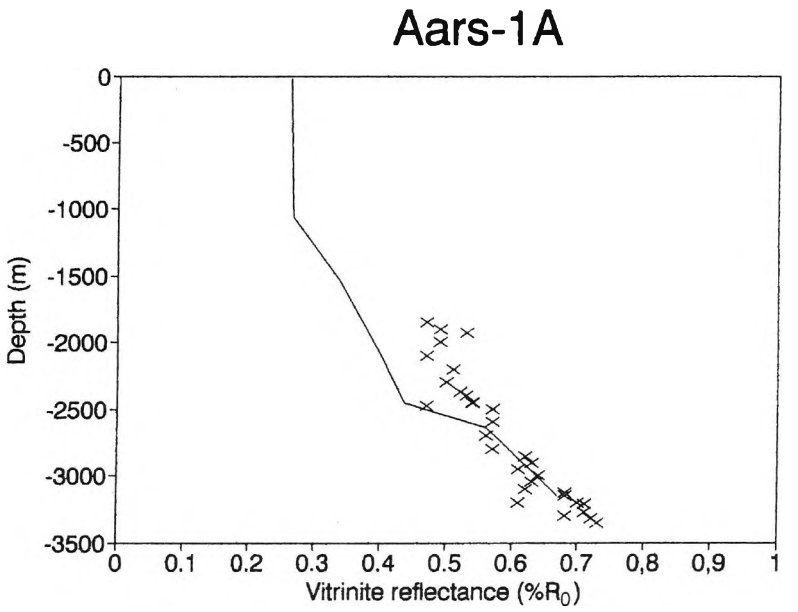

Fig. 9. Measured [THOMSEN 1984] and calculated vitrinite reflectance values
9. ábra. Mért [THOMSEN 1984] és számított vitrinit reflektivitási értékek

temperature by BUCHARDT [1978] when the frequency factors given by BURNHAM, SWEENEY [1989] are multiplied by $0.5\ 10^{-2}$.

The computed vitrinite reflectance values as a function of time are shown in *Fig. 10.* Only the lower part of the Fjerritslev Formation reaches vitrinite reflectance values above 0.6% R_0, which is often regarded as the critical value for onset of oil generation.

Also the recent total oil, gas, water, and carbon dioxide generation of the F-III Member was calculated. According to ØSTFELDT [1986] this rock unit has the most promising potential source rock in the area. LECO-Rock Eval data for the Aars-1A well are reported by ØSTFELDT [1986], *Table I.* The production index (*PI*) shows a mean value around 9%. The bitumen content (*S*1) is around 0.25 (mg oil/g of rock) and the total organic carbon content (*S*2) is around 2.4% (g organic carbon/g of rock) which is equivalent to about 1% (g oil/g organic carbon). The calculations show that 14% of the potential of light hydrocarbons ($CH_{1.7}$) has been generated, methane has not yet been generated. The calculated production index is:

$$PI = \frac{\gamma f_f}{\gamma + \delta} \tag{18}$$

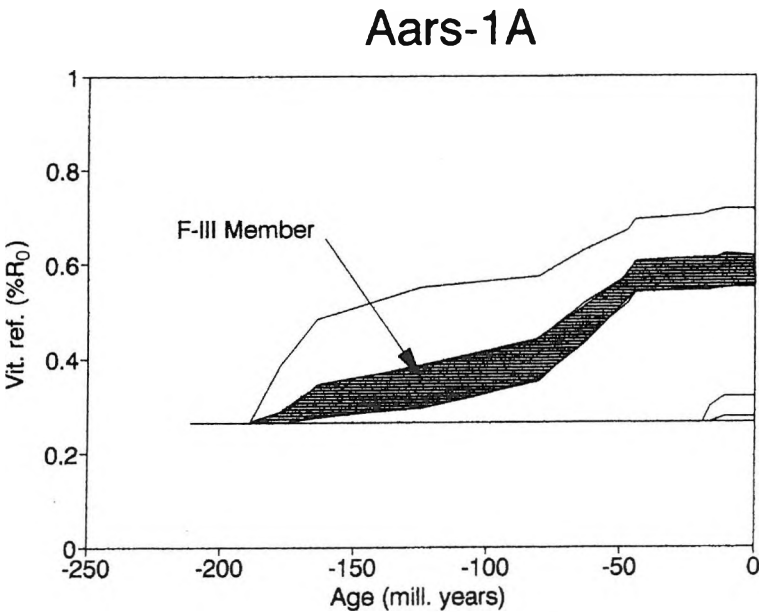

Fig. 10. Simulated vitrinite reflectance values as a function of time
10. ábra. Szimulált vitrinit reflektivitási értékek az idő függvényében

Meter	TC	TOC	T_{max}	S1	S2	PI	HI
2600	6.41	5.05	436	.31	4.37	.07	87
2650	5.02	3.60	427	.72	3.50	.17	97
2700	2.87	1.76	429	.38	3.27	.10	186
2750	2.39	1.63	432	.19	1.65	.10	101
2800	2.27	1.60	432	.24	2.39	.09	150
2855	3.19	1.89	435	.14	1.89	.07	100

Table I. LECO-Rock Eval data from cutting samples of the F-III member of the Fjerritslev Formation at the Aars-1A well [ØSTFELDT 1986]

I. táblázat. LECO-Rock Eval adatai a Fjerritslev formáció F-III tagjából származó metszetekből az Aars-1A mélyfúrásból. [ØSTFELDT 1986]

where γ and δ are the fractions of initial carbon that ultimatly may be removed from the initial kerogen as CH_n and CH_4 respectively, and f_c is the fraction of carbon converted to CH_n. The conversion ratios for H_2O, CO_2, CH_n, and CH_4 are defined: $F_\alpha = [H_2O]/[H_2O]_0$, $F_\beta = [CO_2]/[CO_2]_0$, $F_\delta = [CH_n]/CH_n]_0$, and $f_C = [CH_4]/[CH_4]_0$, where in each case the index 0 indicates initial concentrations. In the calculation example γ is 12.5% and δ is 1% [BURNHAM, SWEENEY 1989], and f_C is here calculated to be 14% which leads to a calculated value for the production index equal to 0.13. The calculated production index may be compared with the measured production index $S_1/(S_1+S_2)$ where S_1 is the volatile hydrocarbons and S_2 is the hydrocarbon derived from kerogen pyrolysis. The calculations as well as the measurement show that a small amount of oil has been generated and only a small fraction of the potential has been transformed. Although the hydrocarbon generation is small in the Aars-1A well it may be higher in areas of the basin where the burial is deeper.

A sensitivity study is performed to see the effect of the assumed linear heat flow function. The results are summarised in *Table II*. The preferred heat flow function linearly increases from 55-67 mWm^{-2} [VEJBÆK 1989]. The simulations show that onset of hydrocarbon generation occurred quits suddenly (within 500,000 years). The onset most likely occurred within the last 30 to 18 mill. years.

Application of the geodynamically calculated heat flow function and the modified kinetic model leads only to a rough match between calculated and

Heat Flow (mWm^{-2})	Onset of Oil Gen. mill. years	Vit. Ref. % R_0	f_c
40	no onset	0.60	0.00
50	18	0.62	0.10
67	**30**	**0.64**	**0.14**
70	37	0.65	0.15
80	50	0.68	0.18

Table II. Parameter study varying the assumed linear heat flow function. For all cases the present heat flow is 55 mWm^{-2}. The F-III Member of the Fjerritslev Formation is considered. Vitrinite reflectance and the fraction of CH_n production, f_c is calculated for the present time. The preferred model is in bold letters

II. táblázat. Paraméter vizsgálatok a feltételezett lineáris hőáram függvény változtatásával. Mindegyik esetben a jelenlegi hőáram 55 mWm^{-2}. A Fjerritslev formáció F-III tagját vizsgálták. A vitrinit reflektivitást és a CH_n termelés frakcióját, az f_c-t a jelenlegi időpontra számították. A kedvezőnek ítélt modellt vastag betű jelöli

measured vitrinite reflectance values (Fig. 9). Refinement of the match is performed by adjusting the heat flow history applying the above described inversion method. Vitrinite reflectance measurements are performed from 10 to 186 times at each depth [THOMSEN 1984]. The standard deviation for each measurement is generally a little less than 10%. In the inversion procedure a general value of 10% has been used. As there are no vitrinite reflectance measurements within the Chalk Group, only a linear heat flow segment can be estimated for that period (corresponding to the base of layer 6). The present day heat flow is assumed to be error-free. Alternative inverted heat flow histories are shown in *Fig. 11* together with the heat flow history calculated by geodynamic modelling [VEJBÆK 1989]. The alternatively inverted heat flow histories lead to calculated vitrinite reflectance values which match measurements within 10%. Only the most recent parts of the heat flow function, which fall within realistic heat flow values, are shown. The inverted heat flow function can thus only be estimated with reasonable error limits 100 mill. years back in time. The heat flow values show higher values than for the heat flow function derived from geodynamic modelling. Due to the limited extent, back in time, the heat flow function derived from geodynamic modelling is used for kinetic modelling.

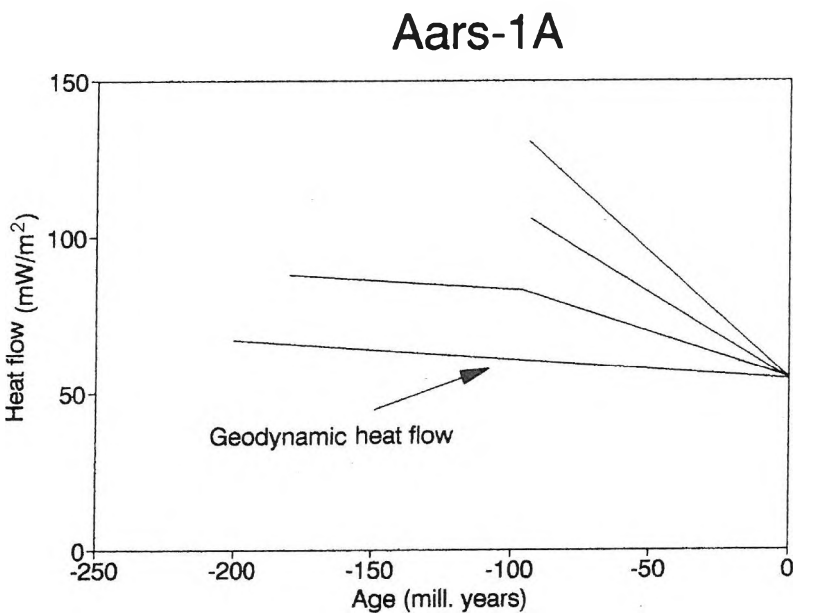

Fig. 11. Alternative heat flow histories calculated by inversion of measured vitrinite reflectance data. The thermal history from geodynamic modelling by VEJBÆK [1989] is also shown

11. ábra. A mért vitrinit refelektivitási adatok inverziójával számított alternatív hőáram változások és a VEJBÆK [1989]-féle geodinamikai modellezésből eredő termikus történet

8. Discussion

A major limitation of the analytical expressions for the burial history of sedimentary sequences outlined in this paper is the predefined porosity–depth function. Although such relations have been used widely in the literature they cannot adequately describe the porosity conditions in overpressured shales. In these zones, compaction ceases because formation water is trapped due to the low permeability. Pre-defined compaction curves can therefore only roughly estimate the natural conditions.

The equations for formation temperature are developed for stationary conditions. This condition is only partly valid since surface temperature and heat flow may vary with time. Also variations of the sedimentation rate cause transient effects. This may be important for rapidly subsiding basins [HUTCHINSON 1985].

Determination of rock heat conductivities is connected with high uncertainties, but a close match of simulated and measured formation temperatures can be obtained despite inaccuracies of the conductivity model. This is done by adjusting the assumed present heat flow model. Basin modelling is therefore not particularly sensitive to the accuracy of the heat conductivity model since a satisfactory match between simulated and measured temperatures can be obtained.

The equations concerning the history of burial and temperature presented here are attractive firstly because the approach is simple and secondly because the results, for 1-D modelling, may be as accurate as more advanced modelling including compaction-driven ground water flow. In advanced 1-D modelling only vertical movements are allowed. This restriction is seldom fulfilled in sedimentary basins [see BETHKE 1985]. Improved estimates of burial and temperature history of sediments can only be obtained by two- or three-dimensional simulations including water movements.

In an earlier study JENSEN [1988] it was shown that if one applies the kinetic model by TISSOT et al. [1987] and a thermal history for the Aars-1A well including compaction, variation of conductivity with time, and a surface temperature history they lead to transformations of the kerogen that are much too high when compared with measured transformation ratios. There may be several reasons for the necessity of modifying the published kinetic models. First of all there may be differences in the chemical composition between the kerogen at the Aars-1A well and the kerogen considered by BURNHAM, SWEENEY [1989] and TISSOT et al. [1987]. Second, there are differences in the basin models used by the different authors. If a basin model is used with kinetic parameters originating from calibrations using a basin model that do not take compaction or surface temperature into account, considerable errors may arise.

The kinetic model given by BURNHAM, SWEENEY [1989] can adequately simulate the transformation ratios observed in the Aars-1A well providing adjustments of the frequency factors are made as described above. To test the predictive force of the kinetic model more well data must be included.

Although the matrix method ensures a flexible input scheme the computing time is high. The steady improvement in the speed of computers makes the matrix method even more attractive in the future.

The inversion method described above is attractive since it avoids unrealistic fluctuations of the calculated heat flow history which are caused by the uncertainty of the vitrinite reflectance measurements. However, the

fluctuations may also be caused by the kinetic model itself, because the kerogen is assumed to be described by a limited number of activation energies.

9. Conclusions

Burial, compaction, and temperature history of sediments may be described by a set of easily solvable equations. The matrix method for calculating chemical reactions by SØRENSEN, STEWART [1980] has successfully been implemented in a chemical kinetic model, the model being flexible in terms of changes of species in the input scheme. Thus, re-evaluation of equations and re-programming are avoided if new species are introduced. However, the matrix approach is not as efficient concerning computing time as the traditional analytical approach.

A 1–D basin model study was performed for the Danish well Aars-1A. The heat flow history was first calculated by inversion of measured vitrinite reflectance data. Due to the uncertainties of the measurements the resulting heat flow history fluctuates especially when the distance between vitrinite reflectance samples is small. If the distance between the samples is increased, it diminishes the fluctuations thereby making the estimated heat flow more reliable. However, this is at the cost of the worsening of the time resolution.

On the basis of the calculated formation heat conductivities the measured temperature depth profile is simulated with good agreement when the present day model heat flow is 55 mWm^{-2}. Vitrinite reflectance values and hydrocarbon generation is simulated satisfactorily using the heat flow history derived from geodynamic modelling [VEJBÆK 1989] and using chemical kinetic data from BURNHAM, SWEENEY [1989] with the modification that all frequency factors are multiplied by 0.5×10^{-2}.

The maturity history for a number of formations is calculated using the heat flow history from geodynamic modelling. The vitrinite reflectance of the F-III Member of the Fjerritslev Formation was close to 0.6% R_0 75 mill. years b.p. and has not increased much since that time. Calculations show that a minor amount of oil has been generated in the last 30–18 mill. years, and only a very small amount of gas has been generated.

Acknowledgement

Thanks are given to Zahari ZLATEV who guided us through the running of the LSODE differential equation solver.

Appendix A

Derivation of burial history equations

The Newton Method

Solving the two transcendental equations (Eqs. 1 and 4) is equivalent to solving the equation $f(z)=0$. The two equations can be transformed to this form by isolating a zero on the right side of the equations. The Newton method [BRONSTEIN, SEMENDJAJEV 1963, p. 123] assumes that if z_i is an approximation to the solution, then

$$z_{i+1} = z_i - \frac{f(z_i)}{f'(z_i)} \tag{A1}$$

is a new and better approximation.

This new approximation may then be used instead of z_i in Eq. (A1) to give an even better approximation. The process converges providing the function is monotonic.

Surface layer

Given the time t in Eq. (4) the corresponding depth z must satisfy the equation

$$\frac{1}{\upsilon_0(1-\Phi_0)}\left[z + \frac{\Phi_0}{a}\left(e^{-az} - 1\right)\right] - t = 0 \tag{A2}$$

The iteration procedure, Eq. (A1), is then

$$z_{i+1} = z_i - \frac{\left[z_i + \frac{\Phi_0}{a}\left(e^{-az_i} - 1\right)\right] - t}{\left[1 - \Phi_0 e^{-az_i}\right]} \tag{A3}$$

It is easily seen by differentiation with depth z, that $f(z)$ is monotonic, knowing that $\Phi_0 < 1$.

Non-surface layers

The unknown depth, z_4, is to be found in Eq. (4) given the depths z_1, z_2, and z_3. The function f in Eq. (A1) is

$$f(z_{4i}) = z_{4i} - z_2 + z_1 - z_3 - \frac{\Phi_0}{a}\left[e^{-az_2} - e^{-az_1} + e^{-az_3} - e^{-az_{4i}}\right] \qquad \text{(A4)}$$

and the derivative

$$f'(z_{4i}) = 1 - \Phi_0 e^{-az_{4i}} \qquad \text{(A5)}$$

Appendix B

The temperature profile in sediments

The expression for the steady state temperature profile, Eq. (6), in sediments with the porosity decreasing exponentially with depth and with the heat conductivity given by Robertson's equation, Eq. (5), will be deduced below. The temperature, $T(z_2)$, at the base of the formation is

$$T(z_2) = T(z_1) + W\int_{z_1}^{z_2} \frac{1}{K(z)}\mathrm{d}z \qquad \text{(B1)}$$

where $T(z_1)$ is the formation temperature at the top of the formation, W is the heat flow, and $K(z)$ is the heat conductivity. The integral, I, in Eq. (B1) may be written as

$$I = \int_{z_1}^{z_2} \frac{\mathrm{d}z}{K_F + (1-\Phi)^2\left[K_s + pC - K_f\right]} \qquad \text{(B2)}$$

Since the porosity $\rho = \rho_0 e^{-az}$ and the derivative $\mathrm{d}\rho = a\rho\,\mathrm{d}z$, the integral becomes, by shift of variable

$$I = \frac{1}{aA}\int_{\Phi_1}^{\Phi_2} \frac{\mathrm{d}\Phi}{\Phi\left[\sqrt{(K_F/A)^2 + (1-\Phi)^2}\right]} \qquad \text{(B3)}$$

where $A = K_s + pC - K_F$. The integral has now a form where an analytical solution can be found [BRONSTEIN, SEMENDJAJEV 1963, p. 302, eq. 82]:

$$I = \frac{1}{aA} \frac{1}{(K_F/A)+1} (g_1 + g_2) \tag{B4}$$

where g_1 and g_2 are defined by Eq. (17).

Appendix C

List of symbols

Explanations of symbols used in the equations are given together with units.

a = compaction coefficient, m^{-1}
A = $K_s + pC - K_F$, $Wm^{-1}K^{-1}$
A_i = frequency factor for reaction i, s^{-1}
c = species concentration, mole cm^{-3}
C = constant for each rock type governing the influence of quartz on heat conductivity, $Wm^{-1}K^{-1}$
E_i = activation energy for reaction i, J mol^{-1}
g_i = function explained by Eq. (7), dimesionless
h = thickness of surface layer at present, m
k_i = chemical reaction rate for reaction i, dimension depends on reaction
K = bulk heat conductivity of sediment, $Wm^{-1}K^{-1}$
$K_{b,i}$ = equilibrium constant at base temperature
K_F = fluid heat conductivity, $Wm^{-1}K^{-1}$
K_i = equilibrium constant, dimension depends on reaction
K_s = solid conductivity for zero content of quartz, $Wm^{-1}K^{-1}$
p = quartz content, percentage
R = production rate, mole $cm^{-3}s^{-1}$
R_{Ad} = Avogadro's constant
R' = reaction rate, mole $s^{-1}cm^{-3}$
R_0 = vitrinite reflectance, percentage
S_j = chemical species

t = time, s
t_b = age date of base of surface layer, s
T = formation temperature, K
$T_{k,i}$ = base temperature for frequency factor
$T_{K,j}$ = base temperature for equilibrium constant
υ_0 = surface grain velocity, ms^{-1}
W = heat flow, Wm^{-2}
z = depth from sediment surface, m
z_i = depth of location i, m
$\underline{\varepsilon}$ = reaction order matrix, dimensionless
ρ_m = matrix (grain) density, kg m^{-3}
ρ_{sol} = bulk solid density (mass of solid particles per volume of sediment), including water, kg m^{-3}
ΔH_i = enthalpy difference
ρ = porosity, dimensionless
ρ_i = porosity of depth z_i, dimensionless
ρ_0 = surface porosity, dimensionless
ν = stoichiometric matrix, dimensionless

REFERENCES

ATHY L. F. 1930: Density, porosity, and compaction of sedimentary rocks. AAPG Bull. **14**, 1, pp. 1–24

BALLING N. 1986: Principal uses of heat-flow data. *In*: MØLLER (ed): Twenty-five years of geology in Aarhus. Geoskrifter, No. 24. 300 p.

BETHKE C. M. 1985: A numerical model of compaction-driven groundwater flow and heat transfer and its application to the paleohydrology of intracratonic sedimentary basins. Journal of Geophysical Research **90**, B8, pp. 6817–6828

BRONSTEIN I. N., SEMENDJAJEV K. A. 1963: Taschenbuch der Mathematik. P. G. Teubner Verlaggesellschaft, Leipzig, 584 p.

BUCHARDT B. 1978: Oxygen isotope paleotemperature from the Tertiary period in the North Sea areas. Nature **275**, pp. 121–123

BURNHAM A. K., SWEENEY 1989: A chemical kinetic model of vitrinite maturation and reflectance. Geochimica et Cosmochimica Acta **53**, pp. 2649–2657

CAO S., LERCHE I. 1986: Fluid flow, hydrocarbon generation and migration: A quantitative model of dynamical evolution in sedimentary basins. Offshore Technology Conference Proceedings, Houston, Texas, Paper 5182, **2**, pp. 267–276

FALVEY D. A., DEIGHTON I. 1982: Recent advances in burial and thermal geohistory analysis. APEA, **22**. pp. 65–81

HAQ B. U., HARDENBOL J., VAIL P. R. 1987: Chronology of fluctuating sea levels since the Triassic (250 million years ago to present). Science **235**. pp. 1156–1167

HINDMARSH A. C. 1980: LSODE and LSODE1, two new initial values ordinary differential equation solvers. ACM-Signum, Newsletter **15**, 4, pp. 10–11

HOOD A., GUTJAHR C. C. M., HEACOCK R. L. 1975: Organic metamorphism and the generation of petroleum. AAPE **59**, 6, pp. 968–996

HUTCHINSON I. 1985: The effect of sedimentation and compaction on oceanic heat flow. Geophys. J. R. Astr. Soc. **82**, pp. 439–459

JAPSEN P. 1993: Influence of lithology and Neogene uplift on seismic velocities in Denmark: Implications for depth conversion of maps. AAPG **77**, 2, pp. 194–211

JENSEN P. K., HOLM L., THOMSEN E. 1985: Modelling burial history temperature and maturation. *In*: THOMAS et al.(eds): Petroleum geochemistry in exploration of the Norwegian shelf. Graham & Trotman, London, pp. 145–152

JENSEN P. K. 1988: Preliminary simulations of transformation ratios for the Danish well Aars-1A: Riso-M-2552, Riso National Laboratory, DK-4000, Roskilde, Denmark. 23 p.

LARSEN F. 1986: A sedimentologic and Diagenetic investigation of the Gassum Formation II. Thesis (in Danish) 100 p.

LERCHE I., YARZAB R. F., KENDALL C. G. ST. C. 1984: Determination of Paleoheat flow from vitrinite reflectance data. AAPG **68**, 11, pp. 1704–1717

LERCHE I. 1988a: Inversion of multiple thermal indicators: Quantitative methods of determining paleoheat flux and geological parameters. I. The theoretical development for paleoheat flux. Mathematical Geology **20**, 1, pp. 1–36

LERCHE I. 1988b: Inversion of multiple thermal indicators: Quantitative methods of determining paleoheat flux and geological parameters. II. The theoretical development for chemical, physical and geological parameters. Mathematical Geology **20**, 1, pp. 73–96

MICHELSEN O. (ed) 1982: Geology of the Danish Central Graben. Series B, No. 8. Geological survey of Denmark, 135 p.

MIDDLETON M. F. 1982: The subsidence and thermal history of the Bass basin, South Eastern Australia. Tectonophysics, **87**, pp. 383–397

ROBERTSON E. C. 1979: Thermal conductivities of rocks. Open File Report 79–356, U. S. Geological Survey, 31 p.

SCLATER J. G., CHRISTIE P. A. F. 1980: Continental stretching an explanation of the post-mid-Cretaceous subsidence of the Central North Sea Basin. Journal of Geophysical Research **85**, B7, pp. 3711–3739

SØRENSEN J. P., STEWART W. E. 1980: Structural analysis of multicomponent reaction models: Part 1. Systematic editing of kinetics and thermodynamic values. AIChE Journal **26**, 1, pp. 98–111

SØRENSEN J. P. 1982: Simulation, regression and control of chemical reactors by collocation techniques. Polyteknisk Forlag, Copenhagen Vol. 1.

TISSOT B. P., PELET R., UNGERER P. H. 1987: Thermal history of sedimentary basins, maturation indices, and kinetics of oil and gas generation. AAPG **71**, 12, pp. 1445–1466

THOMSEN E. T. 1984: A coal petrographical investigation of the well Aars-1. Internal report, Geological Survey of Denmark, 22 p.

THOMSEN E. T, DAMTOFT K., ANDERSEN C. 1987: Hydrocarbon plays in Denmark outside the Central Through. *In*: J. BROOKS K. and GLENNIE (eds): Petroleum geology of North West Europe. Graham & Trotman, London, pp. 375–388

UNGERER P., BESSIS F., CHENET P. Y., DURAND B., NOGARET E., CHIARELLI A., OUDIN J. L., PERREN J. F. 1984: Geological and geochemical models in oil exploration; principles and practical examples. AAPG Memoir **35**, pp. 53–77

VEJBÆK O. V. 1989: Effects of asthenospheric heat flow in basin modelling exemplified with the Danish Basin. Earth and Planetary Science Letters, **95**, pp. 97–114

WAPLES D. W. 1980: Time and temperature in petroleum formation: Application of Lopatin's method to petroleum exploration. AAPG **64**, 6, pp. 916–926

YÜKLER M. A., CORNFORD C., WELTE D. 1978: One-dimensional model to simulate geologic, hydrodynamic and thermodynamic development of a sedimentary basin. Geologische Rundschau **67**, 3, pp. 960–979

ØSTFELDT P. 1986: An organic geochemical investigation of the Aars-1. Internal Report, Geological Survey of Denmark

Üledékes medencék feltöltődésének, hőmérsékletének és a szénhidrogén keletkezésének modellezése az Aars-1A (Dánia) mélyfúrás példáján

Peter Klint JENSEN

Egyszerű analitikai kifejezések segítségével számítják ki az Aars-1A dán mélyfúrás feltöltődési és felszín alatti hőmérsékletének alakulását. Az üledékes szekvenciák kompakcióját figyelembe vették. A vitrinit reflektivitást és a szénhidrogén keletkezést egy általános kémiai szimulációs modell segítségével szimulálják. A kémiai reakciók módosításának tekintetében a modell rugalmas. A hőáram történet kiszámítására a mért vitrinit reflektivitás inverziójának módszerét javasolják. A dán Aars-1A mélyfúrásra 1D medence-modellezést készítettek. A 100 millió évvel ezelőttre számított hőáram bizonytalansága (a jelenlegi hőáramhoz viszonyítva) 25%. Ennél korábbi időkre a bizonytalanság tovább növekszik. A Fjerritslev formáció F-III tagjának szénhidrogén keletkezését a geodinamikai modellezésből levezetett hőáramtörténet felhasználásval számították ki.